高減衰ゴムの微視構造の観察とマイクロメカニクスに基づく構成則の構築

（研究課題番号 12650457）

平成 12 年度から平成 13 年度科学研究費補助金
（基盤研究(C)(2)）
研究成果報告書

平成 14 年 3 月

研究代表者　奥井義昭
（埼玉大学工学部助教授）

ま え が き

本報告書は平成 12 年度から平成 13 年度の２年間に行った文部科学省科学研究費補助金（基盤研究(C)(2)）の補助を受けて実施した研究成果をとりまとめたものである．

研究課題のタイトルとしては「マイクロメカニクスに基づく構成則の構築」とあるが，微視構造の観察の結果，マイクロメカニクスに基づく構成則の構築が困難であることがわかり，報告書で提案する構成則は現象論的なものとなっている．したがって，タイトルと内容が異なるわけであるが，研究計画段階で全てのことを予見することは困難であり，この点ご容赦いただきたい．また，これに伴い英文のタイトルも日本語の研究課題を直訳せず，実際の内容に即したものとなっている．

１．研究課題

高減衰ゴムの微視構造の観察とマイクロメカニクスに基づく構成則の構築

２．研究組織

研究代表者：　奥井義昭　埼玉大学工学部建設工学科

研究分担者：　山口宏樹　埼玉大学工学部建設工学科

研究分担者：　松本泰尚　埼玉大学工学部建設工学科

研究協力者：　A.F.M. S. Amin　埼玉大学理工学研究科博士後期課程（当時）

研究協力者：　M.S. Alam　埼玉大学理工学研究科博士前期課程（当時）

３．交付決定額

	合計
平成 12 年度	2900 千円
平成 13 年度	1200 千円
総計	4100 千円

４．研究発表

(1)学会誌等

Amin, A. F. M. S., Alam, M. Shah and Okui, Y., Development of Rate Dependent Constitutive Model for Elastomers, Creative Systems in Structural and Construction Engineering, Singh (ed.), Balkema, Rotterdam, 2001.

Amin, A. F. M. S., Alam, M. Shah and Okui, Y., Nonlinear viscoelastic response of elastomers: Experiments, parameter identification and numerical simulation, *J. Struct. Engrg, JSCE,* **47A**, 181-192, 2001.

奥井義昭，A.F.M. Saifl Amin，高架橋免震化に使用される高減衰ゴムの特徴と構成則，第２回ダンピングシンポジウム「ダンピング技術の新しい展開」講演論文集，日本機械学会，75-80, 2002

A.F.M.S. Amin, M.S. Alam, Y. Okui, An improved hyperelasticity relation in modeling viscoelasticity response of natural and high damping rubbers in compression: experiments, parameter identification and numerical verification, *Mechanics of Materials*, **34**, 75-95, 2002

(2)口頭発表

Alam, M. Shah, Takanezawa, S., Amin, A. F. M. S. and Okui, Y., Mechanical Behavior of Elastomers Under Compression and Its Microstructure, Proceedings of 55th Annual Conference of Japan Society of Civil Engineers, Sendai, Japan, September, I-A9, 2000.

Amin, A. F. M. S., Alam, M. Shah and Okui, Y., Hyperelasticity Modeling of High Damping Rubber and Finite Element Simulation, Proceedings of 55th Annual Conference of Japan Society of Civil Engineers, Sendai, Japan, September 2000, I-A8, 2000.

Amin, A. F. M. S., Alam, M. Shah and Okui, Y., An Improved Hyperelasticity Relation For Modeling Strain Rate Dependency of High Damping Rubber, Proceedings of 55th Annual Conference of Japan Society of Civil Engineers, Kumamoto, Kyushu, Japan, 2001.

CONSTITUTIVE MODELING FOR STRAIN-RATE DEPENDENCY OF NATURAL AND HIGH DAMPING RUBBERS

REPORT OF RESEARCH PROJECT
GRANT-IN-AID FOR SCIENTIFIC RESEARCH (C) (2)
(Project No. 12650457)

2002, March

Dr. Yoshiaki Okui
Associate Professor

Department of Civil & Environmental Engineering
SAITAMA UNIVERSITY

ACKNOWLEDGEMENT

It is indeed pleasure to express deepest gratitude to Professor H. Horii, Associate Professor M. Abe and Dr. J. Yoshida, Department of Civil Engineering, the University of Tokyo, Tokyo, Japan for their valuable comments and suggestions at various stages of the work. Particularly, the great help of Professor H. Horii by offering the experimental facilities of his laboratory to carry out the mechanical tests of the investigation is gratefully acknowledged.

Acknowledgements are also due to Professor H. Yamaguchi and Dr. Y. Matsumoto for giving enlightening suggestions for the progress of this research at various stages.

At this moment, it is also a pleasure to recall the contribution of Mr. A.F.M. Saiful Amin who carried out this research as a part of his doctoral dissertation. The technical assistances provided by M/S Mr. M.S. Alam, S. Takanezawa and T. Matsuo are also gratefully acknowledged.

Special thanks are due to the Japanese Ministry of Education, Science, Sports and Culture for providing financial supports in the form of Grant-in-Aid for Scientific Research (C) (No. 12650457). The kind cooperation of the Yokohama Rubber Co. for providing the test specimens and the necessary assistance to perform the tension experiments are also gratefully acknowledged.

ABSTRACT

The microstructure and the mechanical behavior of natural rubber (NR) and high damping rubber (HDR) were investigated. In studying the mechanical behavior, most of the attention was paid to the compression regime, whereas some tests in tension were carried out for comparison. The mechanical tests revealed the existence of Mullins' effect, strain-rate dependency, hystersis and residual strain effects in all the specimens. In NR, the extent of these effects were found to have a inherent relation with the presence of microstructural voids. The presence of all these effects was also found to be significant in HDR. In addition, the strain-rate dependent high initial stiffness feature at low compressive stretch levels also became evident from the experiments. However, the microstructural observation of the current study could not explain these features of HDR. This promted for the need of considering a phenomenological approach to reach a general constitutive model for NR and HDR as well.

To this end, a constitutive model based on phenomenological motivation was introduced to model the strain-rate dependency effect. An improved hyperelasticity model was proposed to represent the rate-independent elastic responses including high initial stiffness characteristics. A comparative evaluation was carried out to display the better performance of the proposed hyperelasticity model over the conventional ones over the strain range in representing elastic response of NR and HDR. The hyperelasticity relation was incorporated in a finite deformation rate-dependent model structure. A parameter identification scheme was proposed to identify the parameters for the equilibrium and the instantaneous responses from the experimental data. To this end, the difficulties of direct application of infinitely fast or slow loading rate on such highly viscous material to obtain these responses and thereby to identify the nonlinear elastic parameters were overcome. To do this, experimental results were extrapolated and the proposed hyperelasticity model was used. The proposed scheme was applied on three types of specimens. Numerical simulation of the test results at different deformation modes followed by sensitivity studies verified the adequacy and the robustness of the proposed model and the parameter identification scheme.

CONTENTS

Chapter 1

Introduction

1.1 GENERAL

Rubber is obtained in the form of latex from the tree *Hevea Braziliensis.* A high degree of deformability under the action of comparatively small stresses makes rubber unique among other materials. The typical extensibility falls within the range of 500 -1000% while it can sustain large compressive strain (even up to 90%) without undergoing any failure. The cause of such high deformability lies in the polymeric structure of rubber and it was interpreted from the molecular point of view (Trealor 1975).

As a polymer compound, natural rubber latex consists of long molecular chains with a genuine chemical entity. The molecular weights of such polymers fall in the range of 100,000 – 1,000,000 with a typical value of 350,000. The molecules of such dimensions possess the flexibility associated with internal vibrations and rotations. Figure 1.1a presents a schematic representation of molecular chain structure of latex rubber. In the bulk material, the long chain molecules, however, do not stay in isolation but form a coherent network like structure with freely rotating links. In addition, weak secondary forces and interlocking at few places also do occur between the molecular chains to form a three dimensional network to keep the material in solid phase. Yet, such a material gets a little application in engineering application unless it is vulcanized. During vulcanization process, cross-linkages are introduced between the molecular chains of rubber through sulfur molecules in a chemical process (Fig. 1.1b). Furthermore, carbon-black particles are also added as solid fillers and act as reinforcing agent. These fillers are extremely fine sized particle with the typical mean radii of the order of 100-4700Å (Govindjee 1991). This additive incorporates improved stiffness, toughness, hysteresis and rate dependence properties into the natural rubber (NR) system. Therefore, the extent of improvement of these properties is closely related with the filler concentration (Meinecke and Taftaf 1987; Hamed and Hatfield 1988; Wischt 1998).

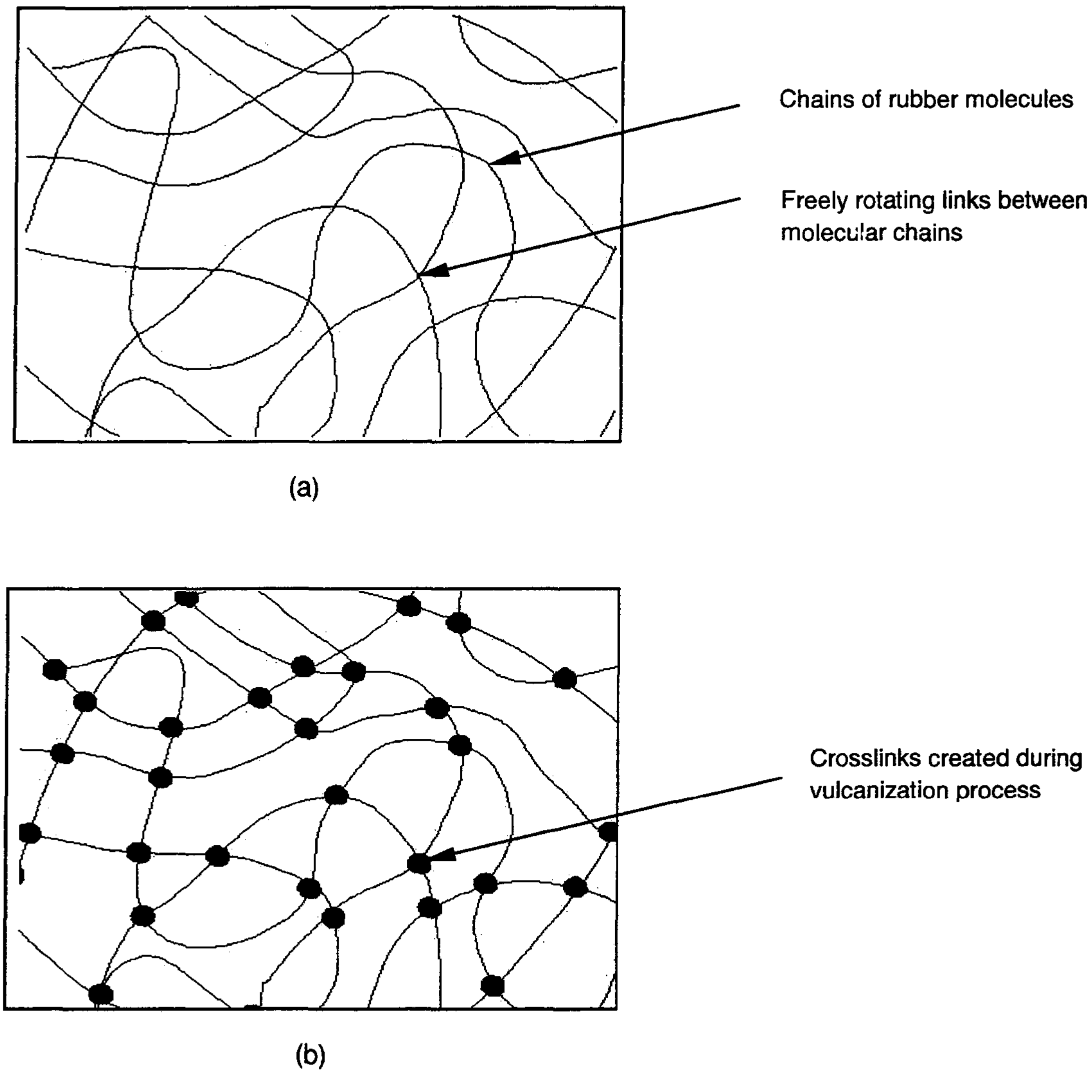

Figure 1.1 A schematic representation of molecular structure of rubber (a) latex rubber, (b) vulcanized rubber

1.2 ENGINEERING APPLICATIONS OF RUBBER

Rubber is a versatile and adaptable material in engineering applications for over 100 years. The use of rubber expanded greatly with the advent of vulcanization process being pioneered by Charles Goodyear in 1839. The very high extensibility and compressive strength together with fatigue, abrasion and corrosion resistant characteristics of the material were the main attractions to the engineers for its application in tires, bearings, seals, shock absorbing bushes, tunnel linings, wind shoes, etc.

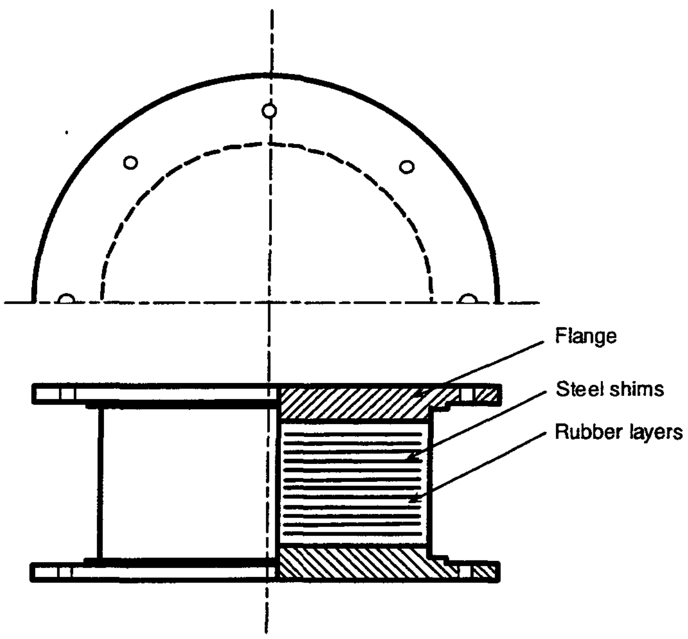

Figure 1.2 Schematic details of high damping rubber bearing

In addition, high damping rubber (HDR) has been developed for specific applications in base isolation bearings to protect structures from earthquakes (Fujita et al 1990; Kelly 1991 and 1997) and vibrations (Castellani et al 1998). The rubber of this kind contains a high proportion of filler (around 31%) and therefore provides better energy absorption property. Figure 1.2 schematically presents the details of a HDR bearing with layers of steel plates. As a requirement of base isolation philosophy, the horizontal layers of steel plates impart a large vertical stiffness in the bearing, while the HDR layers provide a very low horizontal stiffness in the structure subjected to earthquakes or other vibration induced excitations.

In this context, different analytical models were proposed to predict the stability and stiffness of laminated NR bearings at different deformation modes (Lim and Hermann 1987; Hermann et al 1988 and 1989; D'Ambrosio et al 1995). Hwang and Ku (1997) also tried to simulate the responses obtained from HDR bearings using an analytical model. However, these approaches of studying bearing responses were concerned with developing an equivalent homogeneous model for predicting average response of bearings and were not capable of considering the behaviors of rubber and steel as different materials. Hence, the capabilities of these models in predicting local stress and strain conditions that exist between the layers were very limited. To this end, Ali and Abdel-Ghaffar (1995) proposed a finite element model that considered the constitutive behaviors of individual materials through respective constitutive relations and predicted rate-independent response. In a recent study, Dorfmann and Burtscher (2000) studied the development of cavitation damage in HDR bearings through finite-element models. However, these two efforts were concerned with the prediction of rate-independent response and were not considering the strain-rate dependency property.

1.3 GENERAL MECHANICAL BEHAVIOR OF RUBBER

The mechanical behavior of rubbers is dominated by nonlinear rate dependent elastic response (Aklonis et al 1972) and includes other characteristic behaviors like Mullins' effect (Mullins 1947 and 1969) and hysteresis (Gent 1962a,b). Furthermore, incompressibility is an important characteristic feature of this range of materials. All these features are introduced in an illustrated way in the following subsections.

1.3.1 Mullins' effect

The first period of stress-strain curves obtained from cyclic loading test on a virgin specimen differs significantly from the shape of subsequent cycles due to a strain-induced stress softening effect. Mullins (1947) was the first to point out this phenomenon and therefore frequently referred as 'Mullins' effect'. The softening has been attributed to breakdown or slippage of weak linkages between the filler and rubber, filler-filler aggregates and breakdown of molecular network chains. The effect is much more pronounced in the vulcanizates containing high proportion of reinforcing fillers.

Figure 1.3 illustrates an example of typical Mullins' effect exhibited by virgin rubber subjected to a cyclic compression test. In this demonstration, stretches (i.e. 1+dL/L, where L is the undeformed length) were applied in three cycles in each stretch level (Fig. 1.3a). Three maximum stretch levels (namely S1, S2 and S3) were considered. The specimen is initially assumed to be in a reference stress-free virgin state V and loaded in compression to a stretch state S1 along stress- stretch path P1 (Fig. 1.3b).

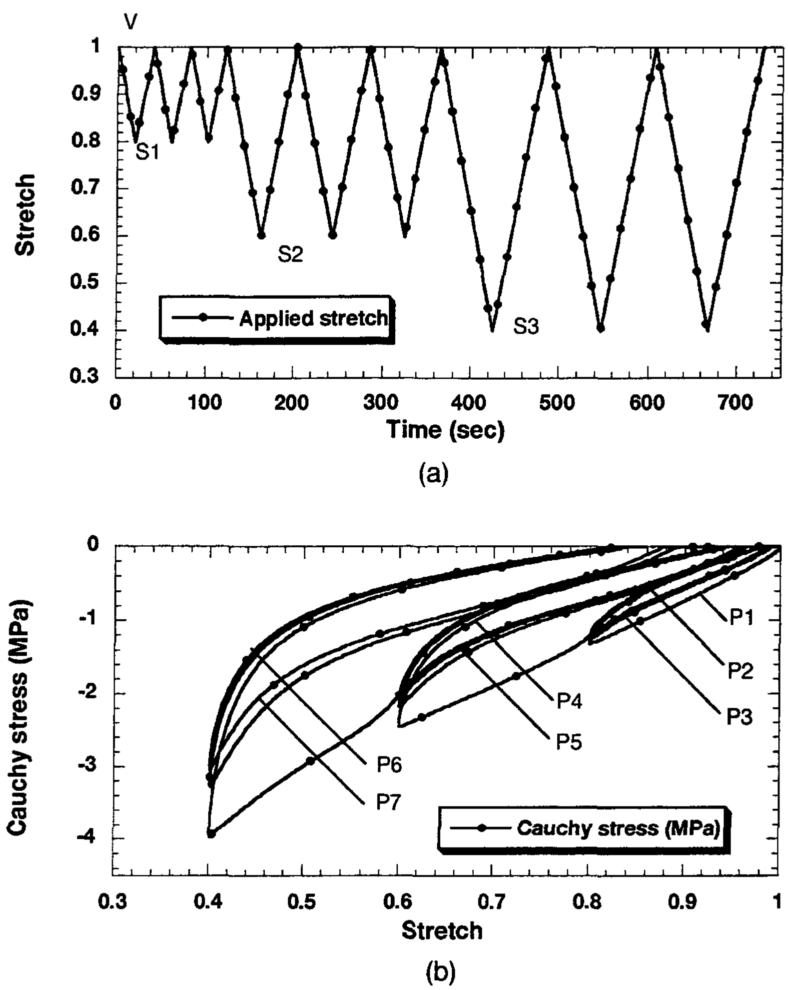

Figure 1.3 A typical example of Mullins' effect observed in virgin rubbers under compression (a) Applied stretch history; (b) Stress-stretch response

At this point, when the specimen is unloaded, it follows path P2 and returns to V. In the second period, when the material is loaded once again up to S1, the stress- stretch response follows P3 path and behaves like a softer material than the virgin one. However, the unloading path remains the same as P2. In the third period, the loading path remains at P3 and unloading path at P2 provided the maximum stretch in loading is kept constant at S1. In a fourth period, when loading is applied up to S2 stretch, the path P3 is followed to reach S1 state, not the P1 path. If additional loading is applied beyond S1, the path P1 is followed again to reach S2 and during unloading, P4 path is followed. In subsequent loading phases up to S2 stretch, P5 path is followed, while in unloading sequence P4 path is maintained indicating a greater loss is material stiffness. In the third maximum stretch level of S3, P1 and P7 loading paths are followed and P6 is maintained for unloading purpose. However, from Fig. 1.3b, the material appears to reach neighborhood of a stable state after the first loading cycle provided the maximum stretch value is maintained constant.

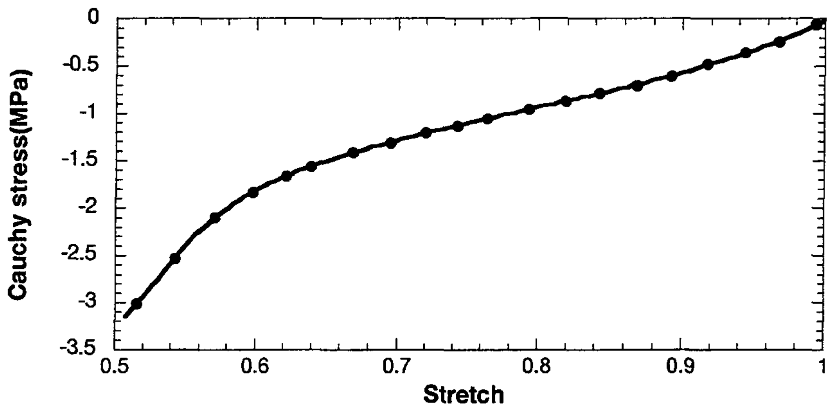

Figure 1.4 A typical nonlinear response obtained from natural rubber under monotonic compression and after removing Mullins' effect

1.3.2 Nonlinearity in monotonic response

Apart from the Mullins' effect present in virgin rubbers, the stress-strain behavior of rubber is recognized to be nonlinearly elastic in its main part. Figure 1.4 presents a typical nonlinear response that one can obtain in a monotonic loading test. The stress-strain response contains three features (Trealor 1944). At the initiation of stretch application, the presence of fillers gives a little bit high stiffness. With increasing applied stretch, the initial stiffness disappears due to the breakdown of rubber-filler bonds. However, at the end, stiffness starts to increase prominently when the free lengths of the molecular network chains (Fig. 1.1) get depleted and the material approaches the ultimate limit of deformability.

1.3.3 Strain-rate dependency

Figure 1.5 presents a schematic representation of typical rate-dependent responses that can be obtained from a viscoelastic solid. When such a solid is loaded at an infinitely slow rate, the stress-strain curve follows the E-E' path. This behavior is called the equilibrium response. On the other hand, in the case of an infinitely fast loading rate, the response takes the I-I' path. Such a response is known as the instantaneous response and defines a domain where viscoelastic effects come into play (Haupt 1993; Gurtin and Herrera 1965). However, in practical experiments, it is quite difficult to apply infinitely fast or slow loading rates to reach these boundaries.

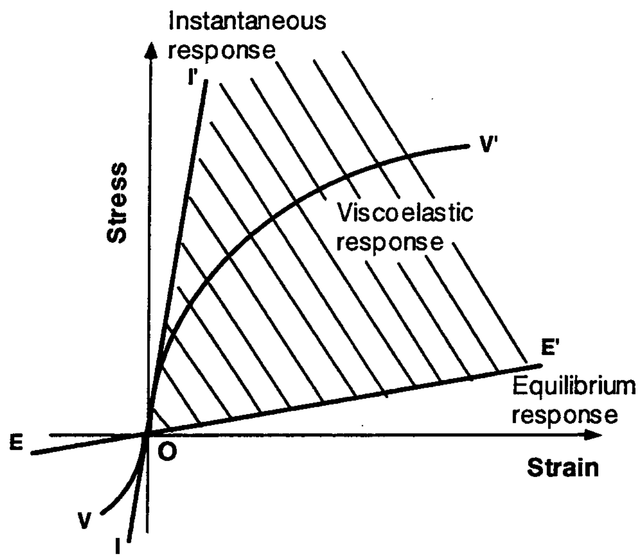

Figure 1.5 A schematic representation of responses obtained from a viscoelastic solid

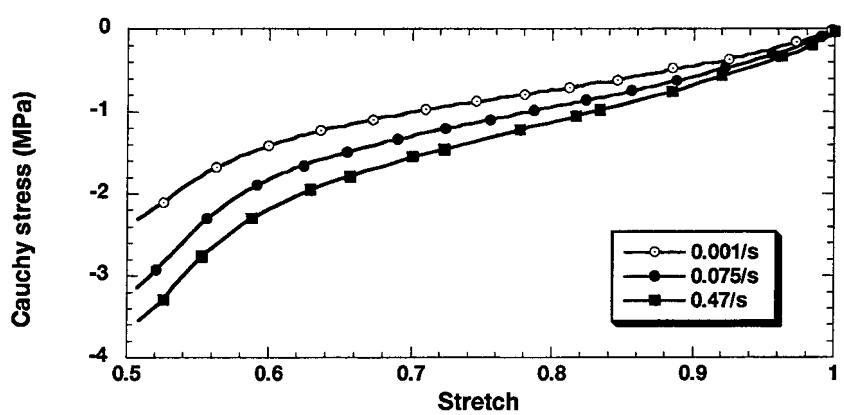

Figure 1.6 Viscoelastic effect exhibited by natural rubber at diffrenet strain rates in monotonic loading under compression

Vulcanized rubber is a typical example of highly viscous solid (Ward 1985), where the stress response is highly dependent on the rate of loading. Figure 1.6 presents some typical rate-dependent response that can be obtained, when rubber is subjected to monotonic compression loading at varied strain rates. The comparison of the curves portrays the presence of strain-rate effect on the stress-strain response.

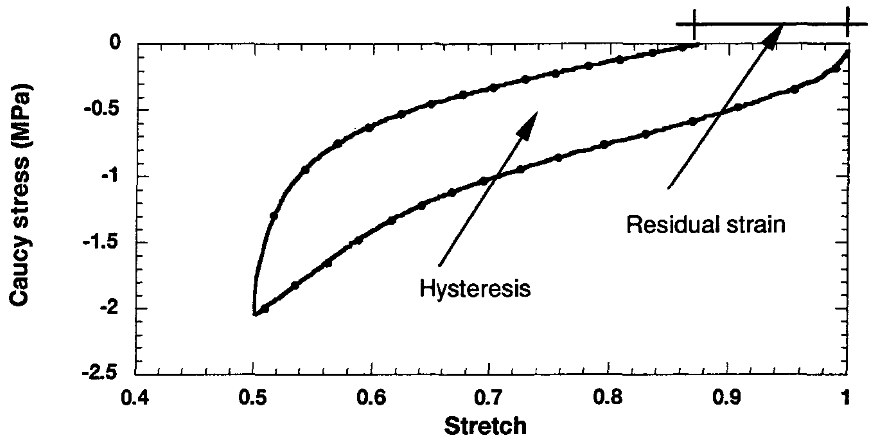

Figure 1.7 Hysteresis and residual strain charactersitics exhibited by natural rubber in cyclic loading under compression

1.3.4 Hysteresis and residual strain

Apart from the strain-rate dependent effects, rubber also exhibits a significant hysteresis phenomenon and residual strain under cyclic loading. Filler concentration plays an important role on these behaviors (Ward 1985). Figure 1.7 illustrates the hysteresis effect and residual strain feature obtained from a rubber specimen subjected to cyclic loading under compression. Here, the term 'residual strain' refers to the 'set' in the specimen at the end of a cyclic test. However, there is an existence of 'healing effect' in the material (Bueche 1961). Due to healing effect, a recovery of molecular damage occurs slowly with time and the material tends to reach the virgin state.

1.3.5 Incompressibility

The resistance of rubber against shear deformation is very low compared to the resistance against volumetric deformation. This gives a very high value of bulk modulus compared to its shear modulus and the material is considered to be incompressible. Under this assumption, the deformed cross-section of the specimen subjected to uniaxial or biaxial deformation can be predicted to calculate the Cauchy (true) stress in the material. However, Herrmann et al (1989) indicated the possibility of the existence of voids in the rubber microstructure that might largely affect the bulk modulus. Yet, no test set-up is reported till now to check the validity of this assumption in a large-strain uniaxial test.

1.4 DEVELOPING A RATE-DEPENDNET CONSTITUIVE MODEL: PRIMARY CONSIDERATIONS

In the past decades, there have been considerable efforts to model, analyze and design structures composed of rubber-like materials using a numerical approach such as finite element methods. Yet, the core of a reliable numerical analysis lies in an adequate constitutive model.

To this end, the large extension feature of rubbers was the prime motivation for the researchers to express the nonlinear elastic behavior through hyperelasticity models (Charlton et al 1993; Boyce and Arruda 2000). In this approach, the rate-independent elastic behavior is expressed in terms of strain energy density functions assuming a complete elastic recovery of strains. Nevertheless, in modeling the nonlinear viscoelastic behavior, a hyperelasticity model is usually combined rate-dependent model structure (Bonet and Wood 1997; Lion 1996 and 1997; Huber and Tsakmakis 2000) to describe the instantaneous and equilibrium responses (Fig. 1.5). In addition, a plasticity/damage modeling approach is needed to account for hysteresis and residual strain effect that appears in rubbers subjected to cyclic loading (Fig. 1.7). Such a model must be developed under the framework of finite deformation kinematics to account for the large strain behavior.

However, in these rate-dependent constitutive models, there must be some parameters to directly express the instantaneous and equilibrium behaviors of the material. These parameters need to be estimated from experimental observations. Yet, due to experimental limitations, it is not possible to apply infinitely fast or slow loading rate on a specimen and obtain the instantaneous and equilibrium response parameters. In such a situation, the published viscoelasticity models either fail to consider these two elastic boundary states or depend on numerical trials to estimate these parameters. Thus the existing constitutive models lose the physical meaning.

1.5 STUDY BACKGROUND

In the preceding sections, the physics, engineering applications, general mechanical behavior and primary considerations for developing a constitutive model for rubbers have been discussed in a summarized way. From the discussion it appears that:

1. The addition of filler and other elements in vulcanization process creates a composite system in the microstructure of rubber. Furthermore, there are possibilities of the presence of voids in the microstructure. Hence the mechanical behavior of a rubber-like material must have a link with its microstructure.

2. In engineering applications, rubbers are used to carry tensile as well as compressive stresses. Hence, the study of rubber mechanics in compression is equally important as that in tension. Furthermore, with a view to developing a constitutive model for newly developed HDR, there is the necessity of having a thorough understanding of its mechanical behavior in terms of nonlinear rate-independent response, strain-rate dependency, hysteresis, residual strain and recovery effects.

3. In testing rubber specimens, incompressibility assumption is employed to predict the deformed cross section of the specimen and thereby to calculate the Cauchy (true) stress. However, any effort to measure the deformed cross section of specimens in large-strain uniaxial testing is yet to appear.

4. The constitutive model for rubbers must be developed under the framework of finite deformation kinematics in order to account for the large strain behavior.

5. In a physically motivated constitutive model developed to represent viscoelastic behavior, there must be an adequate hyperelasticity model in the finite deformation model structure in order to describe the elastic boundary states, namely instantaneous and equilibrium responses. Furthermore, the parameters involved in expressing these responses should be determined from direct experimental observations to retain the physical significance of the model.

1.6 SCOPES AND OBJECTIVES

Based on the background summarized in Section 1.5, the present research was carried out to meet the following objectives:

1. To study the microstructure of NR and HDR through Scanning Electron Microscope (SEM) observation with a view to ascertaining the relation between the microstructure and mechanical behavior.

2. To remove the Mullins' effect from virgin rubbers and thereby to observe the fundamental viscoelastic, hysteresis, residual strain and recovery characteristics of NR and HDR in compression.

3. To check the validity of incompressibility assumption in a large-strain uniaxial test.

4. To develop an adequate hyperelasticity model capable of representing the rate-independent elastic response of NR and HDR in compression.

5. To incorporate the new hyperelasticity relation in a finite deformation rate dependent model structure and to come up with a physically meaningful parameter identification scheme to estimate elastic and viscosity parameters.

6. To verify the adequacy and robustness of the proposed model and parameter identification scheme through numerical simulation of test results.

1.7 CONTENTS OF THE STUDY

The major focus of this research is on studying the fundamental mechanical behavior of NR and HDR in uniaxial compression and to come up with a constitutive model capable of simulating the rate-dependent response of these highly deformable materials.

In this context, Chapter 2 is devoted towards studying the microstructure and mechanical behavior of NR and HDR in compression. A thorough literature review forms the outline of experimental observations carried out on two NR and one HDR specimens of different microstructures. To this end, the microstructures of the specimens in virgin, in-situ tension and after compression loading were compared. An experimental setup capable of measuring the deformed cross-section of specimen subjected to large uniaxial compressive strain at very slow and very fast loading rates has been presented. A preloading sequence was applied on specimens to separate the Mullins' softening effect from other inelastic phenomena. The energy absorption, residual strain and recovery characteristics of each specimen was compared in virgin states and after preloading to quantify the healing effect over the time. In this course, cyclic compression tests at different strain rates and simple relaxation tests at different stretch levels were carried out to observe the viscoelastic effect. On the other hand, cyclic relaxation tests have been carried out to characterize the equilibrium state hysteresis. The experimental scheme was also extended towards tensile regime to compare the viscoelastic effect with that in compressive regime.

Based on the experimental observation made in Chapter 2, a strain energy density function for NR and HDR subjected to uniaxial compression has been developed in Chapter 3. A comparison of the performances of the conventional and proposed relations in representing the elastic compressive response of NR and HDR obtained from slow and fast strain rate tests has been presented.

Chapter 4 reviews the existing finite deformation viscoelasticity models and explains the physical requirements of directly considering instantaneous and equilibrium states of the material in the formulation. Following the review, a finite deformation three component model structure capable of capturing these responses has been introduced. The hyperelasticity model developed in Chapter 3 has been incorporated in this model structure to describe the elastic boundary states of the viscoelasticity response. Some qualitative examples of the resulting model behavior have also been presented.

Chapter 5 addresses the challenges that lie in identifying elasticity and viscosity parameters from explicit experimental observations. In this course, a scheme has been presented to identify the elasticity and viscosity parameters using the proposed model and experimental observations carried out in Chapter 2.

Finally, the Chapter 6 is concerned with the numerical verification of the proposed model and the parameter identification scheme. To do this, numerical experiments were carried out to simulate the monotonic compression response and experimental data were used to verify the adequacy. Efforts have also been made to check the capability of the present model in simulating multi-step relaxation test results. The sensitivity of the change of strain rate in estimating instantaneous response parameters on stress prediction is finally investigated to clarify the importance of an adequate instantaneous response parameter value in stress prediction.

(This page is intentionally left blank)

Chapter 2

Experimental Observation: Microstructure and Mechanical Behavior

2.1 GENERAL

The general mechanical behavior of rubbers mainly concerns with the nonlinear rate dependent elastic response (Aklonis et al 1972). However, other inelastic behaviors like Mullins' effect (Mullins 1969) and hysteresis (Gent 1962) also exist. In addition, rubbers are also believed to fall in the class of incompressible materials. However, all these characteristic behaviors in the material generally originate from its chemical composition and microstructure. In this context, the chapter reviews the experimental efforts made so far for understanding the mechanical behavior and microstructure of rubber. Based on the literature review, the objectives of the present experimental scheme were determined. The scheme comprises of the observations on rubber microstructure through Scanning Electron Microscope (SEM) and mechanical tests in compression as well as in tension regimes. All these aspects are summarized in the subsequent sections.

2.2 LITERATURE REVIEW

The study on the mechanical behavior of rubber dates back to 1940, when Mooney (1940) first attempted to reproduce its large elastic deformation through a strain energy function based on a very limited number of experimental data. However, the theoretical work of Mooney together with immense versatility of the material attracted the contemporary researchers to make considerable experimental efforts. These efforts included the studies on nonlinear monotonic behavior, strain-rate dependency, hysteresis, Mullins' effect and incompressibility as well. Some limited efforts also exist regarding the study of rubber behavior from microstructural viewpoint.

2.2.1 Nonlinearity in monotonic response

Trealor (1944) was the first to report a series of systematic mechanical tests on vulcanized NR and studied the nonlinear responses at different deformation modes including uniaxial tension, biaxial tension and pure shear. The tests were carried out up to 600% tensile strain. These tests revealed the typical nonlinearity of the responses. The evidence for the existence of initial stiffness at low strain level, a large extension at a moderate strain level, and a large-strain hardening feature in the monotonic response in tension became then apparent from these experiments. Even though the experimental setups of Trealor (1944) tests were not so sophisticated like those of the present days, Trealor's work till now provides the baseline data on the nonlinear behavior of rubbers in tension regime. In this connection, the theoretical works of Rivlin and Saunders (1951), Hart-Smith (1966), Alexander (1968), Ogden (1972), Finney and Kumar (1983), Simo and Taylor (1991), Lambert-Diani and Rey (1999), Boyce and Arruda (2000), and Shariff (2000) are examples, where the experimental data of Trealor (1944) were considered as standard reference. Subsequently, the response of rubber under other deformation modes such as flexure, torsion, and shear were also studied by Rivlin (1947, 1948a, 1948b, 1948c, 1949), Rivlin and Saunders (1951) and Rivlin and Thomas (1951) with a view to arriving at a general hyperelasticity theory capable of describing the rubber behavior at all deformation modes. However, all these experimental efforts could not come to a success for characterizing the large extension of rubber until the researchers considered biaxial deformation mode.

James et al (1975) were among the pioneers to obtain biaxial response of NR tested in a biaxial testing device capable of giving a homogeneous deformation by overcoming the boundary effects. They also investigated the applicability of higher order terms of Mooney (1940) and Rivlin (1948) hyperelasticity model through their testing data. To make a similar re-evaluation of the original Mooney-Rivlin model, Fukahori and Seki (1992) investigated the NR under strip-biaxial deformation mode, where deformation in one direction can be kept constant. The necessity of this type of deformation modes was also evaluated by Kawabata and Kawai (1977) and Kawabata et al (1981) to arrive at a general hyperelasticity relation. Finally, Yamashita and Kawabata (1992) reached a general hyperelasticity relation using this testing technique.

In contrast to all these tension regime investigations, Bogert (1991); Bogert and Borst (1994) studied the behavior of NR under the combined action of compression and shear. In a different move, Plumtree and Cheng (1998) made a limited study on the fatigue behavior of NR under cyclic uniaxial compression.

Apart from all these efforts made on NR, the investigation on HDR is very rare. In this context, the preliminary observations of Hernandez (1998) can be referred to, where nonlinearity stronger than the NR was observed in tension regime. A similar observation was also reported in the work of Dorfmann and Burtscher (2000) who investigated the HDR in uniaxial tension and pure shear deformation modes.

2.2.2 Strain-rate dependency and hysteresis

The effect of strain rate on the response of rubber was first known quantitatively through the works of Greensmith (1960), Dannis (1962). In the works, the effect of applied strain rate on the tensile strength was studied in the strain rate range of 0.001/s to 20/s. They reported the existence of a directly proportional relationship between the applied strain rate and the tensile strength at temperatures of 25^{o}C and 90^{o}C. In a contemporary study, Mason (1960) studied the effect of carbon black filler on the strain-rate dependency property.

Subsequently, the work of Gent (1962a,b) revealed the stress relaxation, creep, and hysteresis properties of rubber vulcanizates and their temperature dependency. Gent noted the presence of significant viscosity in his specimens that displayed the major fraction of stress relaxation feature within first two seconds. However, his experimental arrangements did not allow him to make measurements in time intervals less than 6 sec. Due to this reason, the stress relaxation history in the first 6 sec of the tests remained ill-defined.

However, the advent and use of modern high-speed digital computers in data acquisition system has currently solved the problem. Lion (1996, 1997) conducted uniaxial tension and compression tests on NR to study the strain rate dependency and hysteresis property. In the study, specimens were subjected to 100% tensile and 30% compressive strains at a monotonic rate of 0.0002/s to 0.2/s. Furthermore, cyclic relaxation tests with multiple relaxation intervals were also carried out to identify the equilibrium hysteresis.

In a contemporary study, Bergstrom and Boyce (1998) studied the NR behavior in cyclic compression at strain rates from 0.001/s to 0.2/s on specimens with different filler contents and crosslink densities. A directly proportional relation between the filler content and hysteresis was revealed through this investigation. However, normalized hysteresis (dissipated energy during unloading/supplied energy during loading) was found to be independent of filler content. In addition, for a particular filler content, stiffness of rubber was found to increase with increasing crosslink density. Cyclic relaxation tests with multiple relaxation intervals were also carried out to observe the rate dependency along with equilibrium state hysteresis. A similar investigation on NR was also carried out in the tension and compression regimes by Miehe and Keck (2000). Furthermore, Kar and Bhowmick (2000) studied the loss of hysteresis due to cyclic loading in pure shear and constrained extension.

However, none of these efforts reported any inference on the characterization of strain-rate dependency and hysteresis property of HDR either in a tension or in a compression regime.

2.2.3 Mullins' effect

Virgin rubbers exhibit a characteristic stress softening effect on its first loading cycle (Section 1.3.1). Mullins (1947, 1950 and 1969) first noticed this phenomenon. Subsequently, Mullins and Tobin (1956) characterized that the phenomenon is dependent on the maximum level of strain applied in its loading history. In this course, Bueche (1960a and 1961) worked further and reported the healing of the stress softening over the time. A molecular basis of the mechanical degradation of virgin rubbers through the softening effect was given (Bueche 1960b). Also, Mullins and Tobin (1965), Harwood et al (1965 and 1966) and Mullins (1969) put further efforts and confirmed that filler particles do have a significant role on the appearance of such phenomenon. They proposed a strain amplification factor (a function of filler concentration) to describe the appearance of this effect in filled and gum vulcanizates. It was also revealed therein that the stress softening appears at a molecular level through the breakage of chains, breakage of chain linkages to filler particles, or slippage of chains on the filler particle surface. Afterwards, this stress softening effect was named after Leonard Mullins as "Mullins effect" to recognize his significant contribution in this subject (Mullins 1987).

Later on, Govindjee and Simo (1991, 1992a and 1992b) and Govindjee (1991) formulated a constitutive relation based on micromechanics to describe Mullins' effect following the formulation of Simo (1987). In an another effort, Johnson and Beatty (1993a,b) performed stress controlled tests to observe the effect and then proposed a theory from the phenomenological standpoint and also studied the influence of the Mullins' effect on transverse vibration of a rubber string. Furthermore, the strain amplification concept presented by Mullins and Tobin (1965) was also re-evaluated by Govindjee (1996) through Monte Carlo simulation. In a recent work, Krishnaswamy and Beatty (2000) studied the effect considering the compressibility and proposed a general stress softening theory based on a two-phase microstructural damage model.

2.2.4 Microstructural consideration

Natural gum rubber is derived from natural sources and it falls in the class of polymeric materials (Section 1.1). However, such a rubber is unsuitable for engineering applications and it needs vulcanization treatment. During the treatment, carbon black particles are added as filler together with some sulfur and other elements to create crosslinking bonds within the molecular chains of the polymer. Such a treatment changes the rubber microstructure and increases the stiffness, hysteresis, fatigue and strain-rate dependency properties in the material (Meinecke and Taftaf 1987; Hamed and Hatfield 1988; Wischt 1998). Hence, the study in regard to the rubber microstructure and the relation between the microstructure and mechanical properties was considered in the past.

The work of Mullins and Tobin (1956) can be referred to, where electron microscope replica of rubber containing carbon black was considered to describe the origin of Mullins' softening effect.

In a later study, Cornwell and Schapery (1975) studied the fracture of solid propellant (a kind of particulate filled polymeric materials) in tension through SEM. In the study, the role of voids in the fracture process was clarified through SEM observation. In addition, Hermann et al (1989) pointed out the possibility of the effect microstructural voids on incompressibility property.

Kilian et al (1994) also considered SEM observations to explain the effect of filler on the stress-strain pattern of different filler loaded NRs. The study revealed a direct effect of filler concentration on stiffness and hysteresis properties.

Wang et al (1997) characterized the microscopic surface of polyaniline-based rubbers by using SEM and an electron-probe X-ray microanalyzer technique. Also, Liu et al, (1998) considered the effect of rubber-filler particle size distribution on the toughness mechanism of rubber blends.

Recently, Bergstrom and Boyce (2000a,b) employed Transmission Electron Microscopy (TEM) to arrive at a micromechanics based large strain time-dependent constitutive relation that considered the interaction between the NR and filler network structure. However, in the work of Bergstrom and Boyce, no void was present in their specimen. Accordingly no attention was paid to discuss the strain-rate dependency effect in terms of microstructural voids.

2.2.5 Poisson's ratio and incompressibility

The bulk modulus of a solid rubber is usually very large and it is larger than that of several orders of the shear modulus. The rubber is therefore called an incompressible material. Due to this feature, the Poisson's ratio (a function of bulk and shear moduli) takes a value very close to 0.5. In measuring the Poisson's ratio, although the measurement of shear modulus of a rubber specimen can be done using a standard dumbbell specimen in tension (ASTM Standard D 412 98a) or a cubic/cylindrical specimen in compression (ASTM Standard D 395 98), the measurement of bulk modulus brings a great difficulty. This is mostly due to the very little change in volume that is experienced in isotropic compression. Yet, when analyzing the rubber parts subjected to small deformations, a reliable value of Poisson's ratio is the vital information needed in a finite element technique.

To address this problem, Kugler et al (1989) used a direct optical measurement technique to measure the lateral strain and Poisson's ratio in tension experiments. Later on, Fishman and Machmer (1994) devised fluid displacement volume change measurement system and load ram displacement for the measurement of volume change. In another effort, Migwi et al (1994) used thermal mechanical analysis measurement equipment to measure the shear modulus and the Poisson's ratio and also studied the effect of temperature on these parameters. Peng et al (1994) proposed an inexpensive testing method, where a rubber disk can be tested in a fully confined condition achieved by using a metal jacket. Nevertheless, it should be mentioned here that the major motivation for proposing these experimental methods was to measure the Poisson's ratio that is only meaningful in small strain cases.

In contrast to this, in a large deformation test, the deformed cross section of the specimen needs to be measured to calculate the true stress in the specimen. However, due to large deformation (in the range of over 50% strain), the conventional strain gauges cannot measure the strains. This indicates the necessity of an optical measurement on a plane perpendicular to where the displacement is applied. In optical measurement techniques, another problem arises due to the significant shift of the measurement plane on account of the very large applied displacement. In such a situation, the only solution that remains is to consider the incompressibility assumption and predict the deformed cross sectional area from the applied displacement (Peeters and Kussner 1999). On the contrary, the review of rubber microstructure (Section 2.2.4) has indicated some cases where voids can remain present and therefore the validity of incompressibility assumption can be put into question. However, no work is reported until now for a direct approach of measuring the deformed cross section of a specimen subjected to large deformation.

2.3 OUTLINE OF EXPERIMENTAL OBSERVATION

The literatures cited in the Section 2.2 indicated a lacking in the studies on the NR mechanics in compression regime. On the other hand, few preliminary efforts were recorded on HDR that mainly concentrated on its nonlinear monotonic response. Yet, no information is available on the strain-rate dependency and hysteresis properties of this kind of rubbers.

In addition, the cited literatures also indicated the possibilities of variation in microstructure that might include voids. Such microstructural variation is likely to have some definite role on the mechanical behavior. Traditionally, rubber is assumed to be incompressible material and Cauchy stress (true stress) in a rubber specimen can be obtained directly. However, the possibility of the existence of voids in microstructure leaves questions on the validity of incompressibility assumption.

In this context, the present work was undertaken to make qualitative and quantitative studies on the microstructure of NR and HDR specimens in virgin state, states after loading and in-situ loading state as well using SEM. Efforts were also made to ascertain a relation between the microstructure and the mechanical behavior. In this course, an experimental set up was devised to measure the deformed cross section of the specimens in large strain experiments and thereby to check the validity of incompressibility assumption used for calculating the Cauchy stress. The set up was used to study the fundamental strain-rate dependency and hysteresis behavior of the specimens subjected to homogeneous compressive deformation. The experiments comprised of cyclic compression tests, simple relaxation tests and cyclic relaxation tests. To separate the Mullins' effect from other inelastic effects, a preloading sequence was applied on each specimen prior to the actual test. The energy absorption and residual strain characteristics of each specimen during and after preloading were also studied and compared. Some parts of these experimental efforts are also available in Amin et al (2001a,b,c) and Alam et al (2000). Furthermore, in order to have a comparative study on the strain-rate dependency and hysteresis behavior of NR and HDR in the tension regime, an identical experiment was also carried out in tension. The details of the experiments and the inferences observed thereon are described in the following paragraphs.

2.4 SPECIMENS

Two different types of NR and one HDR were investigated in the present study. The details of the specimens are presented in Table 2.1.

Table: 2.1 Details of the specimens

	SPECIMEN DESIGNATION		
	NR-I	NR-II	HDR
Type	NR	NR	HDR
Application	General purpose	Bridge bearing	Bridge bearing
Manufacturer	Shinoda Rubber Co.	Yokohama Rubber Co.	Yokohama Rubber Co.
Strength	4.0 MPa*	0.98 MPa**	0.78 MPa**
MECHANICAL TESTS IN COMPRESSION			
Shape	Cubic	Cylindrical	Cylindrical
Size	H:50mm, L:50mm, W:50mm	H:41 mm, D:49 mm	H:41 mm, D:49 mm
MECHANICAL TESTS IN TENSION			
Shape	—	Sheet	Sheet
Size	—	L:40mm, W:9.5mm, T: 2mm	L:40mm, W:9.5mm, T: 2mm

H: Height, L: Length, W: Width, D: Diameter, T: Thickness. * Tensile strength, ** Shear modulus tested according to JIS K 6301

2.5 MICROSTRUCTURAL OBSERVATION

The SEM observations were recorded with computer controlled JEOL JSM 5600LV SEM machine. Specially prepared samples of the specimens were placed in the SEM chamber after preliminary treatment. The SEM formed an image by moving a beam of electrons across the sample and reading the scattered electrons from the specimen. The image was viewed on a monitor and the image data was captured as bitmap image. The details of the preparation of the sample and the observation are summarized in the following subsections.

2.5.1 Preparation of samples

Sizable samples were prepared for placing and observing in the SEM chamber. Specimens of approximately 1.5 mm thickness were prepared with side dimensions of 2-3 mm x 4-10 mm. A very sharp cutting edge and the same cutting method were used for all specimens. In order to avoid the edge effect on the microstructure, representative samples were cut from different locations (Fig. 2.1) for each specimen and comparative observations were made.

Samples of the investigation in SEM were coated with a conductor as per procedural need to ensure an electron-conducting path for the electron beam. In the present study, a gold-palladium coating was applied by using a vacuum evaporator JEOL JFC 1200 fine coater operated at a pressure of 8 Pa for 45 sec.

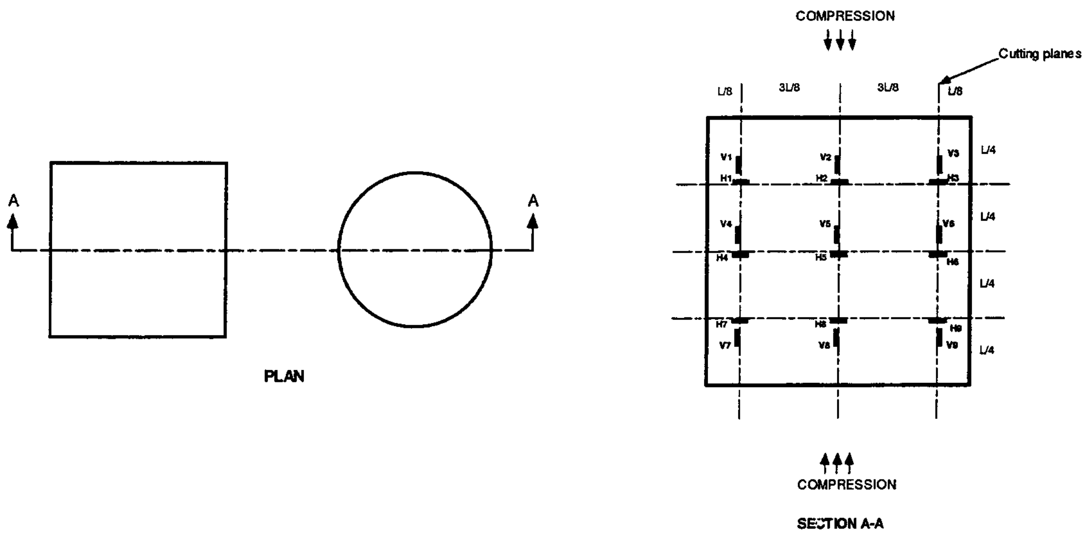

Figure 2.1 Sample collection locations for SEM Observation

2.5.2 Observations

The SEM observations were done on virgin specimens, tested specimens, and in-situ tensile specimens. In-situ tension observations were done at 20% and 40% strain levels. However, due to experimental limitations, observation on in-situ compression was not performed.

Figure 2.2 presents the photomicrographs of NR-I, NR-II, and HDR at virgin state. The figure shows a void dominated microstructure of NR-I in contrast to the NR-II and HDR, where the occurrence of voids is rare. The typical microstructural deformation pattern of NR-I observed for 24 hours after the mechanical testing in compression is

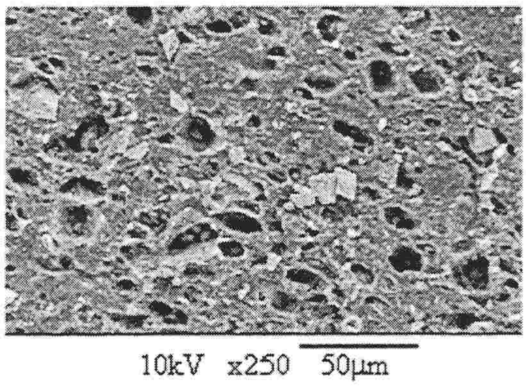

(a)

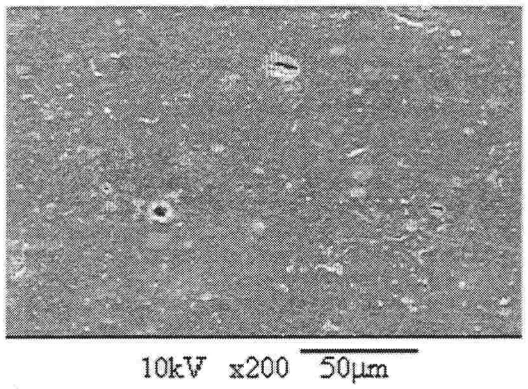

(b)

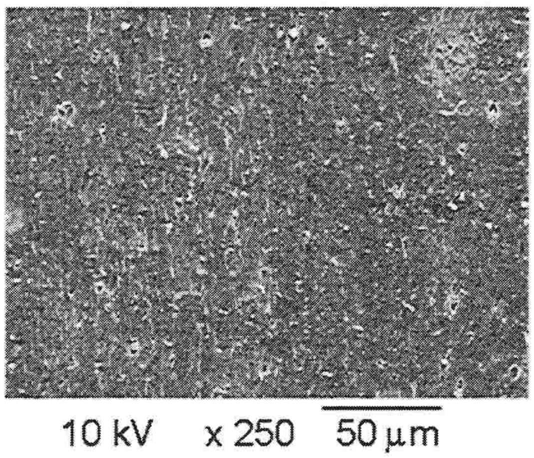

(c)

Figure 2.2. SEM Micro-graphs of (a) NR-I; (b) NR-II; (c) HDR observed at virgin state

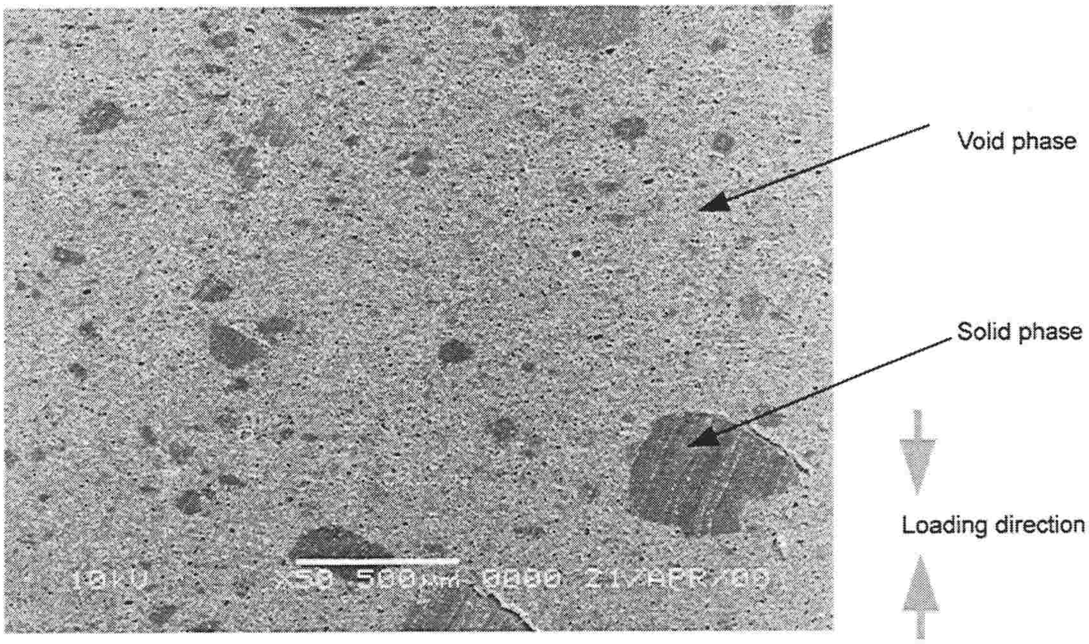

(a)

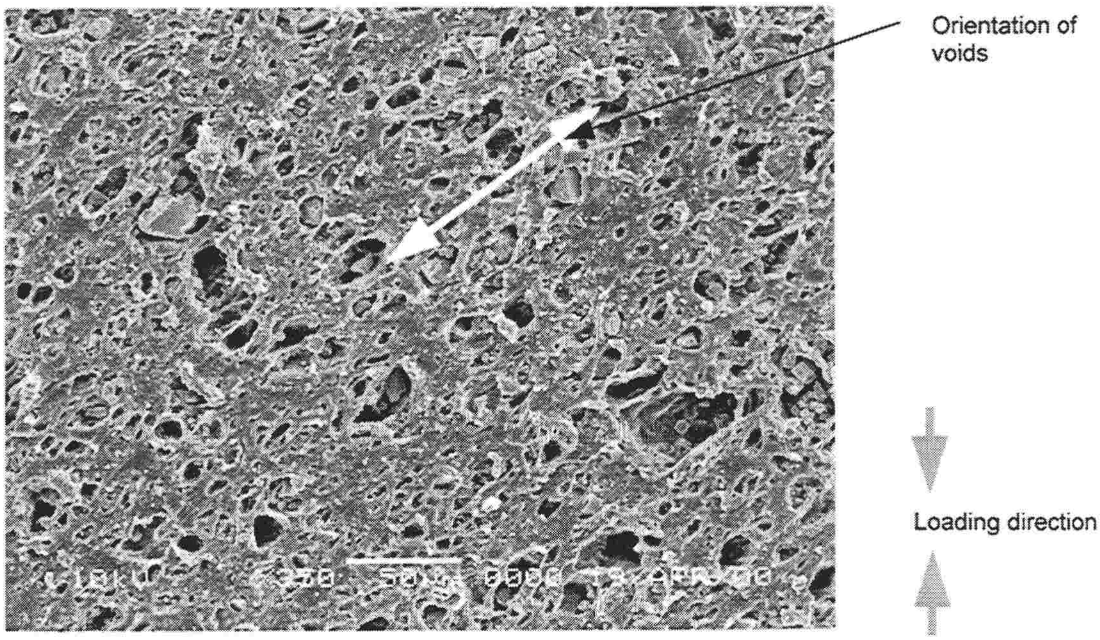

(b)

Figure 2.3 Orientation of voids in NR-I after compressive loading
(a) x50 magnification; (b) x350 magnification observation

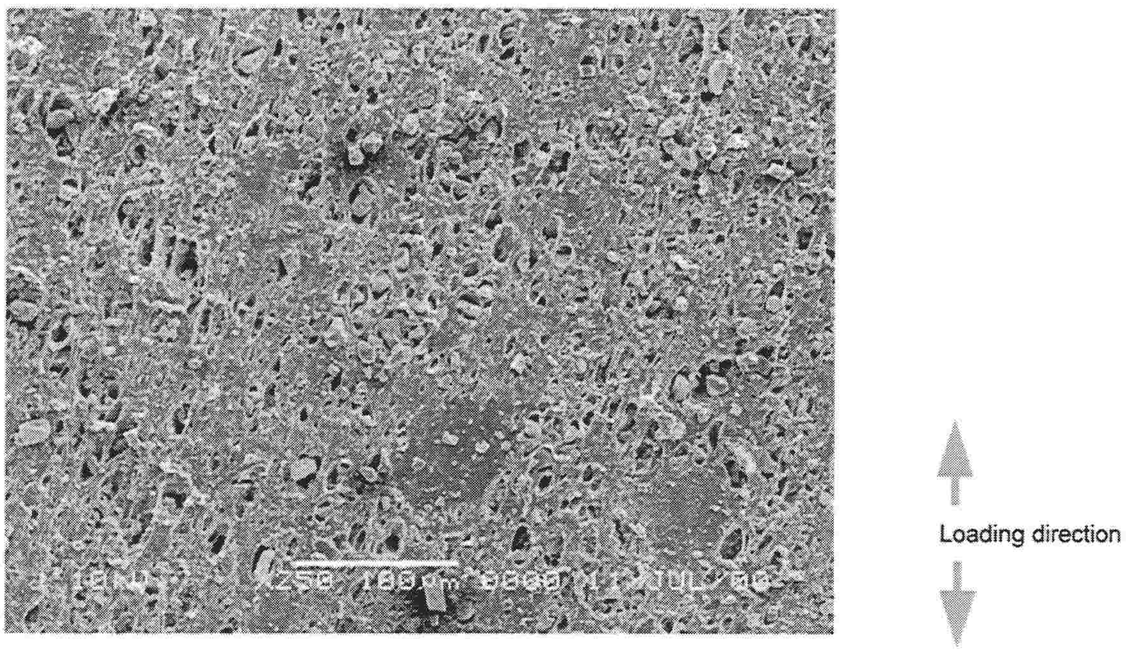

(a)

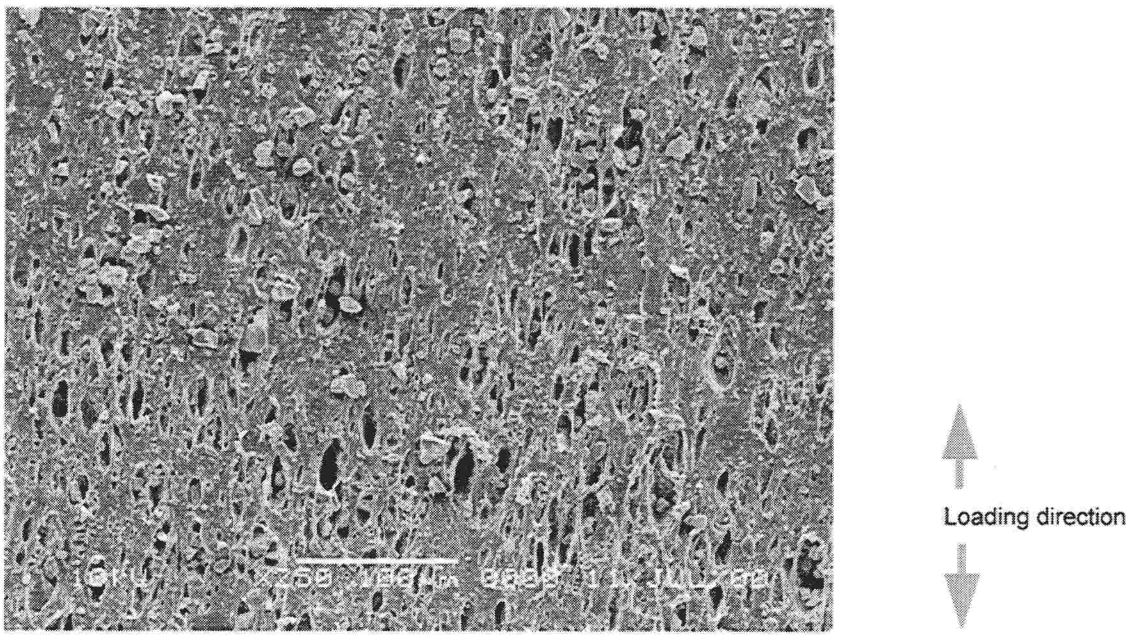

(b)

Figure 2.4 Orientation of voids in NR-I observed during in-situ tension loading
(a) 20% strain; (b) 40% strain

presented (Figure 2.3). The low magnification observation (Fig. 2.3a) illustrates the presence of solid rubber particles surrounded by voided area. Upon compression, the solid rubber particles generally act with the voids and cause an anisotropic deformation pattern in the voids. As a result, the voids take elliptical shapes with an inclined orientation. However, the samples tested in-situ tension loading condition did not show such an anisotropic feature (Fig. 2.4) and the voids were oriented along the stretching direction.

2.5.3 Void area measurement

The observations (presented in Section 2.5.3) revealed the void dominated microstructure of NR-I in a qualitative way. In this section, the SEM images were further analyzed to obtain some quantitative information on the voids of NR-I and its change due to mechanical loading.

Table 2.2 Measured void area ratios in NR-I

SPECIMENS	VOID AREA RATIO (%)
Virgin	15.7 ±0.7
Cyclic relaxation (0.15 strain)	13.6 ±1.4
Cyclic relaxation (0.45 strain)	16.8 ±1.2
Monotonic compression (0.5 strain, 1 cycle)	18.0 ±0.9
Monotonic compression (0.5 strain, 5 cycle)	17.8 ±1.5
In-situ tension (0.2 strain)	16.1 ±0.7
In-situ tension (0.4 strain)	14.2 ±1.0

To do this, the samples were observed in different magnifications so that the precise measurements of voids could be done. Comparative void measurement was done on virgin specimens, loaded specimens and in-situ tension specimens using an image processing and analysis program (Scion Image 2000). At first the SEM photographs were coloured in black and white for voids and solid parts respectively. It was done manually. Then the coloured photographs were scanned to measure the void area using image analysis technique (Scion Image 2000). In order to check the accuracy and to get the average results, the measurement was done twice by two different persons. The variations observed between the two measurements were found within 3%. The comparative voids measured from the SEM photographs are listed (Table 2.2). The void areas in virgin, during in-situ tension loading and after compression loading conditions appear to be well comparable. This observation is also an indication of material incompressibility.

2.6 MECHANICAL TEST IN COMPRESSION

2.6.1 Experimental setup

A schematic detail of the experimental set-up is presented in Fig. 2.5. The specimens were tested in a computer-controlled servo-hydraulic testing machine by using Shimadzu servo-pulser 4800 at room temperature. Displacement controlled tests in compression were carried out. The displacement was applied along the vertical axis and the corresponding force was measured by a load cell in the testing machine. All data were recorded using a personal computer. In order to cut the friction between a sample and the loading plates and thereby to ensure a homogeneous deformation in the specimen, polypropylene films with lubricant on the top and at the bottom of the sample were used. Figure 2.6 illustrates the deformation homogeneity of a specimen that was ensured at about 50% compressive strain level.

In general, rubbers are assumed to be incompressible materials. The Cauchy stress (true stress) can therefore be readily calculated from this assumption (Peeters and Kussner 1999). However, SEM observations of the specimens of the present investigation (Section 2.5) indicated the presence of micro-voids. Hence to make certain the validity of the assumption, the lateral displacement of the specimens was measured. A laser transducer (Ono Sokki LD-1110M-020) was used to measure the mid-height lateral displacement of the specimen surface. Due to a very large applied vertical displacement (resulting up to 50% compressive strain), the midpoint of the specimen surface on deformation practically shifts significantly in the vertical plane from its initial position. To overcome this problem and to catch the midpoint of the deformed specimen in the vertical plane, a special type of jig using a boom device

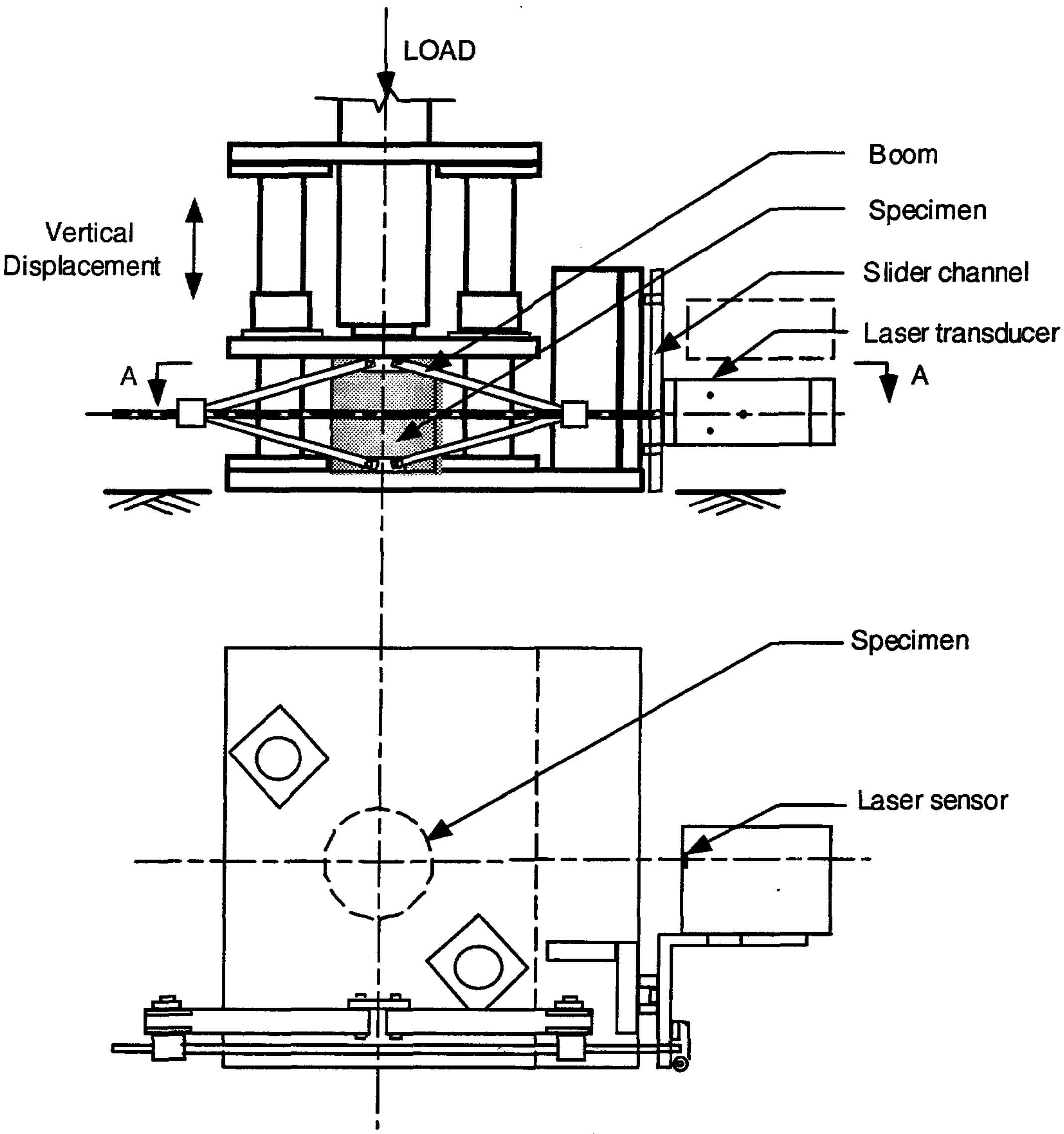

Figure 2.5. Experimental set-up. (a) Elevation; (b) Section A-A.

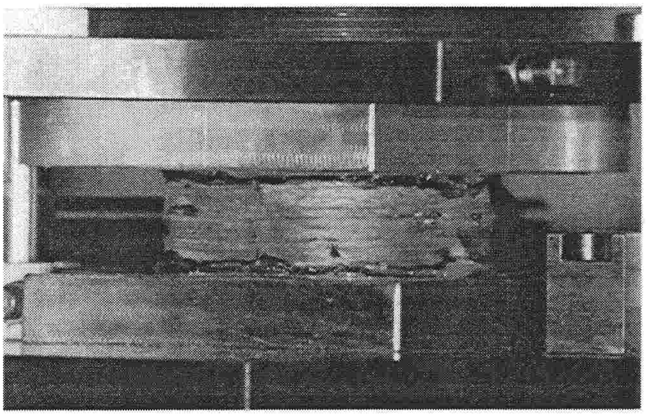

Figure 2.6 Deformation homogeneity of HDR attained at 50% compressive strain.

(Figs. 2.5 and 2.7) was used to move the laser transducer at a rate synchronized with the applied displacement rate. Figure 2.8 presents the measured Cauchy stress vs. applied stretch (i.e. 1+dL/L, where L is the undeformed length) response in comparison to that obtained by using the incompressibility assumption in NR-I. Although a little difference between the measured stress appears at a higher stretch level between the measured and calculated Cauchy stress, the lateral displacement measurement indicates a good reasoning for using the incompressibility assumption. In this situation, the applied stretch and the Cauchy stress of each test were calculated under the assumptions of homogeneous deformation and incompressibility of the specimens.

2.6.2 Preloading

Virgin rubber typically exhibits a softening phenomenon, known as Mullins' effect (Section 2.2.3) in its first loading cycle. This characteristic effect was found to be present in all the specimens at the virgin state. In order to remove the Mullins' effect from other inelastic behavior as well as to obtain a stable material state, all virgin specimens were subjected to a specified pre-loading sequence prior to the actual experiment. In the pre-loading, each virgin specimen was subjected to cyclic uniaxial compressive loading for 5 cycles with a strain rate of 0.01/s.

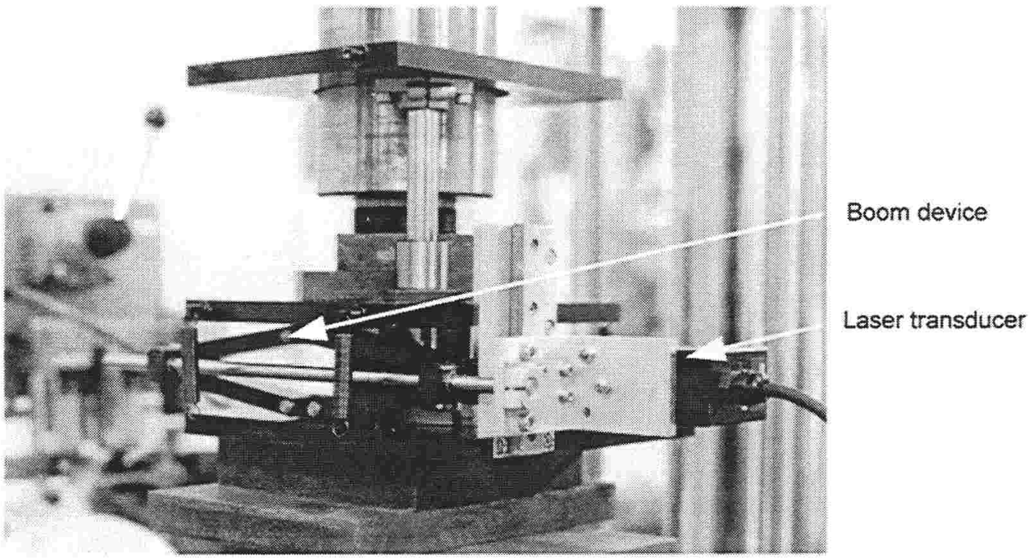

(a)

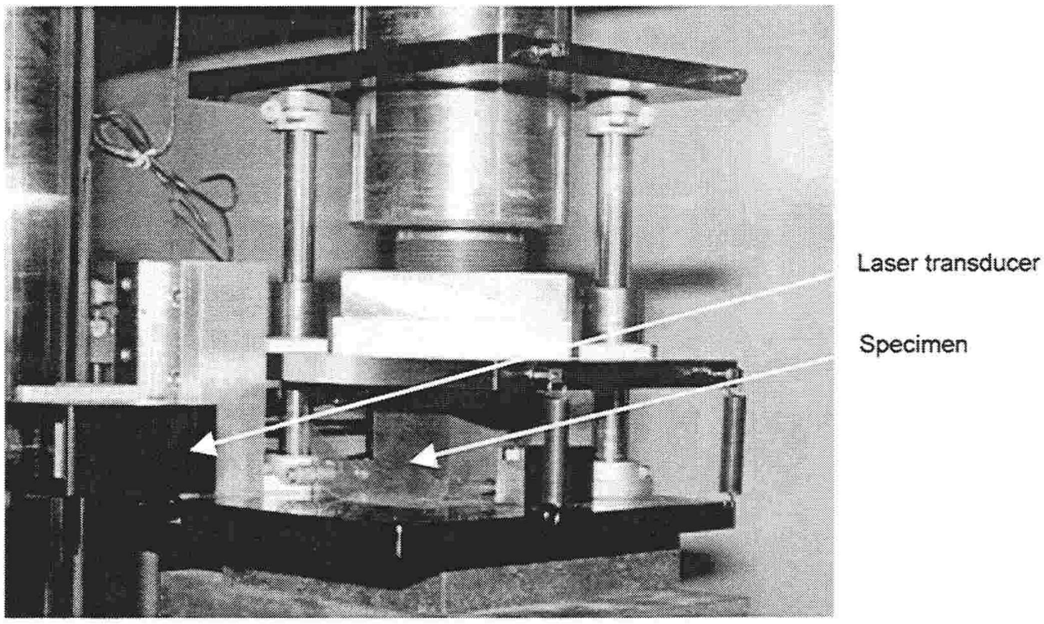

(b)

Figure 2.7 Measurement of lateral displacement using laser transducer and boom
(a) Left-side view; (b) Right-side view

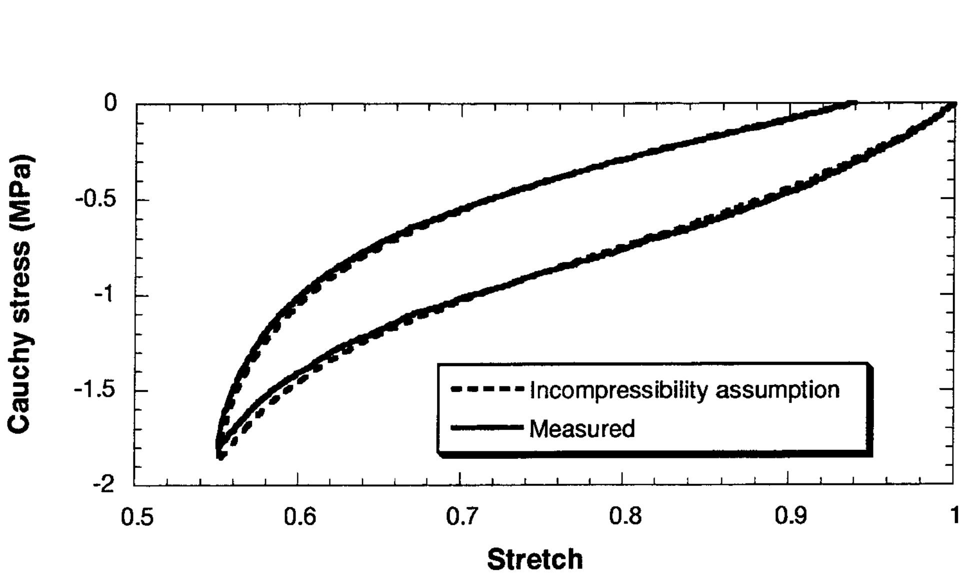

Figure 2.8. Verification of incompressibility assumption through lateral displacement measurement in NR-I.

Figures 2.9 to 2.11 present the typical stress-stretch responses obtained from preloading tests on NR-I, NR-II, and HDR. The softening behavior in the first loading cycle is evident from the figure. In NR-I and HDR, the softening behavior is more pronounced than that of NR-II. All the specimens showed a repeatable stress-stretch response after passing through 2-3 loading cycles indicating the removal of the effect. Apart from the Mullins' effect, the typical strain-hardening feature of virgin rubbers at higher strain levels is more visible in NR-I and HDR than that in NR-II.

Furthermore, the amounts of energy absorption and residual strain in each type of specimens subjected to preloading were compared (Fig. 2.12a and Fig. 2.13a). Figures 2.12a and 2.13a indicate a higher amount of energy absorption and residual strain in the first cycle than that of the subsequent cycles. This feature is considered to be related with the breakage of rubber-filler bonds in virgin specimens. However, in the later cycles, the energy absorption and residual strain values approach a constant value for each specimen. In addition, as a consequence of the presence of microstructural voids, NR-I showed higher energy absorption and residual strain than those of NR-II. Furthermore, when compared between the NRs and HDR, the higher filler content of HDR might be the factor behind the higher energy absorption and residual strain effect in HDR than those of NR.

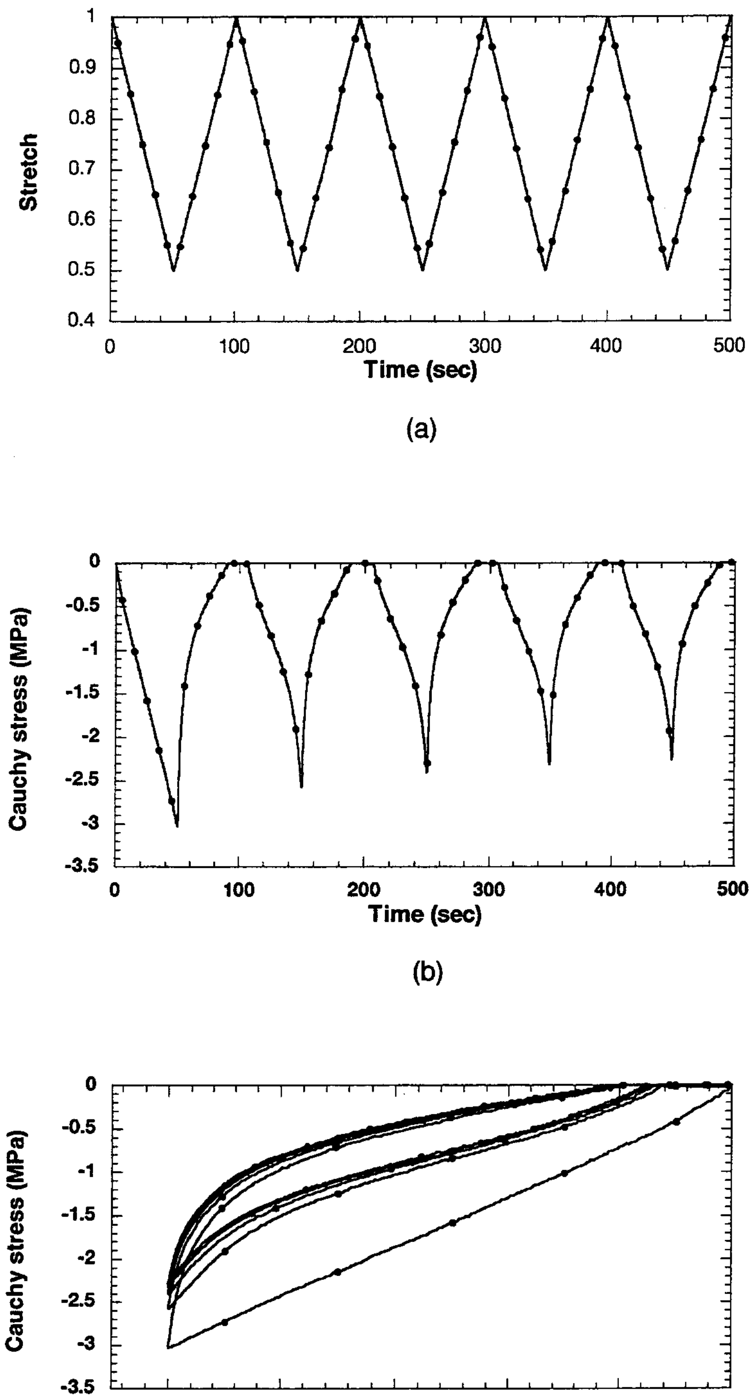

(a)

(b)

(c)

Figure 2.9 5-cycle preloading test on virgin NR-I to remove Mullins effect
(a) Applied stretch history, (b) Stress history, (c) Stretch-stress response

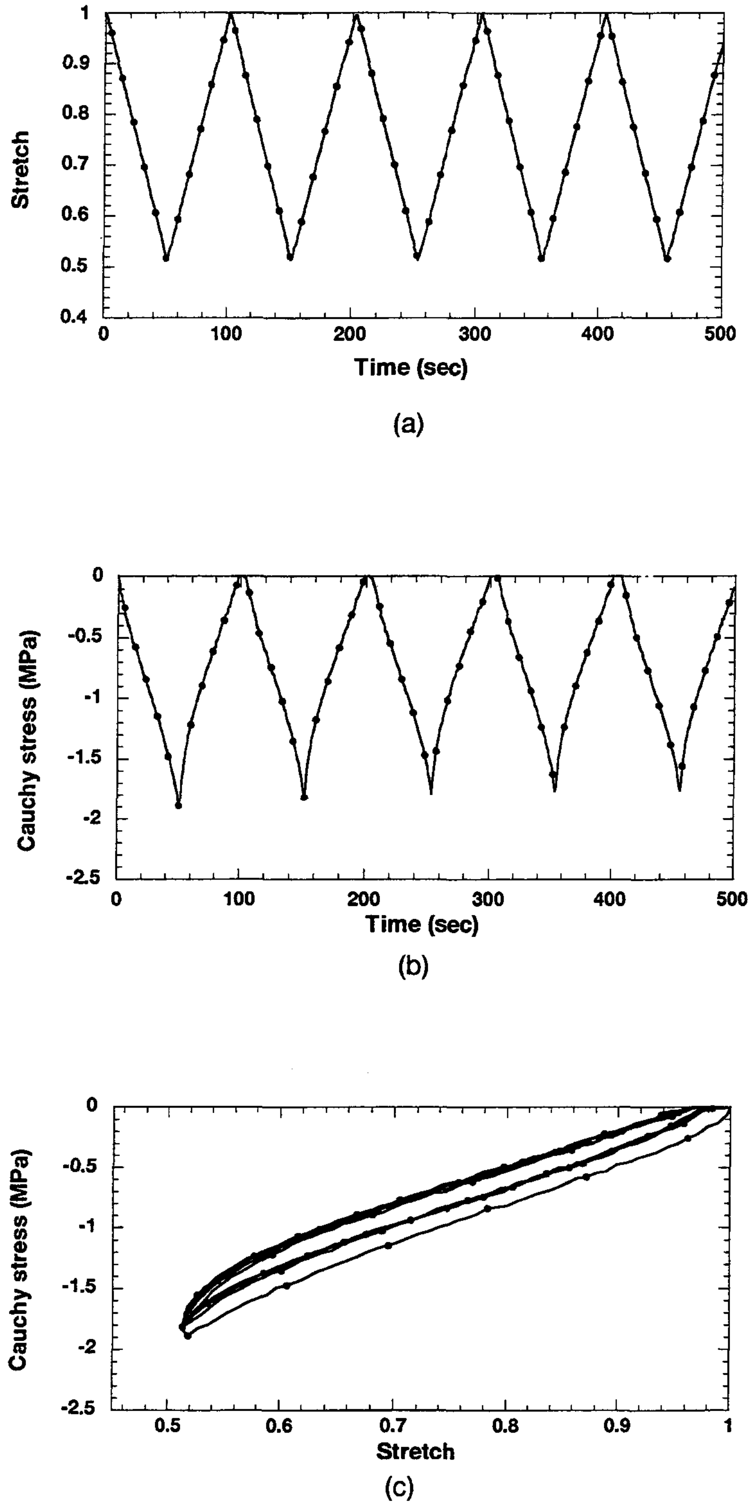

Figure 2.10 5-cycle preloading test on virgin NR-II to remove Mullins effect
(a) Applied stretch history, (b) Stress history, (c) Stretch-stress response

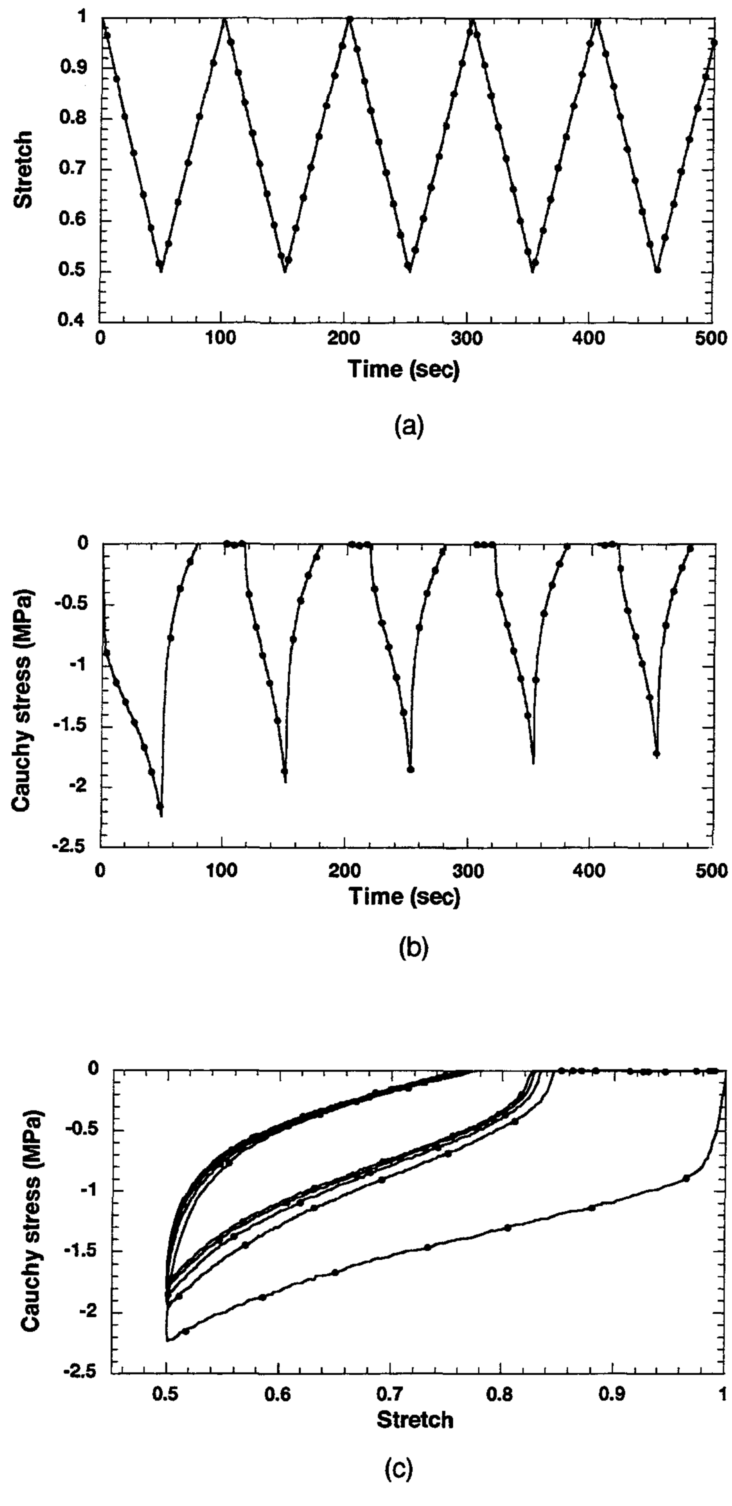

Figure 2.11 5-cycle preloading test on virgin HDR to remove Mullins effect
(a) Applied stretch history, (b) Stress history, (c) Stretch-stress response

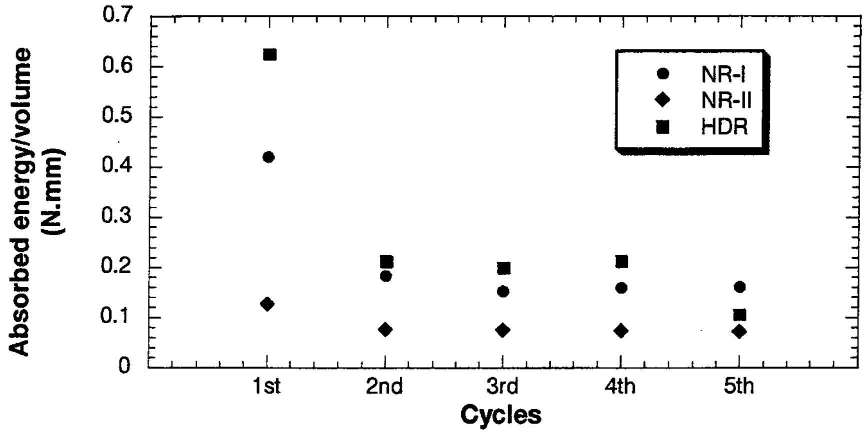

(a)

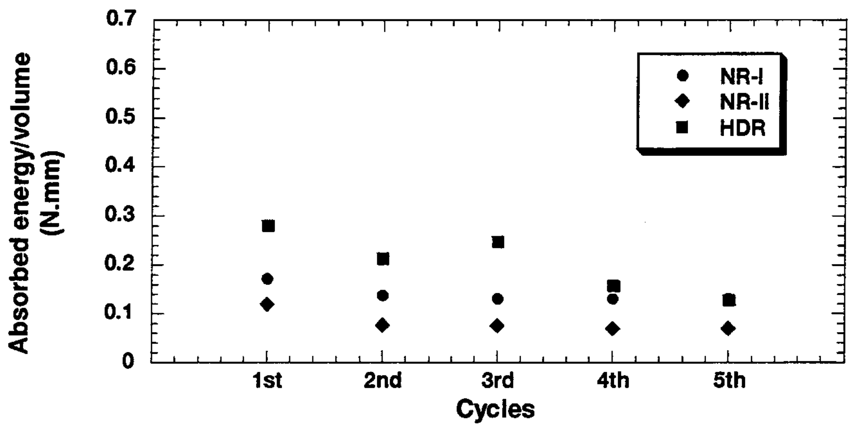

(b)

Figure 2.12 Comparative energy absorption characteristics in each cycle of NR-I, NR-II and HDR in cyclic compression loading (a) virgin specimen, (b) in a specimen preloaded 20 min before the cyclic compression test

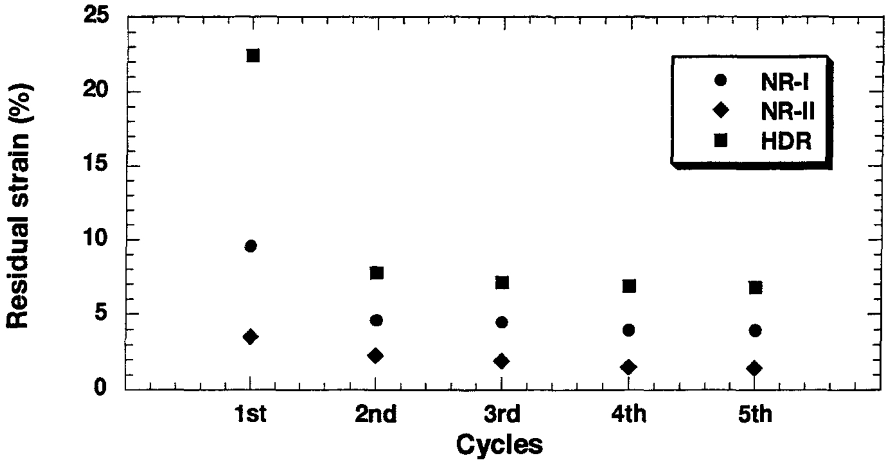

(a)

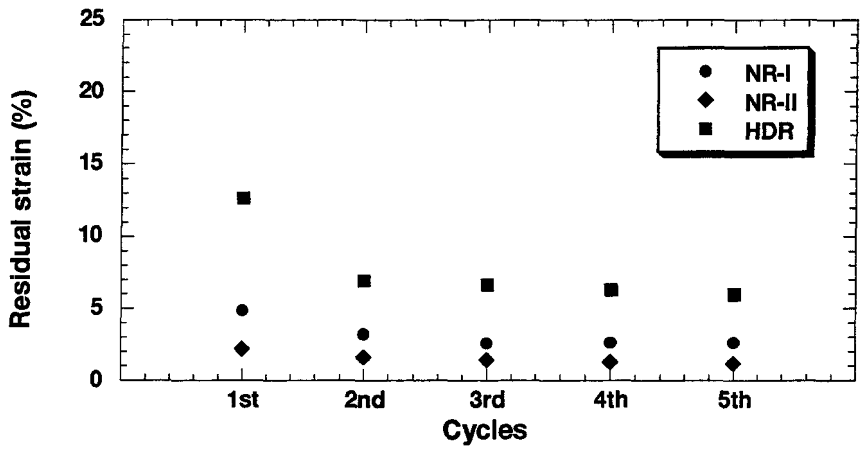

(b)

Figure 2.13 Comparative residual strain characteristics in each cycle of NR-I, NR-II and HDR in cyclic compression loading (a) virgin specimen, (b) in a specimen preloaded 20 min before the cyclic compression test

A similar study on energy absorption was carried out on specimens tested 20 min after the preloading. Figures 2.12b and 2.13b present the results of the energy absorption and residual strain measurement respectively. The values measured in each of the 5-cycle tests are almost comparable with a little bit higher in the first cycle. This is certainly due to the 'healing effect' (Bueche 1961). To keep this healing effect constant for each specimen, 20 min time interval was maintained between the pre-loading and the actual test for each test of each specimen described in the subsequent articles.

2.6.3 Cyclic compression tests

With a view to studying the strain-rate dependency of NR and HDR, cyclic compression tests at different strain rates were carried out. In the test series, a number of constant strain-rate cases within the range of 0.001/s to 0.96/s were considered. Figure 2.14 shows the rate-dependency of stress-stretch responses that were observed in 6 strain-rate cases for NR-I and 4 strain-rate cases for each of the other two specimens.

In general, the stress responses in the loading path contain a three-fold feature like a high initial stiffness feature at low strain level followed by a noticeable large compressibility at moderate strain as well as a large strain-hardening feature at the end part. When compared among the three specimens, the high initial stiffness at a low stretch level is the most prominent in HDR at a higher strain rate. However, a weaker strain-hardening feature in NR-II than that of the other two specimens at higher stretch levels is also noticeable. These observations will be discussed once again in Chapter 3 to derive a new hyperelasticity function to represent all these aspects.

A further comparison between the loading-path responses at different strain-rate cases shows that with increasing strain-rate, the stresses increase due to viscosity. At higher strain rates, however, a diminishing trend in the increase of stress response was observed indicating an approach to the instantaneous state. When compared between the specimens, the viscosity effect was found to be less prominent in NR-II. However, in contrast to the loading-path, a remarkable feature was noticed in the unloading-path in each specimen for the all strain-rate cases with absence of strain-rate dependency

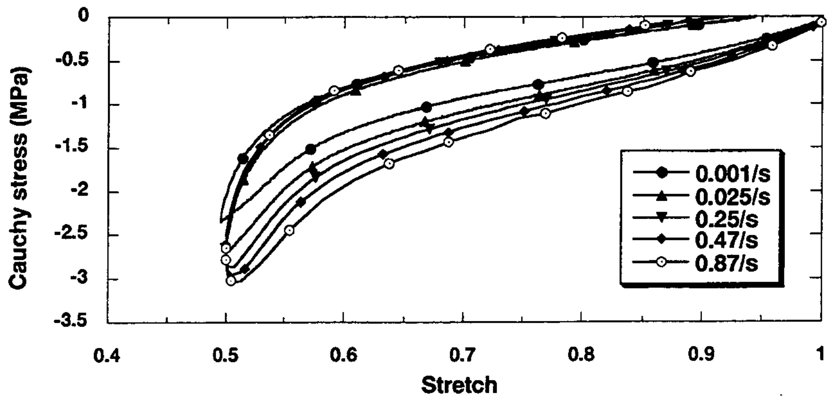

(a)

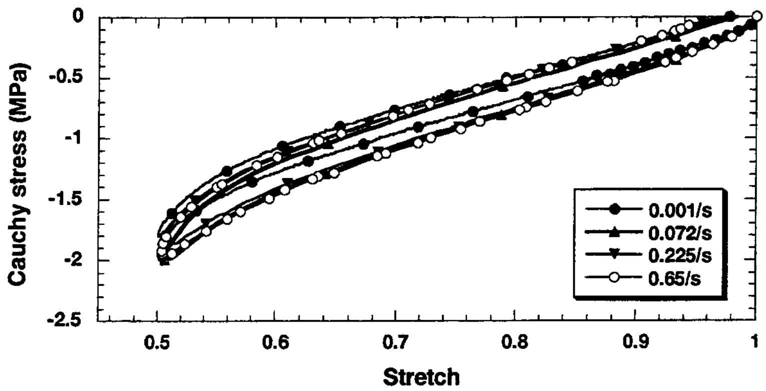

(b)

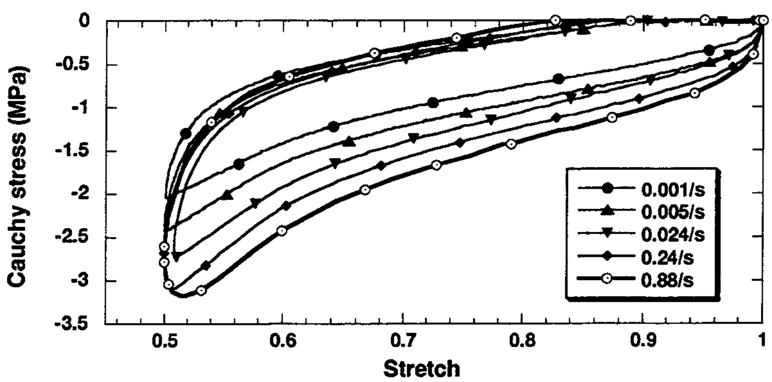

(c)

Figure 2.14 Cyclic compression responses from specimens at different strain rates; (a) NR-I, (b) NR-II, (c) HDR in the response. In general, the energy absorption due to hysteresis was found to be the highest in HDR and the lowest in NR-II.

When compared between the NR specimens, the appearance of viscosity, hysteresis and residual strain in NR-I was found to be more prominent than those of NR-II. The voided microstructure of NR-I (Fig. 2.2) might be a reason behind this significant feature.

2.6.4 Simple relaxation tests

The cyclic compression tests presented in Section 2.6.3 revealed the existence of viscosity in all the specimens. Simple relaxation tests were carried out to study the stress relaxation behavior. The tests were carried out at different maximum stretch levels with a hold time of 10 min. In the loading path, strain rate was specified in between 0.5/s to 1.00/s.

Figures 2.15 to 2.17 illustrate the applied stretch and the corresponding stress histories obtained from tests of NR-I, NR-II, and HDR. The applied strain rates for all these tests have been mentioned in captions. The stress relaxation histories on each specimen illustrate the viscosity induced fundamental viscosity behavior of the materials. In NR-I and HDR, a rapid stress relaxation feature was displayed in the first 2 min of hold time after which it approached asymptotically towards an equilibrium state within next 2 min. The total magnitude of stress relaxation of NR-II was found much lower than that of the other specimen. This observation conforms to the cyclic compression test observations and interpretations as mentioned in Section 2.6.3. In both specimens, however, the stress relaxation characteristic was not found to vary with the change of stretch levels of the simple relaxation tests.

2.6.5 Cyclic relaxation tests

The cyclic compression tests presented in Section 2.6.3 illustrated the strain-rate dependent property. The subsequent simple relaxation tests (Section 2.6.4) further explained the property. The tests carried out at different stretch levels showed reduction in stress response during the hold time and approached the respective equilibrium states in the loading path. In this context, cyclic relaxation tests were

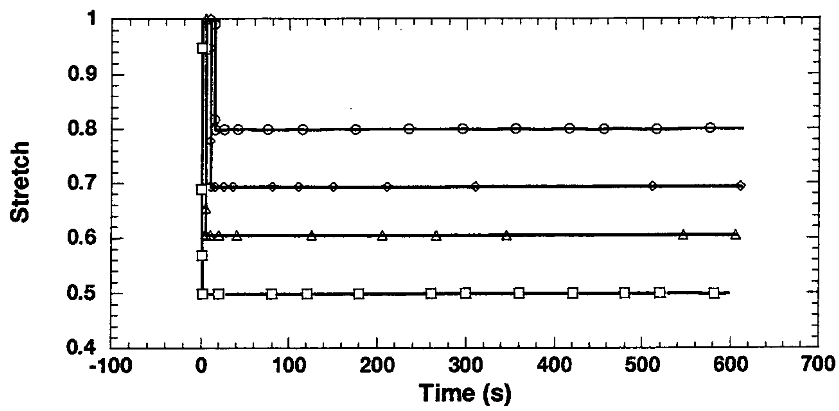

(a)

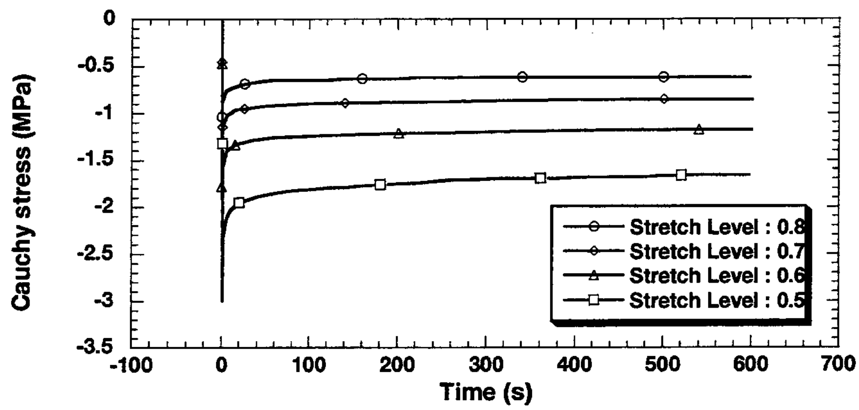

(b)

Figure 2.15 Simple relaxation tests at different stretch levels to observe stress relaxation phenomena in NR-I. The loading rates for 0.8, 0.7, 0.6 and 0.5 stretch levels were maintained at 0.70/s, 0.80/s, 0.97/s and 0.50/s respectively. (a) Applied stretch histories; (b) Stress history.

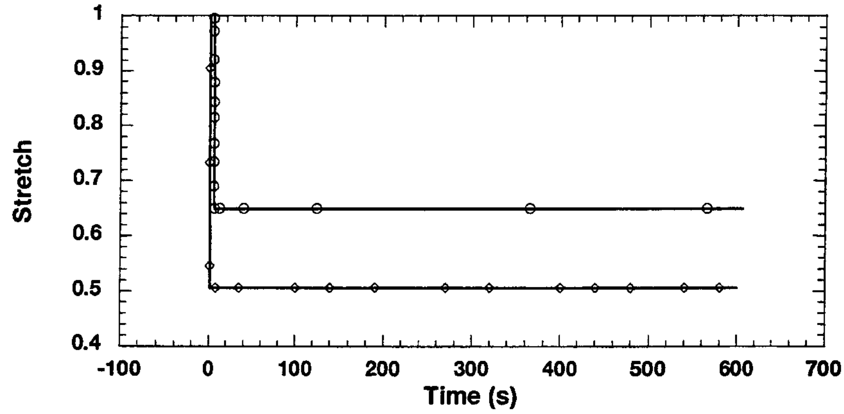

(a)

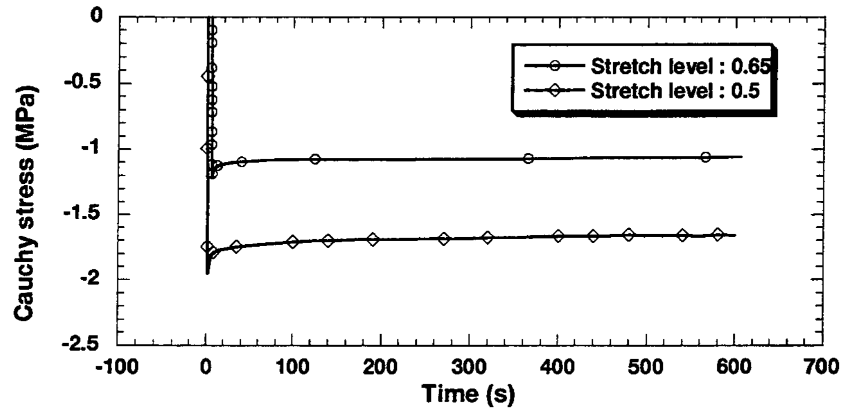

(b)

Figure 2.16 Simple relaxation tests at different stretch levels to observe stress relaxation phenomena in NR-II. The loading rates for 0.65 and 0.5 stretch levels were maintained at 0.41/s and 0.45/s respectively. (a) Applied stretch histories; (b) Stress history.

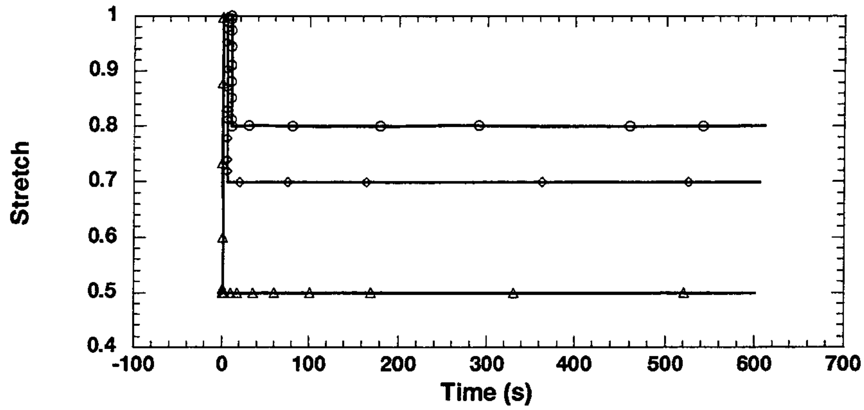

(a)

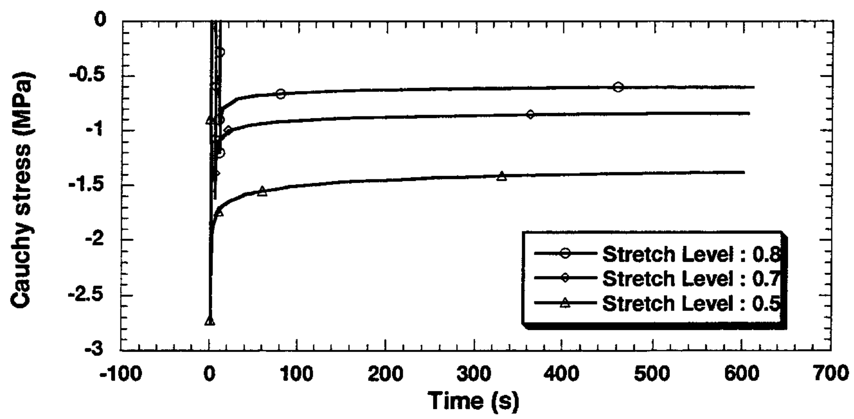

(b)

Figure 2.17 Simple relaxation tests at different stretch levels to observe stress relaxation phenomena in NR-II. The loading rates for 0.8, 0.7 and 0.5 stretch levels were maintained at 0.45/s, 0.45/s and 0.50/s respectively. (a) Applied stretch histories; (b) Stress history.

carried out to observe the relaxation behavior in the unloading paths and thereby to obtain the equilibrium state hysteresis by removing the time-dependent effect.

Figure 2.18 presents the applied stretch and resultant stress histories of the test on NR-I. In the loading path, the maximum stretch level was maintained at 0.55. A strain rate of 0.47/s was maintained in each loading step followed by a hold time of 10 min duration. It is observed that at the end of each relaxation interval in loading and unloading paths, the stress history converges to an almost constant state in all specimens. Although an equilibrium state can be achieved only in an asymptotic sense, the stress states invariably indicate the neighborhood of the equilibrium states. In a consideration similar to Lion (1996 and 1997), these stress states were regarded as the equilibrium states at the respective stretch levels. The difference in the stresses noticed between the loading and unloading paths defines the equilibrium hysteresis (Fig. 2.18b) at a particular stretch level. Kilian et al (1994) attributed this effect as an irreversible slip process between the adjacent filler particles in the rubber microstructure. The equilibrium points obtained in the loading and unloading path give the equilibrium locus of the material (Fig. 2.18c).

Furthermore, with a view to characterizing the dependence of equilibrium hysteresis on loading history, the cyclic relaxation tests were carried out at different maximum stretch levels of the loading paths. Figures 2.19 and 2.20 present the results obtained in testing NR-I at 0.7 and 0.85 stretch levels respectively. Similar to the experiment carried out at 0.55 stretch level, the equilibrium hysteresis effect is also observed in the later two tests. However, the magnitudes were found to decrease with increasing stretch level with a reduced supply of energy. Another two sets of experiments similar to those in NR-I were also carried out on NR-II and HDR. However, in these specimens, the maximum stretch levels were specified at 0.5, 0.7 and 0.85. Figures 2.21 to 2.23 present the results on NR-II, while Figs. 2.24 to 2.26 present those on HDR.

Although in NR-II and HDR a trend similar to NR-I in the appearance of equilibrium hysteresis was noticed, the magnitudes were found to differ in specimen to specimen. Figure 2.27 summarizes the equilibrium hysteresis values of each specimen at different stretch levels. The comparison of the results indicates stronger dependence of equilibrium hysteresis on the past maximum stretch level for each specimen.

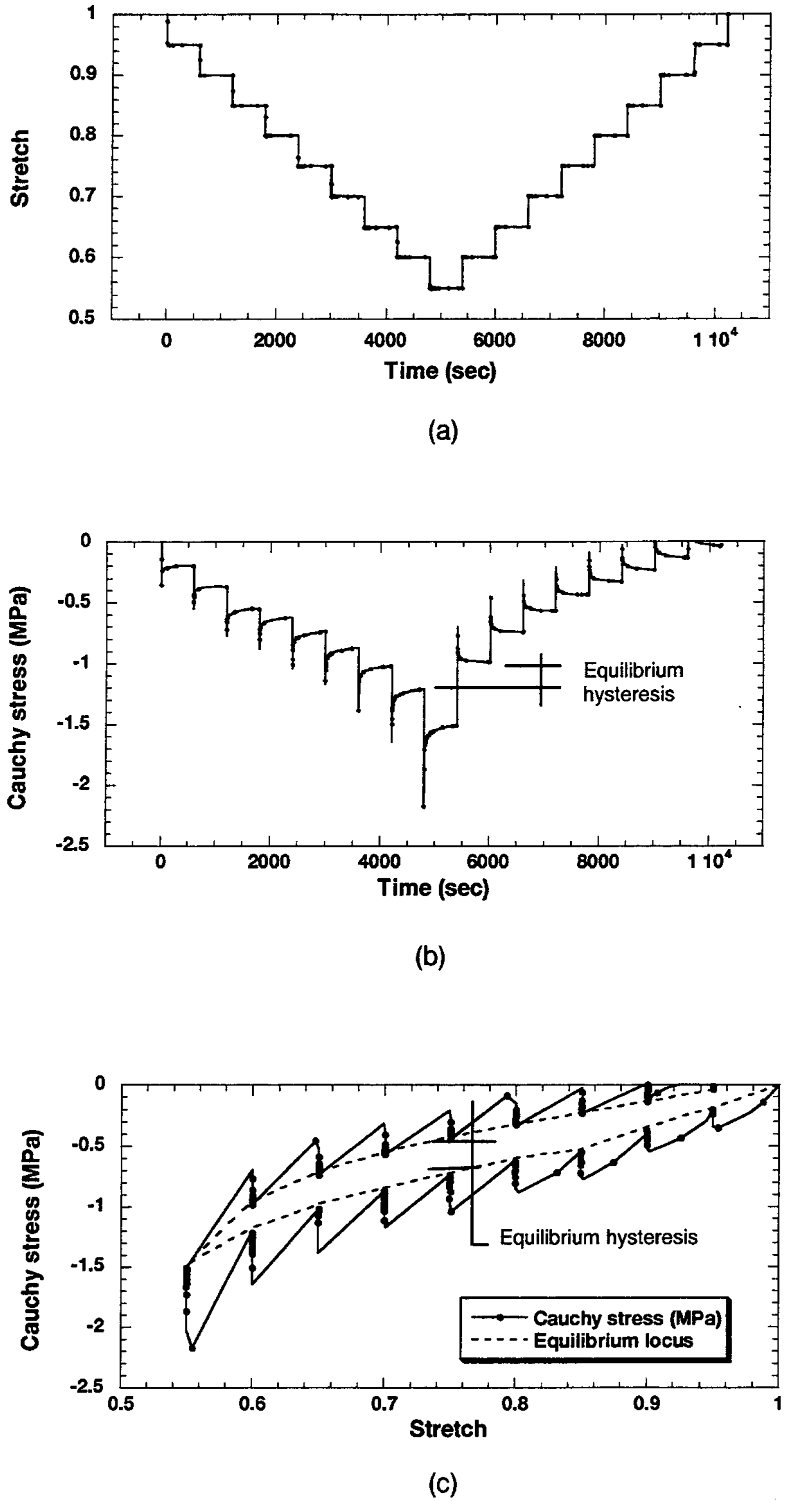

Figure 2.18 Cyclic relaxation test at 0.55 maximum stretch level to observe equilibrium state hysteresis behavior in NR-I.
(a) Applied stretch history; (b) Stress history; (c) Stress-stretch response

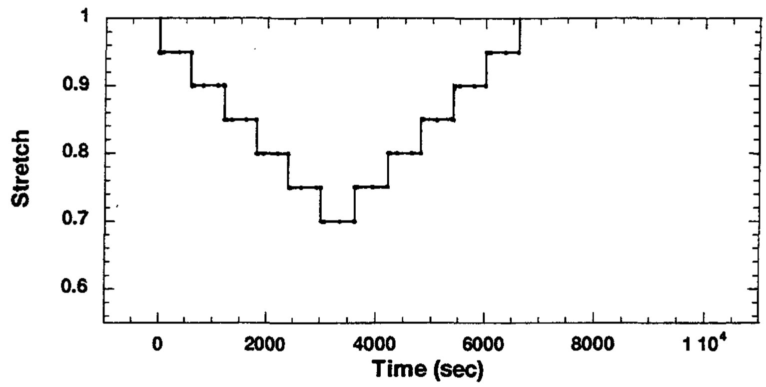

(a)

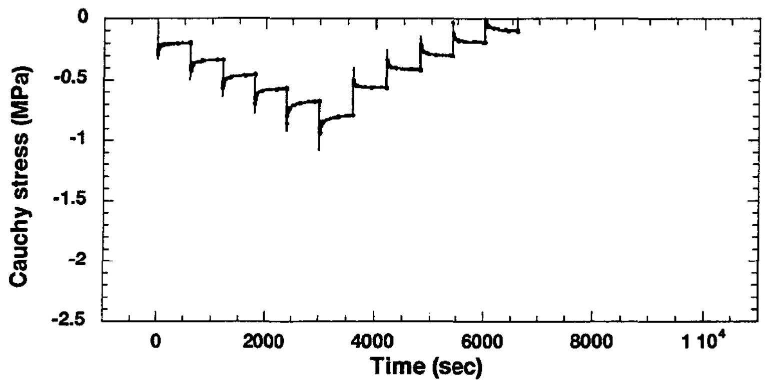

(b)

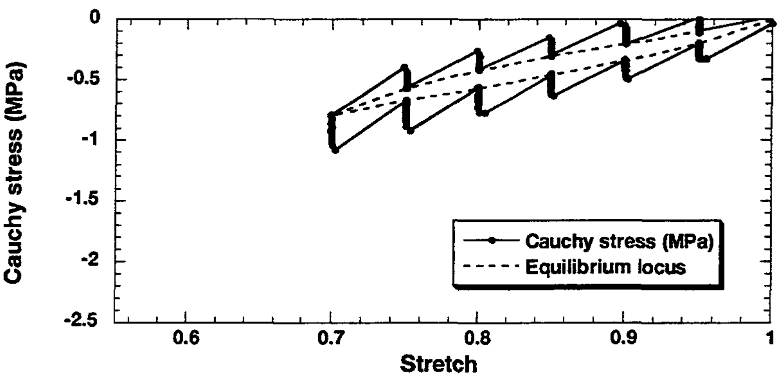

(c)

Figure 2.19 Cyclic relaxation test at 0.70 maximum stretch level to observe equilibrium state hysteresis behavior in NR-I.
(a) Applied stretch history; (b) Stress history; (c) Stress-stretch response

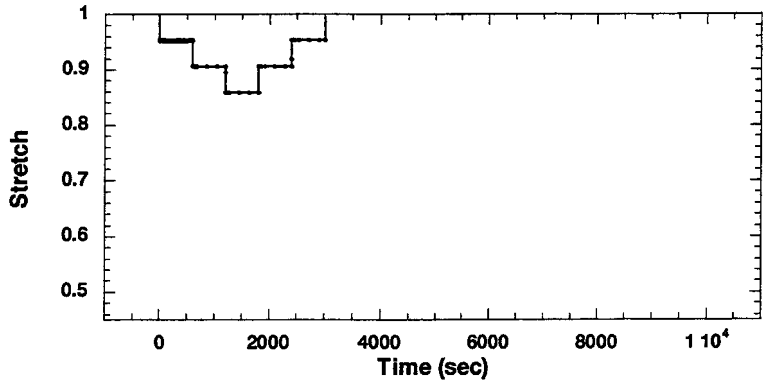

(a)

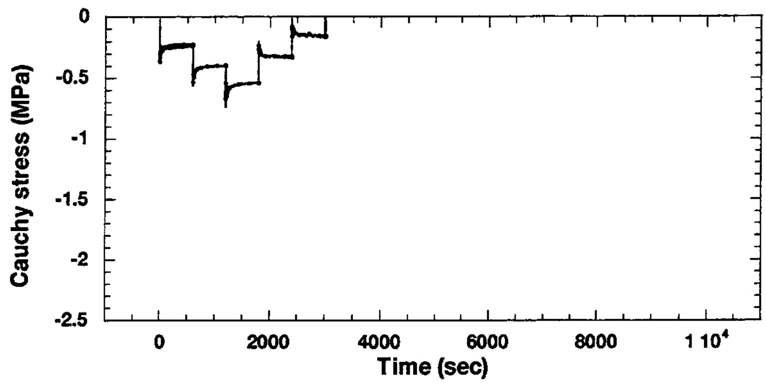

(b)

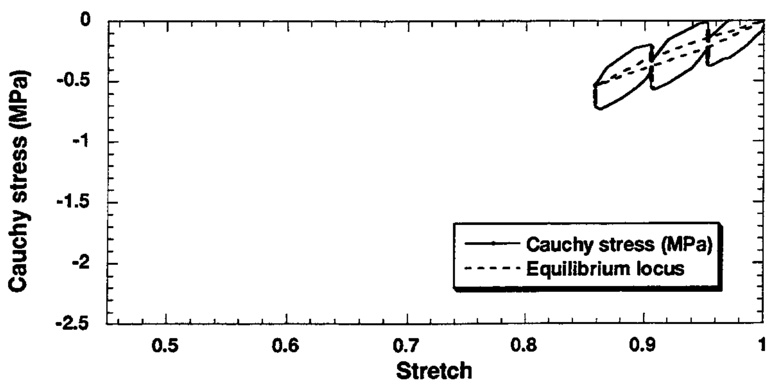

(c)

Figure 2.20 Cyclic relaxation test at 0.85 maximum stretch level to observe equilibrium state hysteresis behavior in NR-I.
(a) Applied stretch history; (b) Stress history; (c) Stress-stretch response

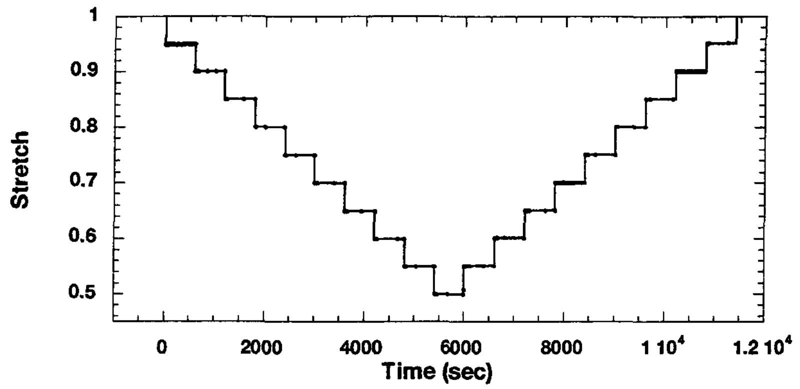

(a)

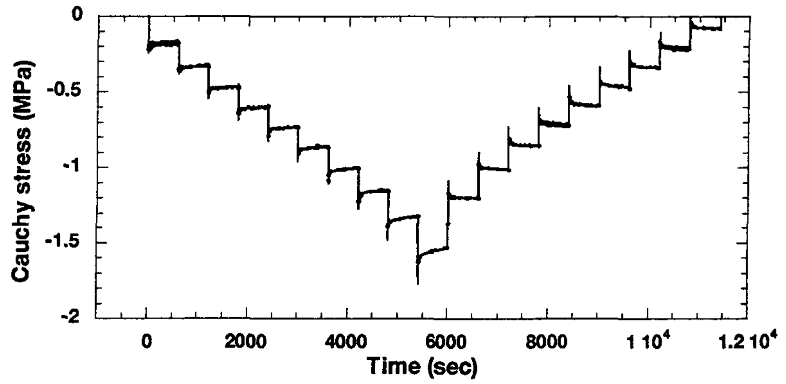

(b)

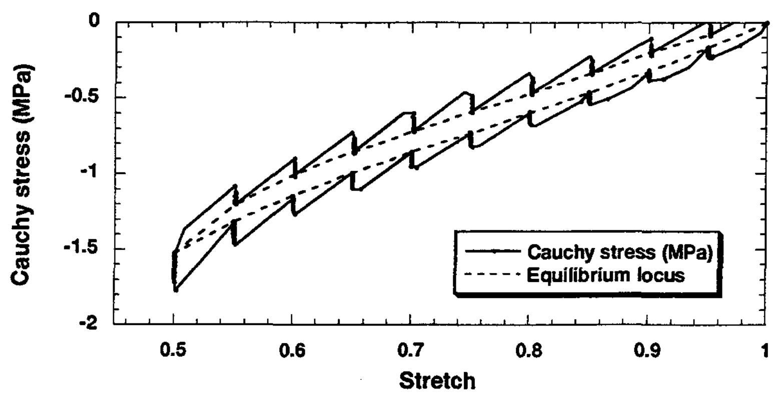

(c)

Figure 2.21 Cyclic relaxation test at 0.50 maximum stretch level to observe equilibrium state hysteresis behavior in NR-II.
(a) Applied stretch history; (b) Stress history; (c) Stress-stretch response

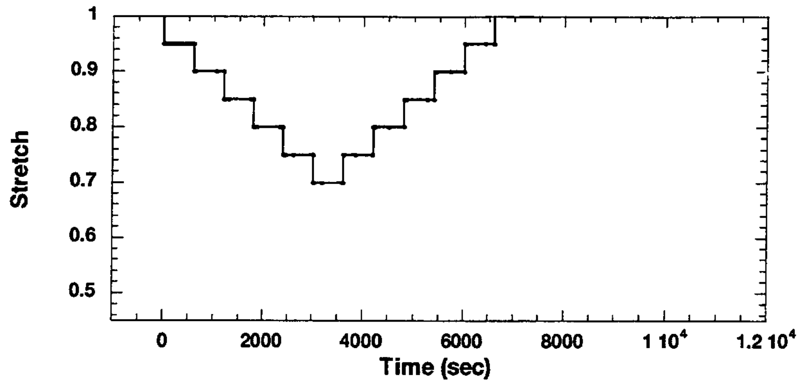

(a)

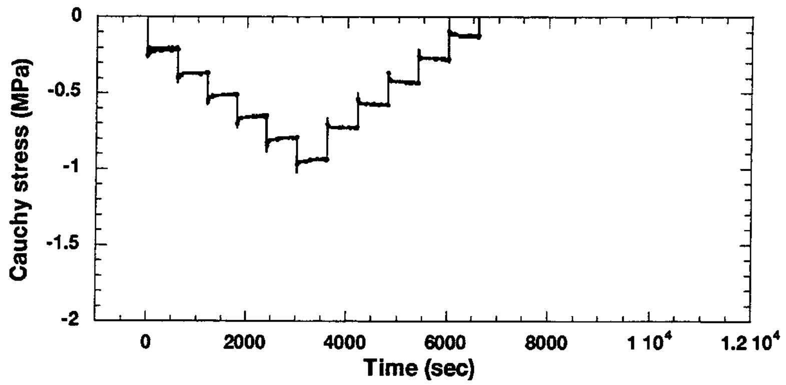

(b)

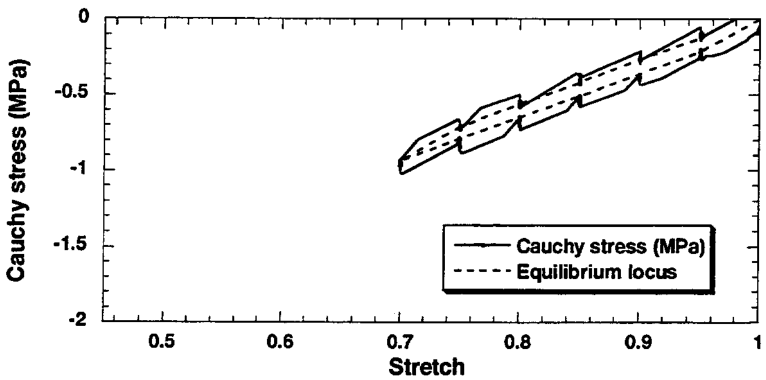

(c)

Figure 2.22 Cyclic relaxation test at 0.70 maximum stretch level to observe equilibrium state hysteresis behavior in NR-II.
(a) Applied stretch history; (b) Stress history; (c) Stress-stretch response

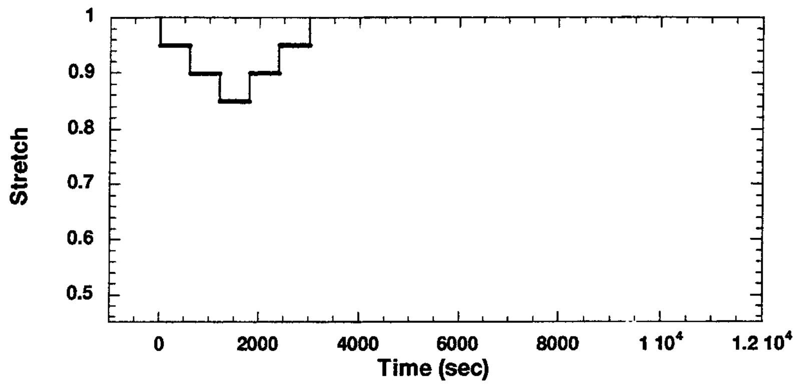

(a)

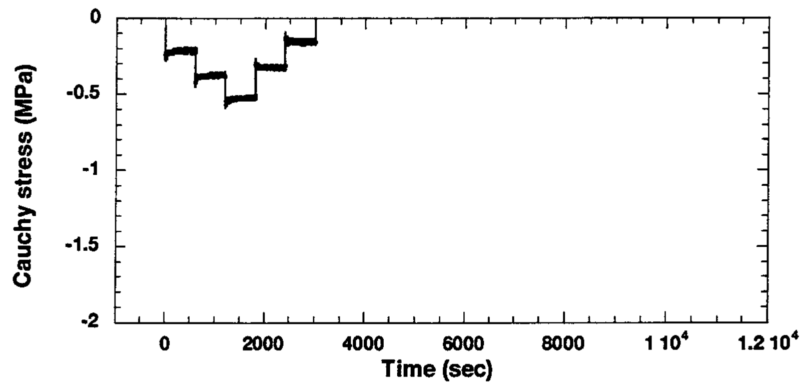

(b)

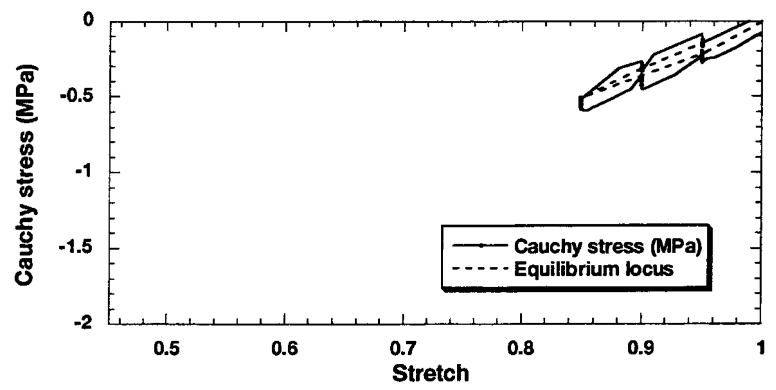

(c)

Figure 2.23 Cyclic relaxation test at 0.85 maximum stretch level to observe equilibrium state hysteresis behavior in NR-II.
(a) Applied stretch history; (b) Stress history; (c) Stress-stretch response

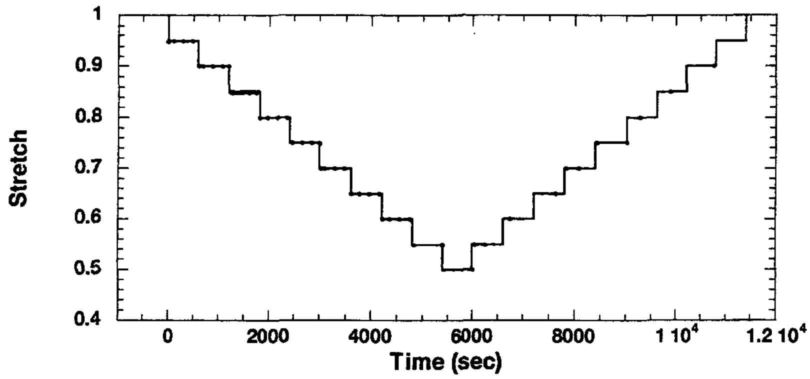

(a)

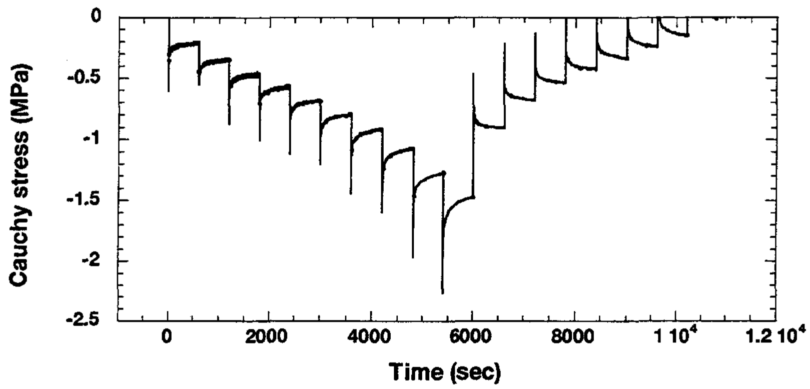

(b)

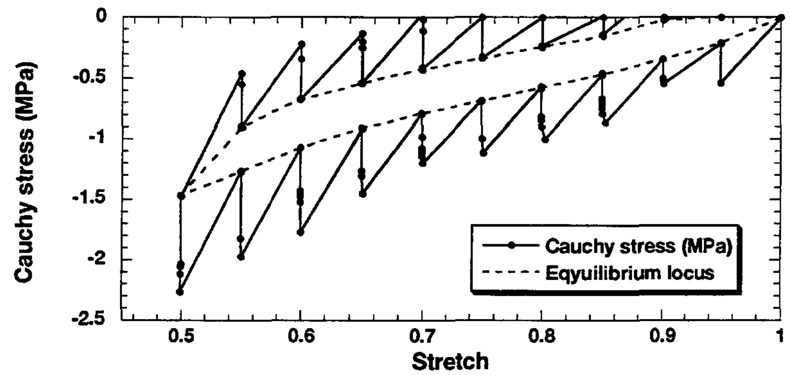

(c)

Figure 2.24 Cyclic relaxation test at 0.50 maximum stretch level to observe equilibrium state hysteresis behavior in HDR.
(a) Applied stretch history; (b) Stress history; (c) Stress-stretch response

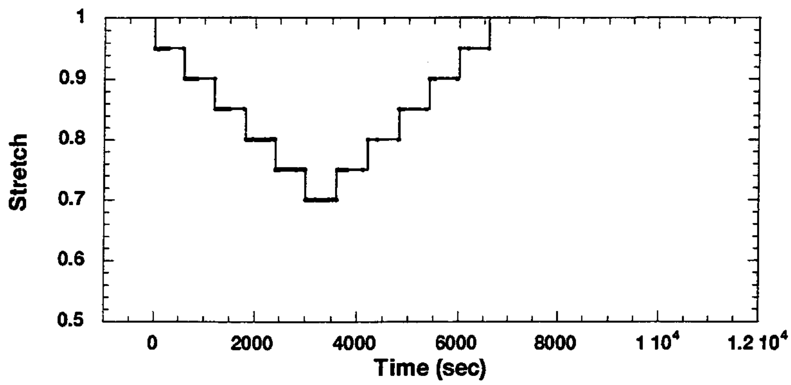

(a)

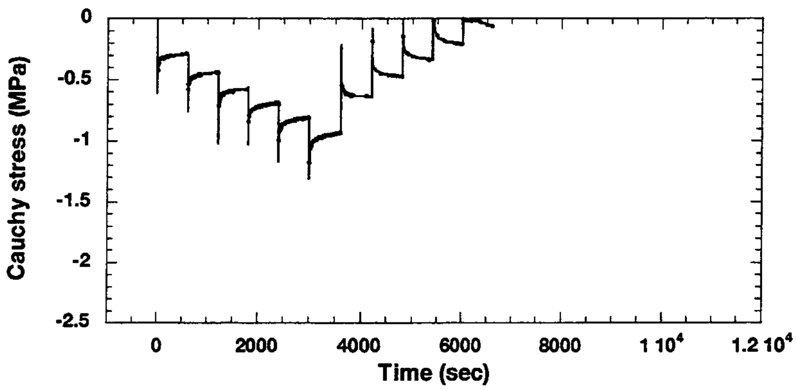

(b)

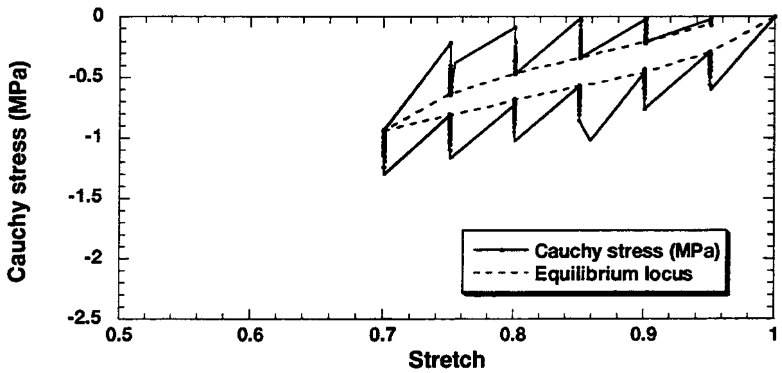

(c)

Figure 2.25 Cyclic relaxation test at 0.70 maximum stretch level to observe equilibrium state hysteresis behavior in HDR.
(a) Applied stretch history; (b) Stress history; (c) Stress-stretch response

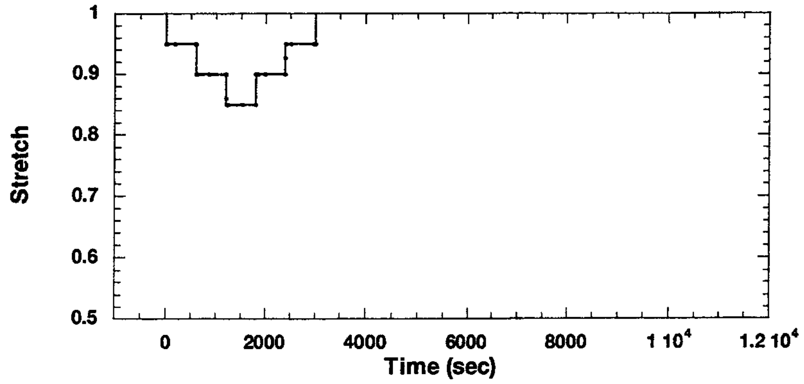

(a)

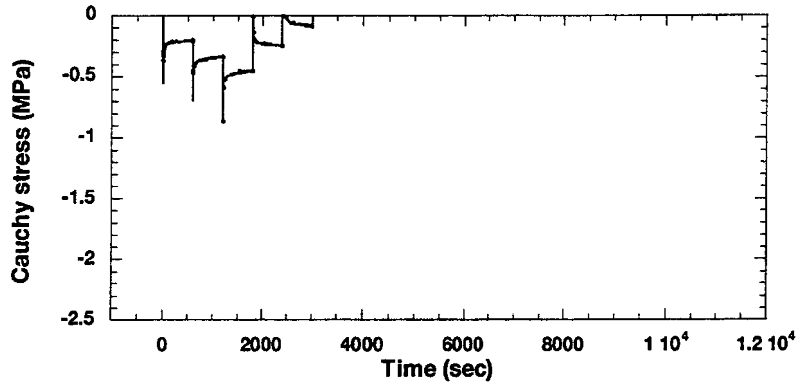

(b)

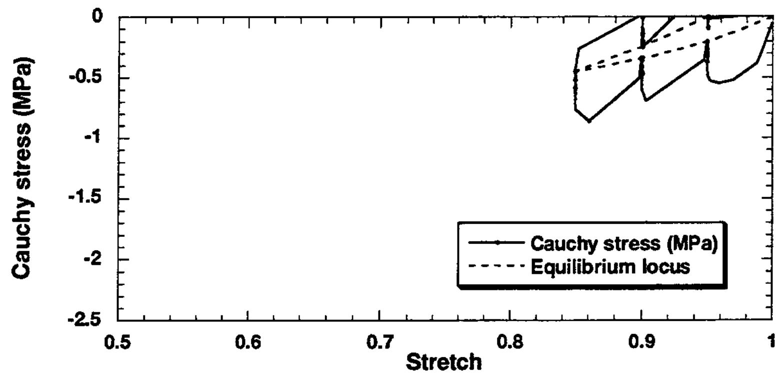

(c)

Figure 2.26 Cyclic relaxation test at 0.85 maximum stretch level to observe equilibrium state hysteresis behavior in HDR.
(a) Applied stretch history; (b) Stress history; (c) Stress-stretch response

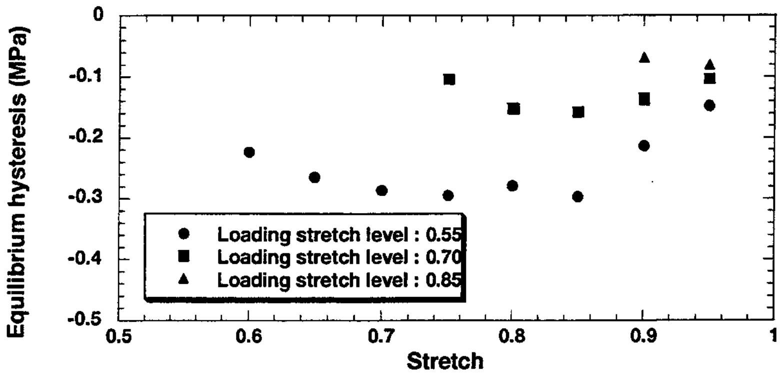

(a)

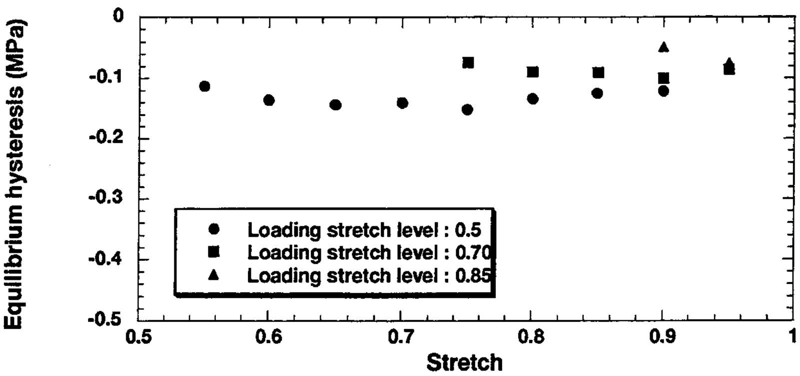

(b)

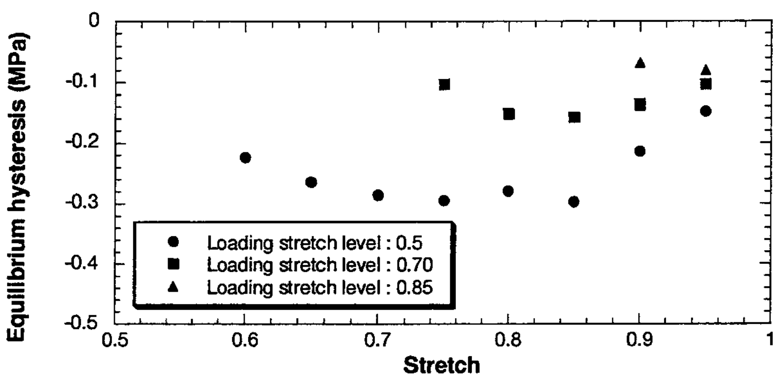

(c)

Figure 2.27 History and path dependence of equilibrium hysteresis phenomenon observed from cyclic relaxation tests carried out at different stretch levels.
(a) NR-I, (b) NR-II, (c) HDR

In addition, the equilibrium hysteresis was also found to be strongly dependent on the current stretch values in NR-I and HDR. However, in NR-II, the dependence on the current stretch was noticed to be somewhat weaker. When compared between the specimens at a particular past maximum stretch level, the equilibrium hysteresis was found to be of comparable magnitude in NR-I and HDR. It was found to be a bit lower in NR-II.

2.6.6 Recovery of residual strain

The preloading test results presented in Section 2.6.2 illustrated the appearance of residual strain at the end of each cycle with a decreasing trend at the later cycles. The residual strain is related to the damage in the rubber-filler bonds that the specimens experience during each loading cycle. The strain was found to be greater in magnitude in NR-I and HDR. However, due to 'healing effect' (Bueche 1961), the microstructural damage is believed to be self-cured with time. In this context, the influence of past strain history on the residual strain and the recovery were studied in preloaded NR-I and HDR specimens subjected to different strain rates and maximum stretches.

Figure 2.28 presents the results on NR-I and HDR, where a linearly logarithmic relation in the recovery of residual strain over the time can be well noted. The figure presents the recovery paths of residual strains of preloaded NR-I and HDR specimens subjected to cyclic compression tests at different strain rates. However, in the loading paths, the maximum stretch values were maintained at a constant 0.5 value. The figure shows an inverse relation between the applied strain rate and the residual strain. This perhaps may inevitably be due to a longer stretch history applied on the specimens in the cases of slower strain rate.

Figure 2.29 presents the residual strain and the recovery characteristics of preloaded NR-I subjected to different stretch levels at a constant strain rate of 0.001/s. However, no effect of past maximum stretch value was noticed. This might be due to the effect of previous preloading histories with 0.5 maximum stretch levels applied on the specimens. Generally, the residual strain values were found to be higher in the HDR than those of NR-I.

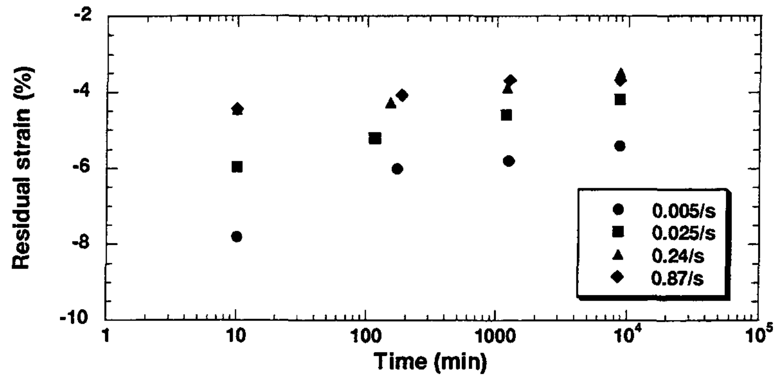

(a)

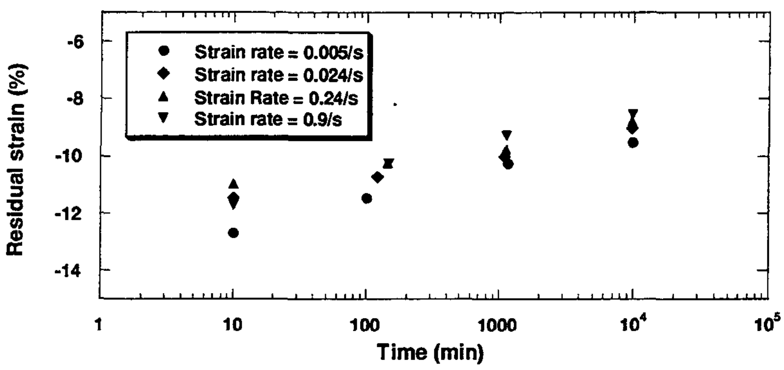

(b)

Figure 2.28 Residual strain and recovery characteristics. Measurements have been carried out on preloaded specimens subjected to cyclic compression tests at different strain rates but constant 0.5 stretch level. The finish of the cyclic compression experiment marks the beginning of recovery history. (a) NR-I, (b) HDR

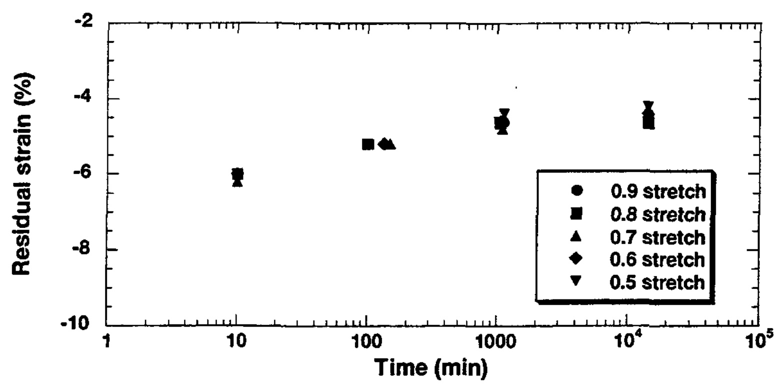

Figure 2.29 Residual strain and recovery characteristics of NR-I. Measurements have been carried out on preloaded specimens subjected to cyclic compression tests at different stretch levels but constant strain rate of 0.001/s. The finish of the cyclic compression experiment marks the beginning of recovery history.

2.7 MECHANICAL TEST IN TENSION

The cyclic compression, simple relaxation, and cyclic relaxation tests in the compression regime revealed the nonlinear strain rate dependent response of NR and HDR along with the hysteresis effect. In this section, the NR-II and HDR specimens were investigated in an identical experimental scheme in tension in order to have a comparative picture in this regime. The following subsections summarize the observations.

2.7.1 Experimental setup

The NR-II and HDR specimens were tested in tension using a universal testing machine (Shimadzu AGS-G). Rubber sheets with dimensions listed in Table 2.1 were stretched between chucks. Displacement was applied at the end of the specimen and the resulting reaction was recorded in a personal computer. However, unlike compression tests, a homogeneous state of deformation could not be maintained in tension experiments due to the boundary effects. To minimize this problem, a gauge length of 20mm was specified at the middle of the specimens. The strains were measured over the loading history using a digital video camera and image analysis technique (Scion Image 2000). Figure 2.30 illustrates the details of the set up.

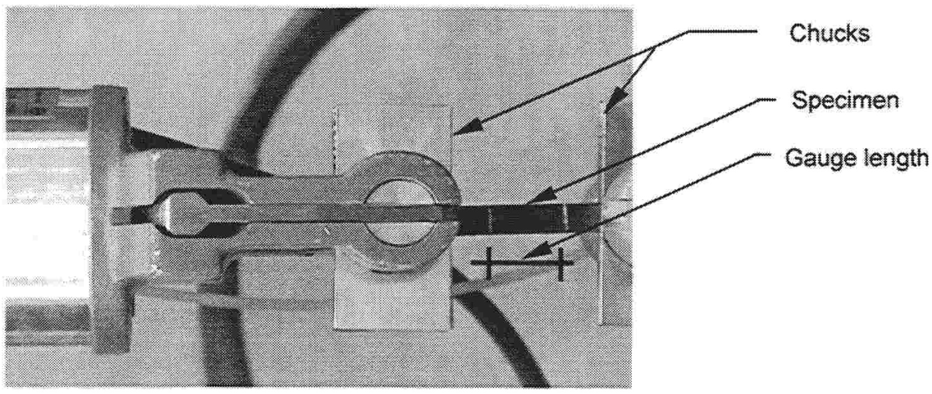

Figure 2.30 Experiment-set up for testing in tension regime.

2.7.2 Preloading

In order to remove the Mullins' effect, 5-cycle preloading with 0.5 maximum stretch level was applied on each specimen prior to the actual test. Actual tests were carried out 20 min after the preloading.

2.7.3 Monotonic tension tests

With a view to investigating the effect of strain rate in stress response, monotonic tension tests at different strain rates were carried out. Figure 2.31 presents the Cauchy stress-stretch responses obtained from NR-II and HDR respectively. The increase in the response due to the increase of strain rate is evident in both specimens. However, in NR-II (Fig. 2.31a), the neighborhood of equilibrium response is visible around 0.0027/s and 0.027/s, while an approach to the instantaneous response is visible around 0.14/s and 0.25/s strain rates. In HDR (Fig. 2.31b), a similar trend is noticeable except the case of 0.25/s strain rate where a scattered data was obtained after 2.25 stretch level. This might be due to low stiffness of the testing machine inadequate for performing the tests at such high strain rates.

In general, when compared with compression regime responses, the strain-hardening feature of both specimens was found to be more significant in tension regime. In contrast, the initial stiffness feature of HDR was less prominently observed here.

2.7.4 Simple relaxation tests

In order to observe the viscosity effect in NR-II and HDR in tension, simple relaxation tests with 0.14/s strain rate were carried out in the loading path following a hold time of 10 min. Figures 2.32 and 2.33 illustrate the stress relaxation behavior in each material. In both specimens, the major fraction of stress relaxation was found to take place within the first 200 sec of the relaxation history. However, the extent of stress relaxation (Fig. 2.32) was a bit lower in NR-II than that of HDR indicating a minimal material viscosity. This conforms to the observation made in the compression regime (Section 2.6.4).

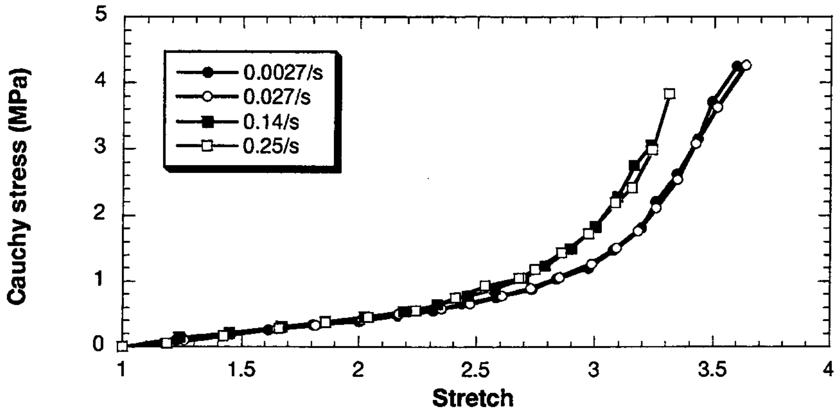

(a)

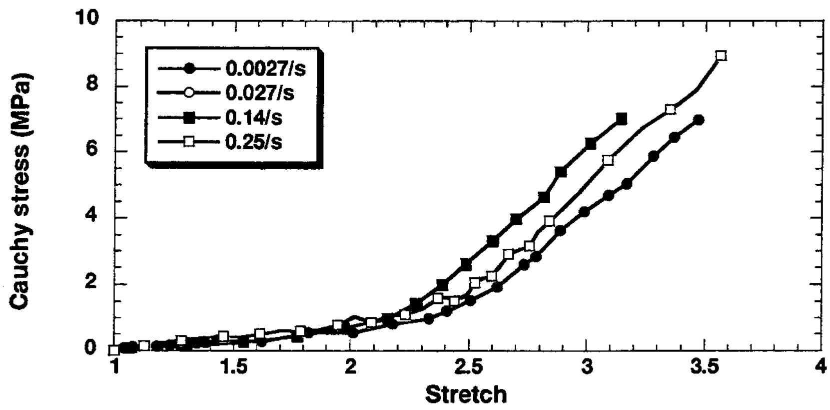

(b)

Figure 2.31 Monotonic tension responses at different strain rates. (a) NR-II; (b) HDR.

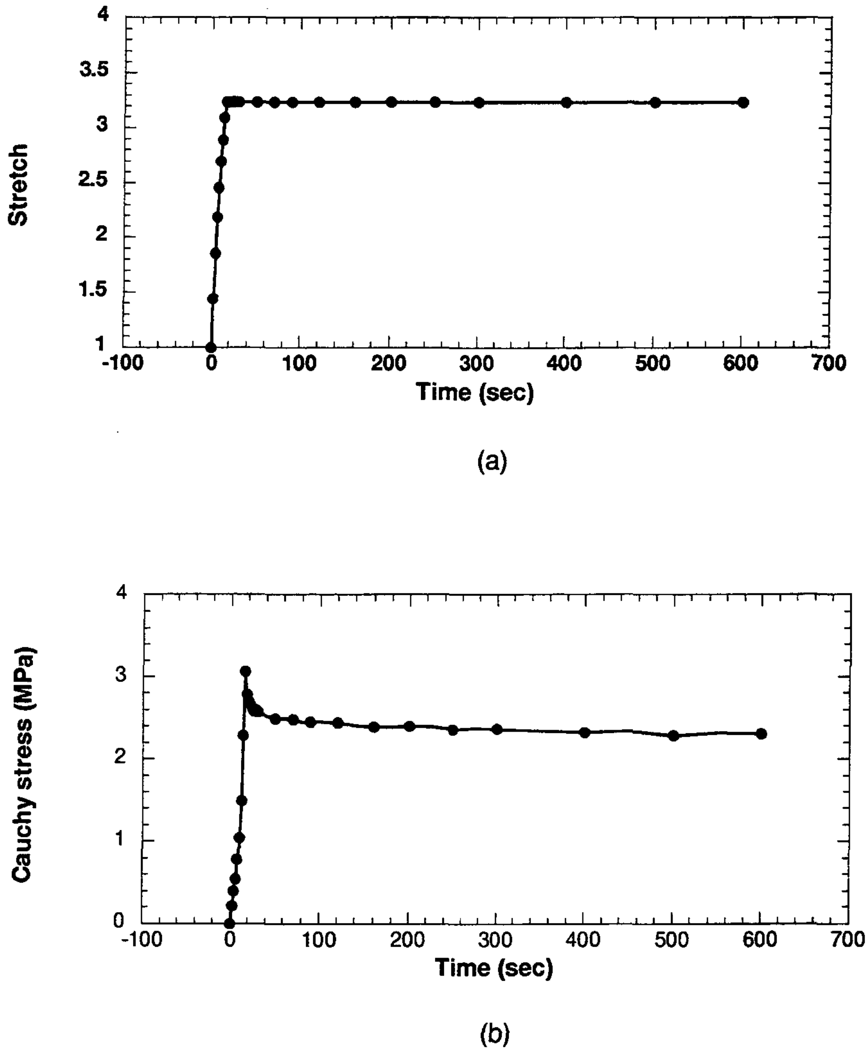

Figure 2.32 Stress relaxation phenomenon observed from NR-II in tension.

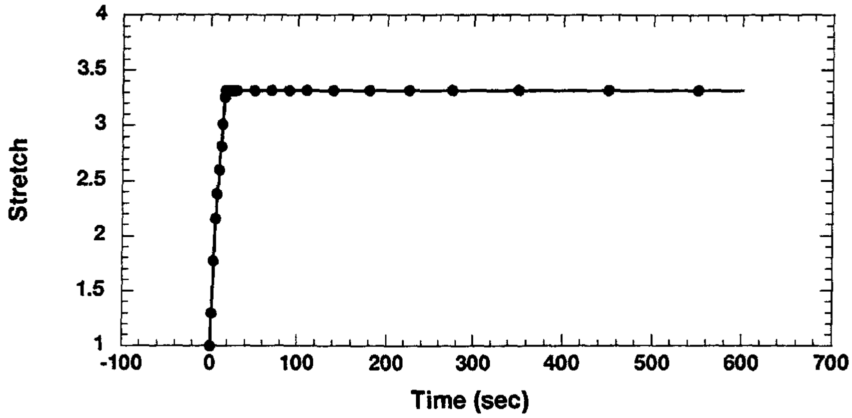

(a)

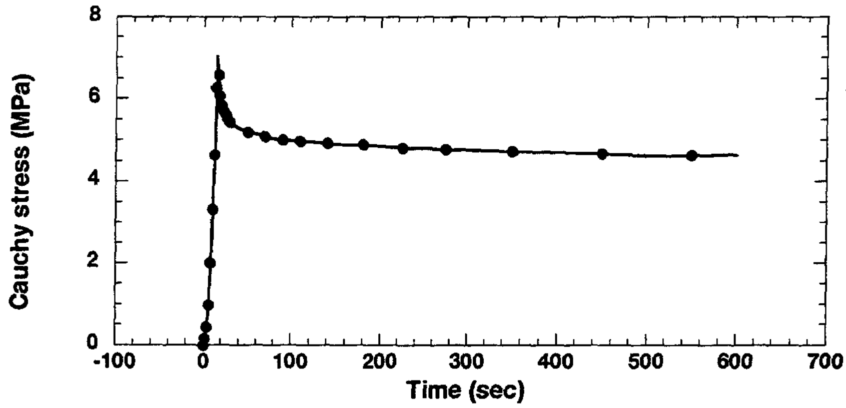

(b)

Figure 2.33 Stress relaxation phenomenon observed from HDR in tension.

2.7.5 Cyclic relaxation tests

Cyclic relaxation tests in tension were also carried out to identify the equilibrium loci of the specimens in the loading and unloading paths. To do this, similar to the compression tests, each specimen was subjected to 16 relaxation steps in the loading and unloading paths with 10 min hold time in steps. A strain rate of 0.14/s was maintained in each loading step. Figure 2.34 presents the equilibrium loci obtained from NR-II and HDR. A comparison between the specimens indicates a larger amount of equilibrium hysteresis in HDR than that in NR-II. This observation is in line with that of the compression regime.

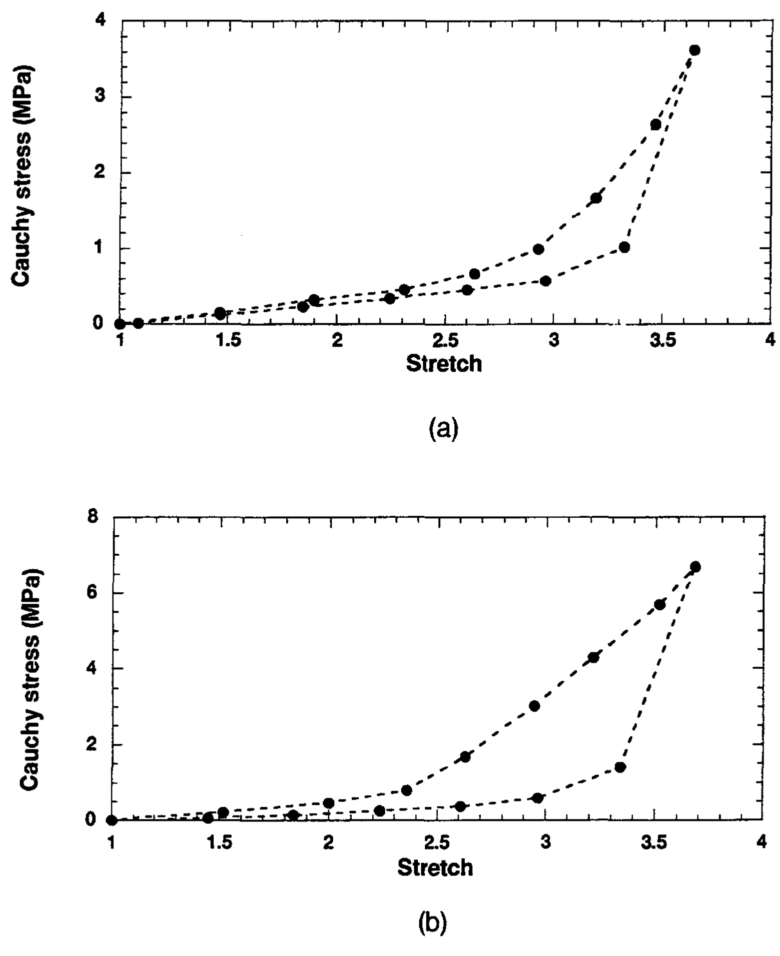

Figure 2.34 Equilbrium hysteresis effect obtained from cyclic relaxation tests in tension regime. (a) NR-II, (b) HDR .

2.8 SUMMARY

In this chapter the experimental results have been presented. At first, SEM investigation was carried out to study the microstructure of NR and HDR in qualitative and quantitative ways. Following the presentation of SEM investigation results, the mechanical tests in compression were presented to illustrate the material behavior with respect to Mullins' effect, nonlinearity in stress-strain response, strain-rate dependency, hysteresis and residual strain behavior. A limited investigation results in tension was also presented to give a comparative picture of the strain-rate dependency and hysteresis property in tension regime. The objectives and inferences of the different microstructural observations, mechanical tests in compression and tension are summarized respectively in Tables 2.3 to 2.5.

Table 2.3 Microstructural observations at a glance

TESTS	OBJECTIVES	OBSERVATIONS
Virgin specimen	To ascertain the presence of voids in the specimens.	NR-I contained significant amount of voids. NR-II and HDR contained no voids.
After mechanical tests in compression	To ascertain the change in microstructure in terms of void orientation and void area ratio in NR-I.	Due to the presence of large rubber solids, the compressive loading caused an isotropic orientation of voids in the microstructure. No significant change in void area ratio with respect to virgin specimens was observed.
In-situ tension	To ascertain the change in microstructure in terms of void orientation and void area ratio in NR-I.	Upon in-situ tension loading, the voids got oriented along the direction of loading. No significant change in void area ratio with respect to virgin specimens was observed.

Table 2.4 Mechanical tests in compression at a glance

TESTS	OBJECTIVES	OBSERVATIONS
Preloading	To remove Mullins' effect.	Within first 2-cycles of the 5 cycle preloading test, the Mullins' effect was found to be removed. The healing effect was observed even within 20 min after the end of preloading. However, the extent was insignificant.
Cyclic compression at different strain rates	To know the strain-rate dependency effect.	A very significant strain-rate dependency phenomenon was observed in the loading path of NR-I and HDR. In NR-II, the effect was somewhat weaker. In the loading path, with the increase of strain-rate, the approach of the response towards the instantaneous state was noticed in all the specimens. However, in the unloading path, no effect strain-rate was observed.
Simple relaxation	To investigate the viscosity effect.	At all the considered stretch levels, the viscosity induced stress relaxation phenomenon was noticed in all specimens. In NR-II, the effect was found to be somewhat weaker than that of NR-I and HDR.
Cyclic relaxation	To remove the viscosity effect and thereby identify the equilibrium locus and equlibrium hysteresis.	In all specimens, equilibrium hysteresis effect was observed. However, in NR-II, it was lower than those of other two. The direct dependence of equilibrium hysteresis on loading path maximum strain and current strain level was revealed.
Residual strain measurement	To know the effect of cyclic loading history on residual strain.	Residual strains were found to be higher when cyclic loadings of slower strain-rates were applied. A logarithmically linear recovery path of residual strain was revealed.

Table 2.5 Mechanical tests in tension at a glance

TESTS	OBJECTIVES	OBSERVATIONS
Preloading	To remove the Mullins' effect	–
Monotonic tension at different strain rates	To investigate the strain-rate dependency.	In both NR-II and HDR, the strain-rate dependency effect was observed. In NR-II, the approach towards instantaneous state was distinctly noticed.
Simple relaxation	To investigate the viscosity effect.	Effect of viscosity induced stress-relaxation phenomena was noted in NR-II and HDR as well.
Cyclic relaxation	To identify the equilibrium locus and thereby know the extent of equilibrium hysteresis.	In HDR, equilibrium hysteresis was found to be higher than that of NR-II.

In general, among the NR specimens, the presence of Mullins' effect, strain-rate dependency, hysteresis and residual strain was found to be more significant in NR-I than those of NR-II. Such a characteristic mechanical behavior of NR-I can be explained from the presence of microstructural voids in the specimens. However, in case of HDR, although these mechanical effects were found to be prominent, the microstructural observations made in the present study could not throw any light on such facts. All these experimental observations indicate the necessity of a phenomenological consideration for constructing a general constitutive model that will be capable of simulating the mechanical behavior of NR and HDR as well.

Chapter 3
Hyperelasticity Modeling

3.1 GENERAL

The experimental observations in Chapter 2 revealed a strong nonlinearity in response along with significant time-dependent and hysteresis properties. Typically, hyperelasticity functions are used to model the response of rubbers at a particular strain rate assuming the complete elastic recovery of the material (Bonet and Wood 1997; Charlton et al 1993; Davis et al 1994). These functions are purely concerned with the current strain and are independent of the path followed to reach that strain. Hence, these are confined to elastic behavior and are needed to be combined with other models through a suitable model structure to include the other effects. However, even in such situation, an adequate hyperelasticity function is the major building stone in a complete constitutive model for rubbers representing all kinds of effects. In this context, the existing hyperelasticity functions are reviewed in this chapter and an improved relation is proposed to represent the elastic response of NR and HDR in compression. Finally, efforts were made to compare the performance of the proposed as well as the conventional functions for representing the elastic response of the specimens in compression regime.

3.2 LITERATURE REVIEW

3.2.1 Preliminaries

The large strain elastic response of rubber-like solids is described either by using an approach based on statistical thermodynamics or by adopting a phenomenological approach considering the material as a continuum (Trealor 1975). The first approach generally considers the rubber from the molecular network point of view and it assumes a statistical distribution of chain lengths, orientations and molecular structures. In contrast to the first approach, however, the phenomenological approach considers the rubber to be a homogeneous material in an undeformed state and thus it assumes random orientation of the polymer molecules. However, in both approaches the stress-strain relationship is derived from a strain energy density function (W) that depends on the final state of strain and is independent of loading history. The construction of W either by statistical mechanics or continuum mechanics forms the basis of the hyperelasticity theory.

In general, the deformation of a body may be resolved into principal strains corresponding to the three principal directions along the three mutually perpendicular axes (Figure 3.1).

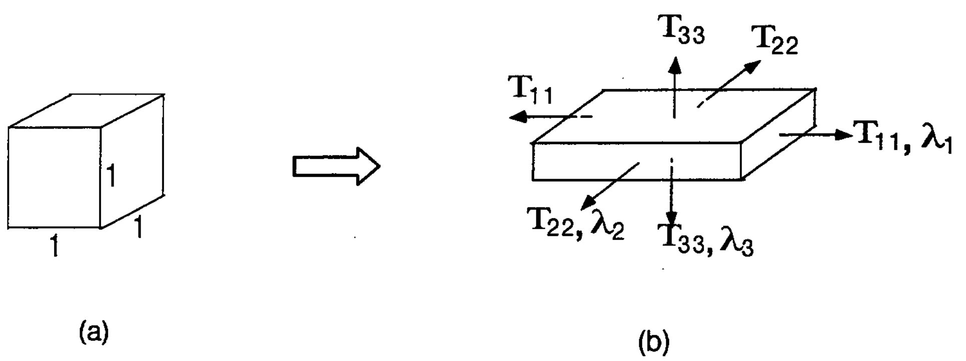

Figure 3.1 Definition of stretch and stresses in principal directions. T_{11}, T_{22}, T_{33} are the Cauchy stresses while λ_1, λ_2, λ_3 are the stretches in the three principal directions. (a) Undeformed; (b) Deformed conditions. Stretch, $\lambda = 1+(\Delta L/L)$, L= undeformed length.

For a complete specification of elastic properties of the material, it is sufficient to know the form of the strain energy function, W. For isotropic elastic materials, the strain energy function W can be expressed as a function of invariants of a deformation tensor I_i, (i=1,3):

$$W = W(I_1, I_2, I_3). \tag{3.1}$$

If the left Cauchy Green deformation tensor **B** is employed as the deformation tensor, the deformation invariants can be rewritten in terms of the principal stretches λ_i (i=1,3):

$$I_1 = \mathrm{tr}\mathbf{B} = \lambda_1^2 + \lambda_2^2 + \lambda_3^2,$$
$$I_2 = \frac{1}{2}\left\{(\mathrm{tr}\mathbf{B})^2 - \mathrm{tr}(\mathbf{BB})\right\} = (\lambda_1\lambda_2)^2 + (\lambda_2\lambda_3)^2 + (\lambda_3\lambda_1)^2, \tag{3.2}$$
$$I_3 = \det\mathbf{B} = (\lambda_1\lambda_2\lambda_3)^2.$$

When the material is incompressible, the third invariant $I_3=1$, and W is represented as a function of I_1 and I_2 only:

$$W = W(I_1, I_2). \tag{3.3}$$

From Truesdell and Noll (1992), it follows that the Cauchy stress $\mathbf{T}$ is expressed as:

$$\mathbf{T} = -p\mathbf{1} + \mathbf{T}_E, \tag{3.4}$$
$$\mathbf{T}_E = 2\frac{\partial W}{\partial I_1}\mathbf{B} - 2\frac{\partial W}{\partial I_2}\mathbf{B}^{-1}, \tag{3.5}$$

where $\mathbf{1}$ is the identity tensor, p is the hydrostatic pressure, and the subscript 'E' denotes the deviatoric part.

From Eqs. (3.1) to (3.5) it becomes clear that the representation of incompressible hyperelastic material behavior is solely dependent on the definition of $W(I_1, I_2)$.

However, there exists an alternate path where W is directly expressed in terms of principal stretches following the Valanis and Landel (1967) hypothesis:

$$W(\lambda_1,\lambda_2,\lambda_3) = w(\lambda_1) + w(\lambda_2) + w(\lambda_3) \tag{3.6}$$

In the following subsections, the models reached from both approaches will be discussed.

3.2.2 Strain invariant based models

Among the W functions based on statistical molecular theory, Arruda and Boyce (1993) function is the most successful one (Seibert and Schoche 2000; Boyce and

Arruda 2000). A compressible version of the Arruda and Boyce model is also available in Anand (1996). The Arruda and Boyce model is expressed in terms of I_1 and it needs only two parameters, namely the μ and λ_m:

$$W(I_1) = \mu\left\{\frac{1}{2}(I_1-3) + \frac{1}{20\lambda_m^2}(I_1^2-9) + \frac{11}{1050\lambda^4_m}(I_1-27)^3 + ...\right\} \quad (3.7)$$

Among the strain invariant based models, a polynomial form of energy density as proposed by Rivlin (1948a,b) is the first and the commonest one. Eq. 3.8 depicts the general polynomial form with C_{ij} as the material parameters:

$$W(I_1,I_2) = \sum_{i,j}^{\infty} C_{ij}(I_1-3)(I_2-3) \quad (3.8)$$

The Rivlin model in its most general form (Eq. 3.8) is reasonably complicated. This led many researchers to develop variations on the general form to suit their own applications. The most commonly referred Mooney-Rivlin function (Mooney 1940; Rivlin 1948a,b) (Eq. 3.9) is derived as the first order polynomial expansion of Eq. 3.8 with C_{10} and C_{01} as material parameters. Sometimes, the single term Neo-Hookean form (Eq. 3.10) is also employed.

$$W(I_1,I_2) = C_{10}(I_1-3) + C_{01}(I_2-3) \quad (3.9)$$

$$W(I_1,I_2) = C_{10}(I_1-3) \quad (3.10)$$

While the Mooney-Rivlin form is convenient for its simplicity, it is often found to be inadequate for predicting the stresses associated with other modes of deformations. This failure of Mooney-Rivlin equations to provide adequate multi-axial data predictions was thought to arise not for taking enough terms of the possible expansions of Eq. 3.8, (Tschoegl 1972). Hence, efforts were made to include higher order of expansion terms to obtain better prediction.

In this course, James and Green (1975) employed various higher order expansions of the general Rivlin function in their attempts to reliably fit and use test data from rubber compounds having high carbon-black loadings. The second order and the third order invariant expansion with 5 and 9 terms were also tried there (Eqs. 3.11 and 3.12).

$$W(I_1,I_2) = C_{10}(I_1-3) + C_{01}(I_2-3) + C_{11}(I_1-3)(I_2-3) + C_{20}(I_1-3)^2 + C_{02}(I_1-3)^2 \quad (3.11)$$

$$W(I_1,I_2) = C_{10}(I_1-3) + C_{01}(I_2-3) + C_{11}(I_1-3)(I_2-3) + C_{20}(I_1-3)^2 + C_{02}(I_1-3)^2$$
$$+ C_{21}(I_1-3)^2(I_2-3) + C_{12}(I_1-3)(I_2-3)^2 + C_{30}(I_1-3)^3 + C_{03}(I_1-3)^3 \quad (3.12)$$

In the trial, the third order expansion was found to give acceptable predictions within the range of fitted data ($1<\lambda<2$). The extrapolation ability beyond that range was found not to be so good as to the expectation. The large strain-hardening feature of rubbers cannot therefore be modeled.

This prompted other contemporary researchers to include different forms of I_2. In this course, Rivlin and Saunders (1951) found that $\partial W/\partial I_1$ is substantially constant and that $\partial W/\partial I_2$ is independent of I_1, but varies with I_2. They performed experiments on two different types of vulcanized rubbers and proposed a strain energy density function, assuming incompressibility in the following form,

$$W(I_1,I_2) = C_{10}(I_1-3) + f(I_2-3) \quad (3.13)$$

where, C_{10} is constant and the function I_2-3 should be left to be determined by specific experiments. They proposed to include an independent function of I_1 in the W function.

Hart-Smith (1966); Hart-Smith and Crisp (1967) followed this path and proposed a modified form of expression based on their test data with C_1, C_2 and C_3 as material parameters:

$$W(I_1,I_2) = C_1\int \exp\{C_3(I_1-3)^2\}dI_1 + C_2\ln\left(\frac{I_2}{3}\right) \quad (3.14)$$

Subsequently, the idea conceived by Hart-Smith was further elaborated by Alexander (1968), where a more complicated five parameter expression was derived (Eq. 3.15). In deriving the equation, the idea of Rivlin-Saunders (1951) was blended with those of

Hart-Smith (1966). Alexander (1968) improved the Hart-Smith function and included a more complicated form of expression of I_2:

$$W(I_1,I_2) = C_1\int \exp\{C_3(I_1-3)^2\}dI_1 + C_2\ln\left(\frac{(I_2-3)+\gamma}{\gamma}\right) + C_3(I_2-3) \tag{3.15}$$

where, C_1, C_2, C_3 and γ are material parameters.

In this course, the idea of Tschogel (1972) was recollected once again by Yeoh (1990, 1993), and suggested an approximate function of W which expresses as a cubic function of I_1:

$$W(I_1) = C_{10}(I_1-3) + C_{20}(I_1-3)^2 + C_{30}(I_1-3)^3 \tag{3.16}$$

where, C_{10}, C_{20} and C_{30} are material parameters.

Apart from all these approaches, Yamashita and Kawabata (1992) considered the strip-biaxial and bi-axial test results and proposed two alternate forms of W:

$$W(I_1,I_2) = C_5(I_1-3) + C_2(I_2-3) + \frac{C_3}{N+1}(I_1-3)^N \tag{3.17}$$

$$W(I_1,I_2) = C_5(I_1-3) + C_2(I_2-3) + \frac{C_3}{n+1}(I_1-3)^{n+1}(I_2-3)^{n-m} \tag{3.18}$$

where, C_5, C_2, C_3, N, n and m are the material parameters with $N=n-m$. In the parameter identification procedure, based on Rivlin and Saunders (1951); Kawabata et al (1977, 1981) and also Fukahori and Seki (1992) noted the W to be decomposed into the sum of two independent functions of I_1 and I_2. This striking idea was further considered in a general form by Lambert-Diani and Rey (1999) to arrive at a general strain energy density building procedure. According to that proposal, one experiment with only one principal stretch ratio greater than one is required to obtain the function of I_1. However, to obtain the other part of W through an adequate function of I_2, they suggested for another experiment with two principal stretch ratios greater than one. In the present work, this concept was to be followed to obtain an improved W function for NR and HDR in compression. The details in this regard are presented in Section 3.4.

3.2.3 Stretch ratio based models

Among the stretch ratio based models, Ogden (1972, 1984, 1986) model is the most popular one (Eq. 3.19). The model requires six parameters to describe the stress-stretch relation and it performs well up to a very large deformation range (above 600% strain).

$$W(\lambda_1,\lambda_2,\lambda_3) = \sum_{n=1}^{m} \frac{\mu_n}{\alpha_n}\left(\lambda_1^{\alpha_n} + \lambda_2^{\alpha_n} + \lambda_3^{\alpha_n} - 3\right) \tag{3.19}$$

where, μ_n, α_n are the material parameters.

In a parallel work, Peng & Landel (1972) also proposed other forms of strain energy density functions presented in Eq. 3.20 with c as the only material parameter.

$$W(\lambda_1,\lambda_2,\lambda_3) = \sum_{i=1,3} c[\lambda_i - 1 - \ln\lambda_i - \frac{1}{6}(\ln\lambda_i)^2 + \frac{1}{18}(\ln\lambda_i)^3 - \frac{1}{216}(\ln\lambda_i)^4] \tag{3.20}$$

However, because of complete phenomenological nature, these functions need a large number of experiments at different deformation modes for the determination and the calibration of a true set of material parameters (Shariff 2000). The other path was undertaken in the present research to reach an adequate hyperelasticity function for NR and HDR in compression.

3.2.4 Finite element implementation aspects

The finite element method (FEM) that was developed first in the early 60's (Irons and Ahmad 1980; Zienkiewicz and Taylor 1996) is the prime constituent in the computer-aided-engineering of the present days. The FEM is the ultimate beneficiary of any successful material constitutive model. In this context, although a lot of efforts were made for developing an adequate hyperelasticity model (Sections 3.2.1 and 3.2.2) to represent the elastic behavior of rubber, a direct and reliable use of these models through a robust FEM technique is still hindered to some extent. The main reason behind this delay is due to the higher resistance of rubbers to volumetric deformation than that of distortion deformation (Section 2.2.5) that brings incompressibility in the material. In the FEM analysis, the incompressibility causes an ill-conditioned system of equations, which in other turn brings a disaster in numerical results (Fried and Johnson 1988). To address this problem, the early practice was to use a linearly elastic FEM code with Poisson's ratio was taken as, say, 0.49, whereas the value 0.50 corresponds to an absolute incompressibility condition and produces a singular stiffness matrix (Nicholson et al 1998). However, even in small strain FEM simulation following that approach evoked serious errors in result, specially in highly confined locations of the mesh. To overcome such a problem, single-field penalty methods using some pre-determined penalty parameters were formulated to impose incompressibility conditions (Jankovich et al 1981; Simo and Taylor 1982; Haggblad and Sundberg 1983; Peng and Chang 1997; Sussman and Bathe 1987; Bathe 1996) in computation. However, when applied to practical fields, the penalty approach suffered robustness problem, specially at large-strain simulations (Nicholson et al 1998).

In a further effort, Simo and Taylor (1991) proposed a three field mixed formulation to account for the incompressibility. In the formulation, closed form expressions for tangent moduli were derived and a quasi-incompressible response was accounted through the additive decomposition (Flory 1961) of deformation gradient into volume preserving and dilational parts (Simo et al 1985). The FEM coding of the formulation is now available in standard finite element codes, like FEAP (Taylor 2000).

Amin et al (2000) used FEAP and incorporated Simo's formulation to investigate its applicability in simulating the elastic response of HDR in tension using Ogden hyperelasticity model (Section 3.2.2). The results of the investigation on HDR carried out in the University of Tokyo (Yoshida 1998) were used in this study to verify the applicability of hyperelasticity model. Yoshida tested the dumbbell shaped HDR specimen in tension following a standard testing method for overcoming the edge effects. The interested readers can refer to the main publication for the details of test condition.

Using the test data, the six material parameters needed in Ogden model were determined by a standard method (Finney and Kumar 1987). The parameters were determined and found to be μ_1 = 0.57 MPa, μ_2 = -2.65 x 10^{-10} MPa, μ_3 = 0.06 MPa, α_1 = 2.85, α_2 = 15.00, α_3 = -3.00. Figure 3.2 presents a comparison of the stress-stretch relation with experimental result, where a good conformity is apparent.

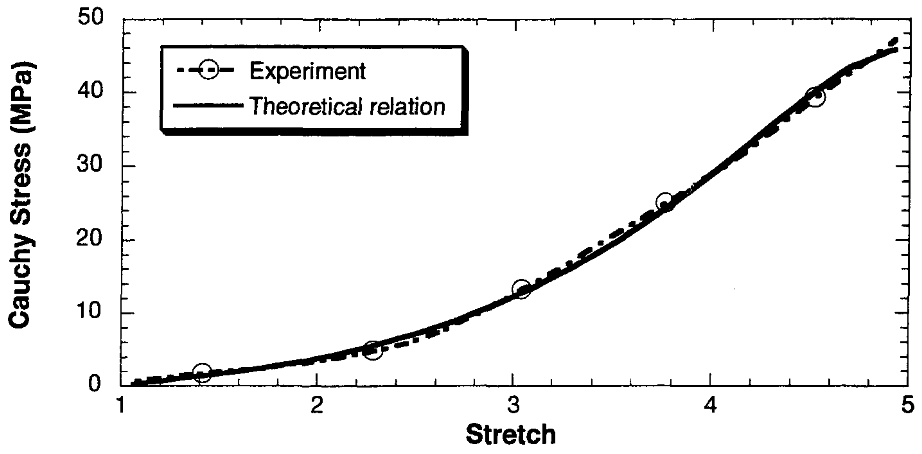

Figure 3.2 Comparison of Ogden stress-stretch relation with experimental data

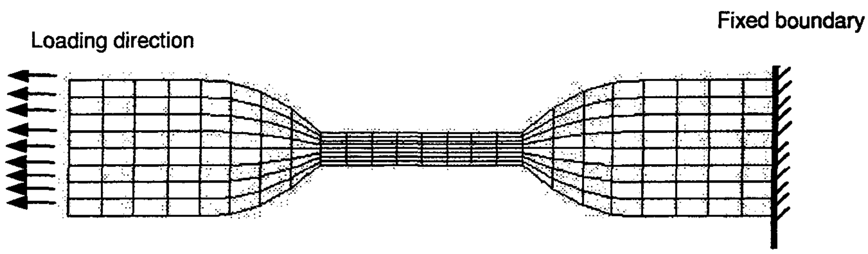

Figure 3.3 FEM mesh of dumbbell specimen with 192 elements.

Finally, for the FEM simulation of the dumbbell testing, the experimental dumbbell shaped specimen was discretized into 192 2-D solid elements. Figure 3.3 presents the FEM mesh and Fig. 3.4 presents the true stress vs. stretch relation obtained from the computation in comparison to experimental observation. The comparison shows marked deviation from the experimental result when the stretch value exceeds 3 i.e. 200% strain. This is a contrast to Fig. 3.2. It may be pointed out here that, in Ogden strain energy formulation, an absolute incompressibility condition was assumed but in the FEM formulation a quasi-incompressible formulation was needed to be used to overcome the ill-conditioning problem associated with the incompressibility. This might be one of the reasons behind this deviation. However, further study in this regard is required to verify this hypothesis.

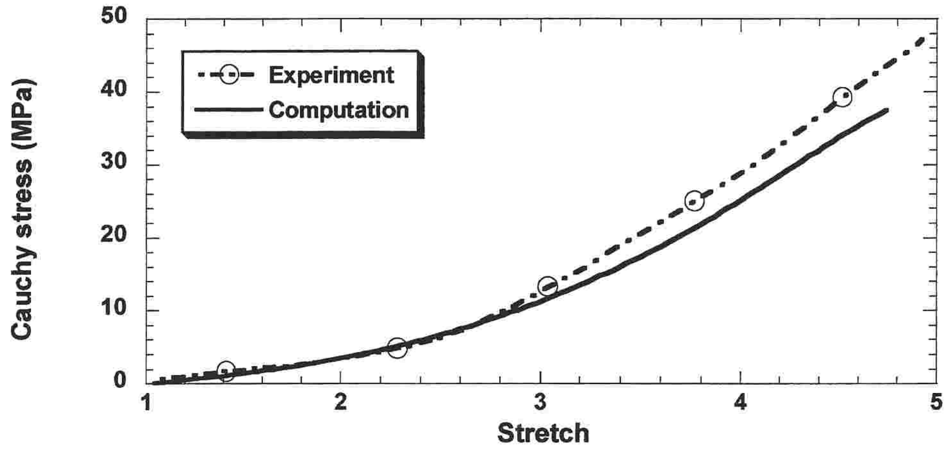

Figure 3.4 Comparative stress-stretch relation as observed from experiments and FEM computation.

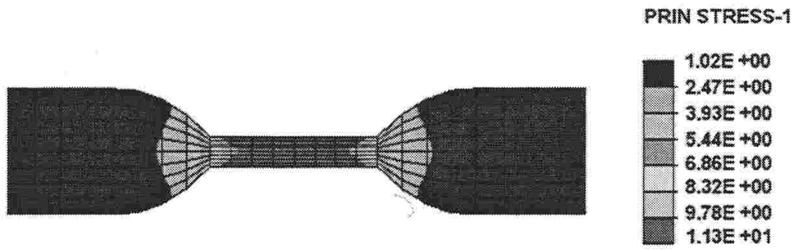

Figure 3.5 Stress contours along the loading direction.

Figure 3.6 Deformed mesh in uniaxial tension loading.

Figure 3.5 presents the stress contours along the loading direction as obtained at 200% strain level. A uniform distribution of stress appears at the central part of the neck. This agrees with the condition assumed in the dumbbell testing. The deformed shape of the mesh is presented in Fig. 3.6, where the large deformation at the neck is distinctly apparent.

3.3 NATURAL AND HIGH DAMPING RUBBER RESPONSES: A COMPARISON

The monotonic compression test results presented in Fig. 2.19 show the typical nonlinear response. When compared between each specimen and different strain rate cases, the nonlinearity was found to be stronger in the HDR at lower stretch levels for the faster strain rate cases. However, for NR-I, it was somewhat weaker. In NR-II, it was almost absent. A similar characteristic feature of the HDR was also noticed in other previous works (Dorfmann and Burtscher 2000; Hernandez 1998).

The characteristic difference in response between NR and HDR has had interpretation from the molecular standpoint. The characteristic difference is attributed to originate from the difference in naturally occurring vulcanization processes followed to produce each material. During vulcanization process in producing HDR, around 31% filler is added (Kelly 1997). The addition of such a high amount of filler creates a large number of bonds of crosslinking within the rubber molecular network (Dorfmann and Burtscher 2000) and incorporates improved energy absorption together with a high initial stiffness feature. In contrast, NR contains lower filler content and therefore the initial stiffness feature is not so prominent. However, in the experiments, the high initial stiffness was found to decrease with increasing strain, and remained approximately constant at the intermediate strain values. The initial reduction of stiffness was mainly associated with breakage of rubber-filler bonds. On the contrary, at large strain values, the stiffness was found to increase once again due to the limited extensibility of polymer chains (Dorfmann and Burtscher 2000). A new strain energy density function is derived in the following section to account for all these aspects from a phenomenological standpoint.

3.4 A NEW STRAIN ENERGY DENSITY FUNCTION

Due to the strong dependence of the stress response on the state of strain, experiments are required to identify an adequate form of W. In this context, tests in uniaxial tension/compression, bi-axial tension and pure shear deformation modes were proposed in the early works of Rivlin and Saunders (1951). The main motivation of conducting tests at different deformation modes was to come up with a W function that is adequate enough in predicting material behavior in different deformation modes. Kawabata et al. (1977, 1981) investigated the dependence of $\partial W/dI_1$ and $\partial W/dI_2$ on I_1 and I_2 using uniaxial and biaxial test data. They showed that $\partial W/dI_1$ and $\partial W/dI_2$ depend only on I_1 and I_2, respectively. This led to the separation of W into two individual functions namely $f(I_1)$ and $g(I_2)$:

$$W(I_1,I_2) = \int f(I_1)dI_1 + \int g(I_2)dI_2 , \tag{3.21}$$

where

$$f(I_1) = \frac{\partial W}{\partial I_1}, \quad g(I_2) = \frac{\partial W}{\partial I_2}.$$

Lambert-Diani and Rey (1999) further considered this notion to propose a general procedure for identifying the strain energy density function. In their work, the effect of the maximum principal stretch, λ_1 on the values of I_1 and I_2 in uniaxial tension, pure shear and equi-biaxial tension modes were considered. It was there concluded that an experiment with either $\lambda_1>1$ or $\lambda_2>1$ is sufficient to determine $f(I_1)$. However, they clarified the necessity of an biaxial experiment with $\lambda_1>1$ and $\lambda_2>1$ for obtaining $g(I_2)$. As far as the prediction of incompressible uniaxial deformation is concerned, it can be seen that from the condition of incompressibility, $I_3=1$ gives $\lambda_2=\lambda_3=\lambda_1^{-1/2}$. Therefore, for uniaxial compression, $\lambda_1<1.0$ gives $\lambda_2>1.0$ which is the sufficient condition to determine $f(I_1)$ as proposed by Lambert-Diani and Rey. In this paper, this condition has been utilized to modify the Yamashita and Kawabata (1992) model and thereby to propose the strain energy function in terms of I_1 for NR and HDR in uniaxial compression. Eq. 3.22 presents the proposed strain energy density relation as a function of I_1:

$$W(I_1) = C_5(I_1-3) + \frac{C_3}{N+1}(I_1-3)^{N+1} + \frac{C_4}{M+1}(I_1-3)^{M+1} \tag{3.22}$$

where, C_5, C_3, C_4, M, and N are material parameters with $N \geq 1.0$ and $0.0 \leq M \leq 1.0$. For uniaxial incompressible deformation, the expression of T_{11E} for the proposed function can be derived from Eq. 3.23 as

$$T_{11E} = 2\left(\lambda_1^2 - \frac{1}{\lambda_1}\right)\left[C_5 + C_3(I_1 - 3)^N + C_4(I_1 - 3)^M\right] \tag{3.23}$$

It should be noted that the first term with coefficient C_5 is a component of original Mooney-Rivlin model (Mooney 1940; Rivlin 1948), while the term with C_3 and N coefficients was proposed by Yamashita and Kawabata to include the hardening feature observed at higher strain levels. In order to incorporate the initial stiffness part, we propose the incorporation of the third term associated with coefficient C_4 and M.

Figure 3.7 presents a comparative representation of $\partial W/\partial I_1$ by the present model for NR-I, NR-II and HDR:

$$\frac{\partial W}{\partial I_1} = \frac{T_{11E}}{2(\lambda^2 - \frac{1}{\lambda})} = C_5 + C_3(I_1 - 3)^N + C_4(I_1 - 3)^M \tag{3.24}$$

The plot indicates the adequacy of the W function over the stretch range with also some improvement at low strain level.

Finally, a comparative representation of elastic responses of NR-I, NR-II, and HDR at slower and faster strain rate cases by the proposed model has been presented in Fig. 3.8. The figures clearly indicate the capability of the proposed model for representing all the features of the response over the strain range. When compared between the specimens, the model is found to perform better in NR specimens because of weaker nonlinearity. On the other hand, in case of stronger nonlinearity of HDR, the performance is a bit lower. This comment is specially true in the low strain region and faster strain-rate case.

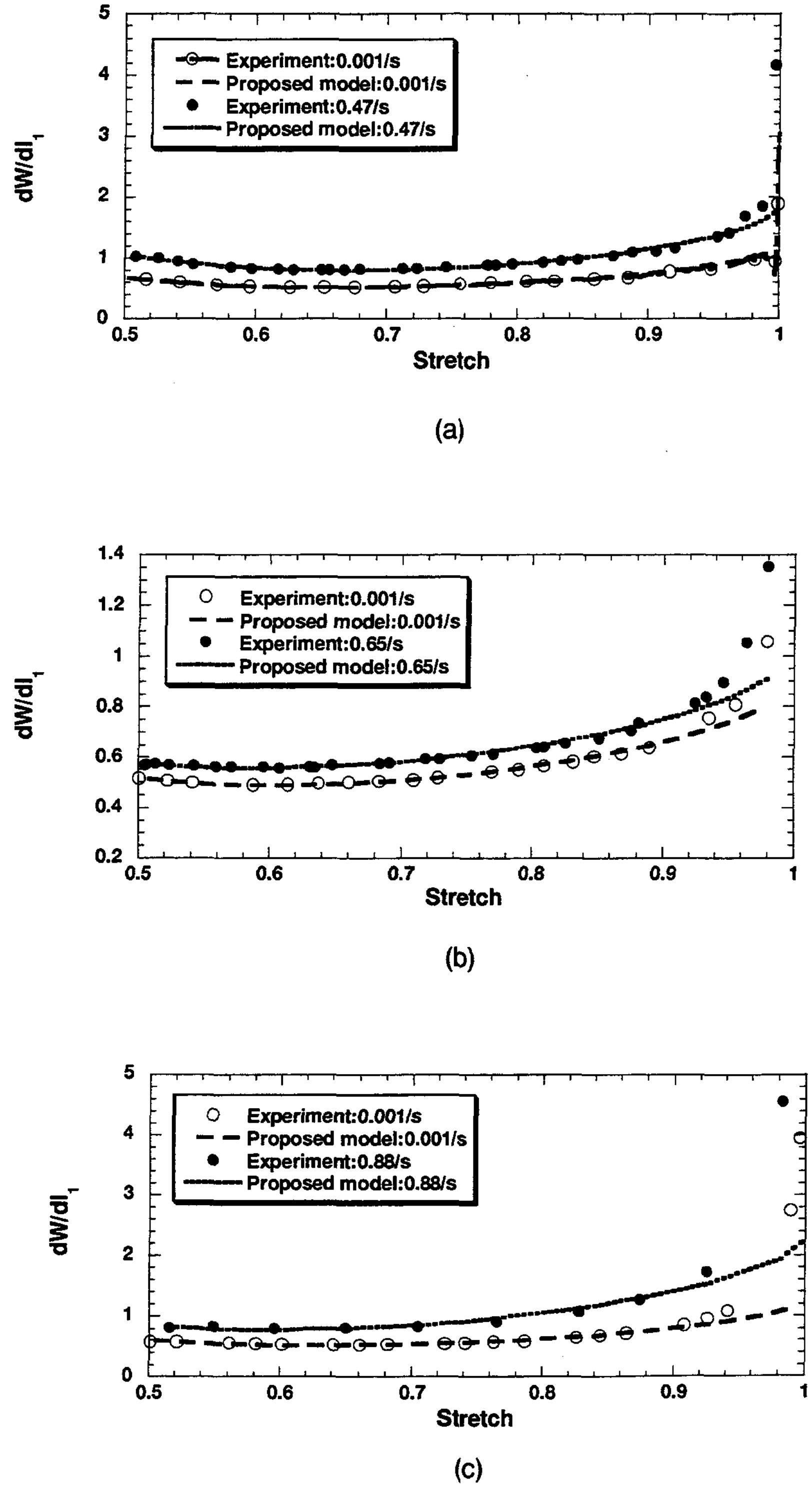

Figure 3.7 Comparative representation of $\partial W/\partial I_1$ by the proposed model at slower and faster strain rates. (a) NR-I, (b) NR-II, (c) HDR.

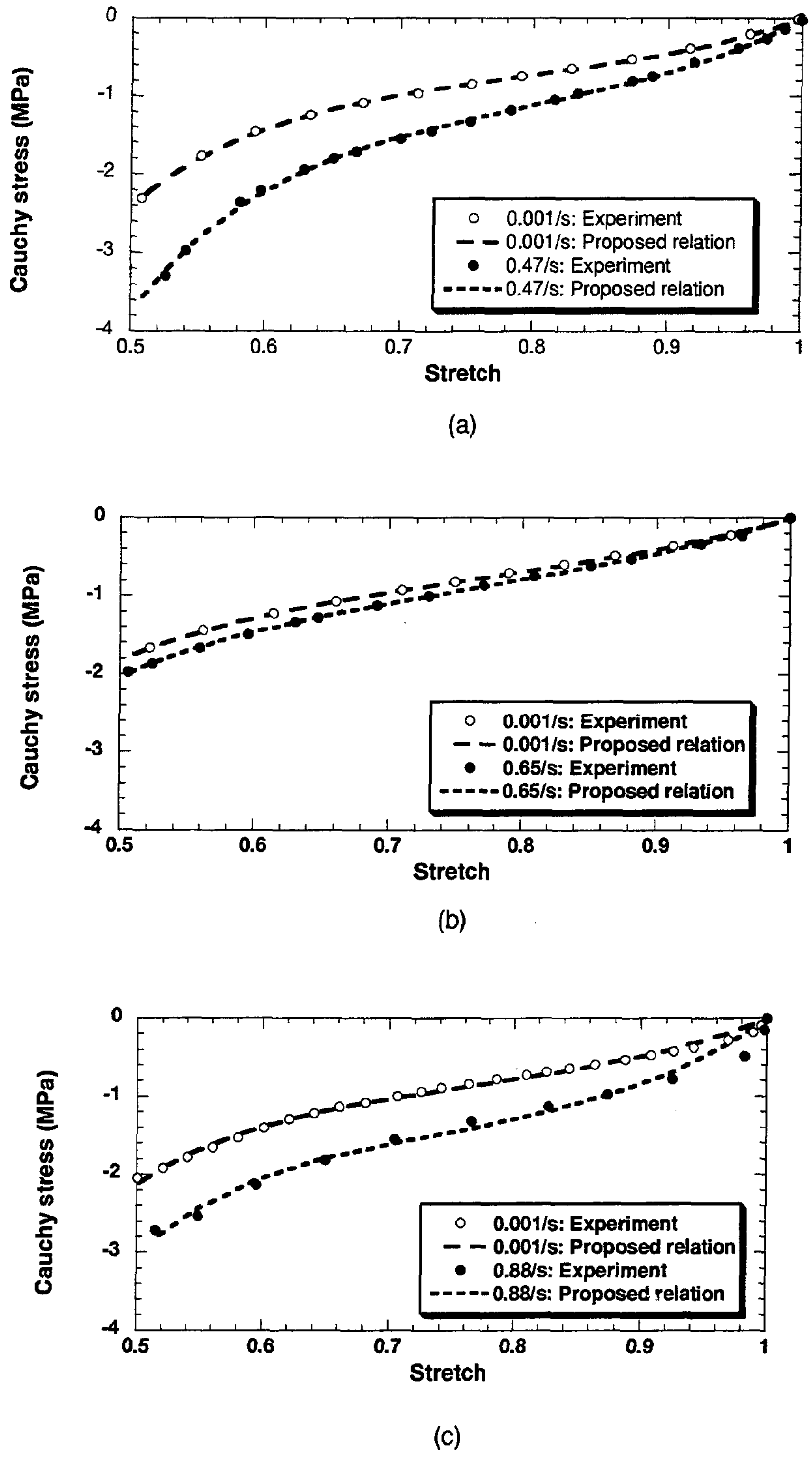

Figure 3.8 Representation of slow and fast strain rate responses by the propose hyperelasticity model (a) NR-I, (b) NR-II, (c) HDR.

3.5 COMPARATIVE PERFORMANCES OF THE PROPOSED AND CONVENTIONAL MODELS

At this moment, the performance of the proposed W relation in comparison to that of the conventional hyperelasticity relations in terms of Error (%) in Cauchy stress (T) prediction was compared, where:

$$\%\mathrm{Error} = \frac{T_{\mathrm{Expt}} - T_{\mathrm{Predicted}}}{T_{\mathrm{Expt}}} x100 \qquad (3.25)$$

Here, the Cauchy stresses obtained from experiments and theoretical prediction are expressed by T_{Expt} and $T_{Prediction}$ respectively.

Figures 3.9 to 3.11 present the performance evaluation results for NR-I, NR-II, and HDR for slower and faster strain rate cases. The comparison indicates the better performance of the proposed and the conventional models in representing the slower strain rate cases than those of faster ones. However, when compared to all the cases, the proposed model was found to perform better than the conventional models in representing the stress-stretch response in low stretch level (up to 0.85) and to display the improvement achievable with the proposed relation. However, above 0.80 stretch levels, all the models were found to show good performance.

3.6 SUMMARY

Due to the low filler content in the traditional NR, the high initial stiffness at a low stretch level is not so prominent. Hence, the available hyperelasticity models developed for the NR cannot adequately represent the high initial stiffness feature of the HDR in the compression regime. The proposed hyperelasticity model on the other turn improves the representation at low stretch levels for both the slow and the higher strain rate cases. The improvement in hyperelasticity modeling at the low stretch level also appears to be significantly promising for NR specimens.

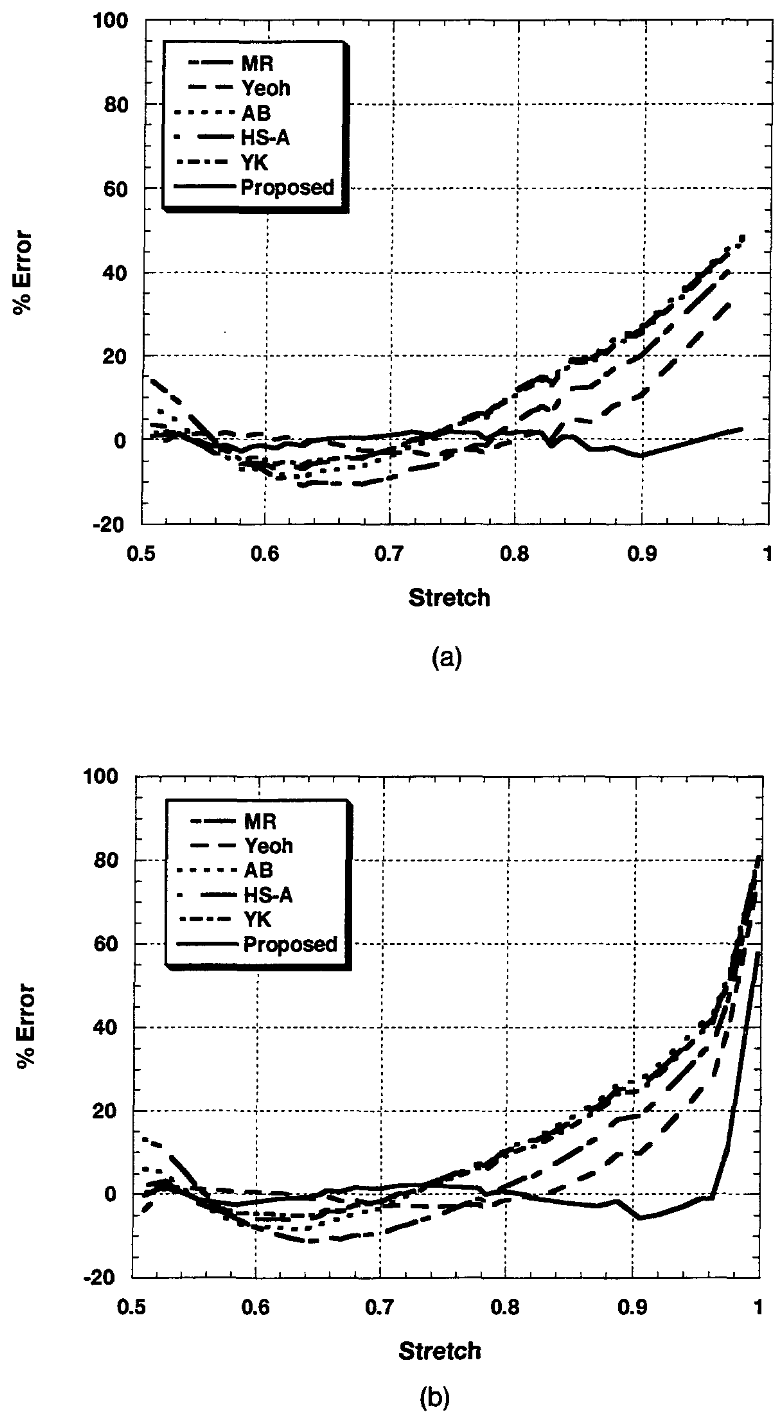

Figure 3.9 Comparative performances of conventional and proposed hyperelasticity models in representing NR-I responses at different strain rates . (a) 0.001/s, (b) 0.47/s. MR: Mooney Rivlin model, Yeoh: Yeoh model, AB: Arruda-Boyce model, HS-A: Hart Smith-Alexander model, YK: Yamashita-Kawabata model, Proposed: Proposed model.

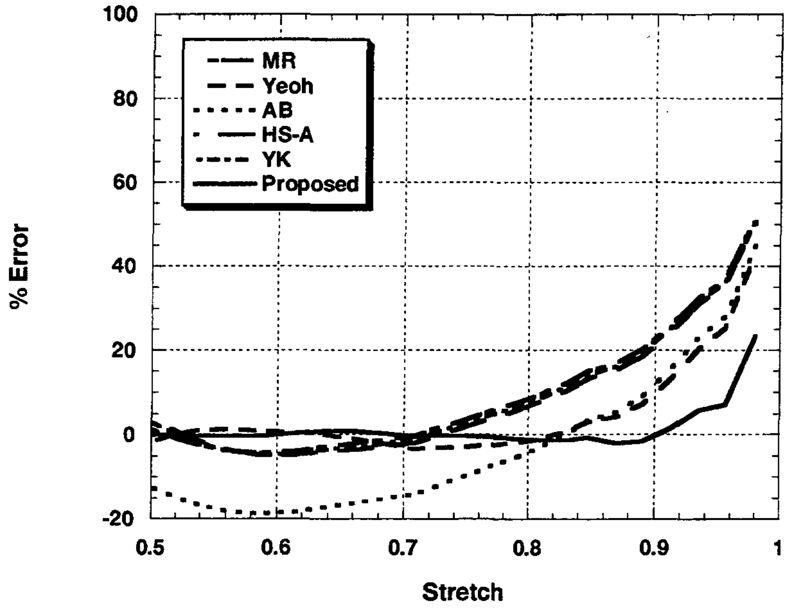

(a)

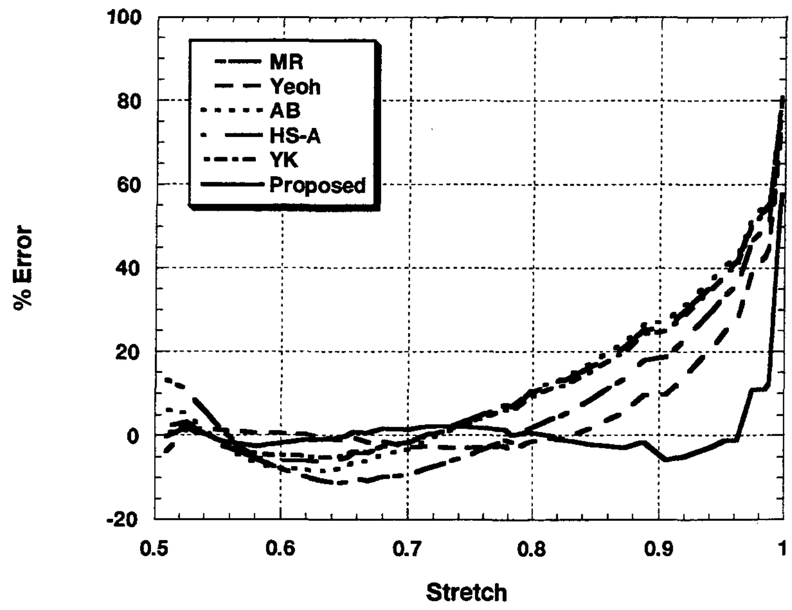

(b)

Figure 3.10 Comparative performances of conventional and proposed hyperelasticity models in representing NR-II responses at different strain rates . (a) 0.001/s, (b) 0.65/s. MR: Mooney Rivlin model, Yeoh: Yeoh model, AB: Arruda-Boyce model, HS-A: Hart Smith-Alexander model, YK: Yamashita-Kawabata model, Proposed: Proposed model.

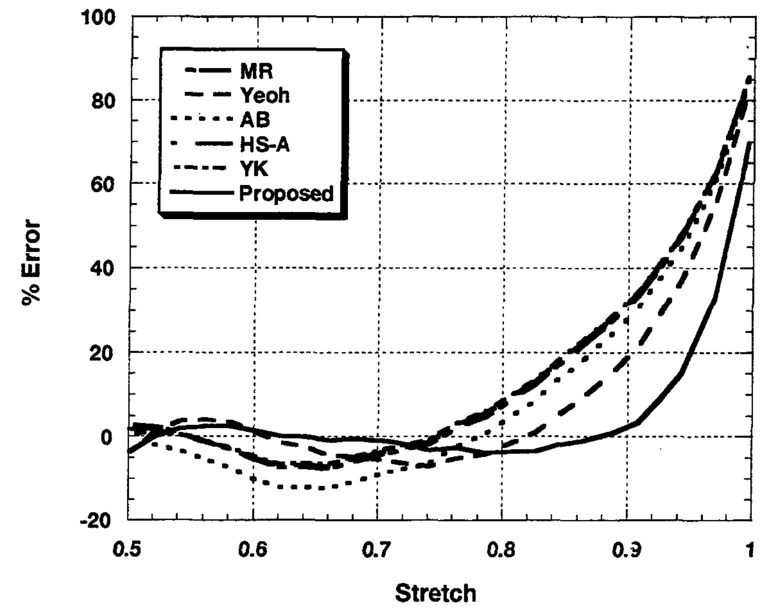

(a)

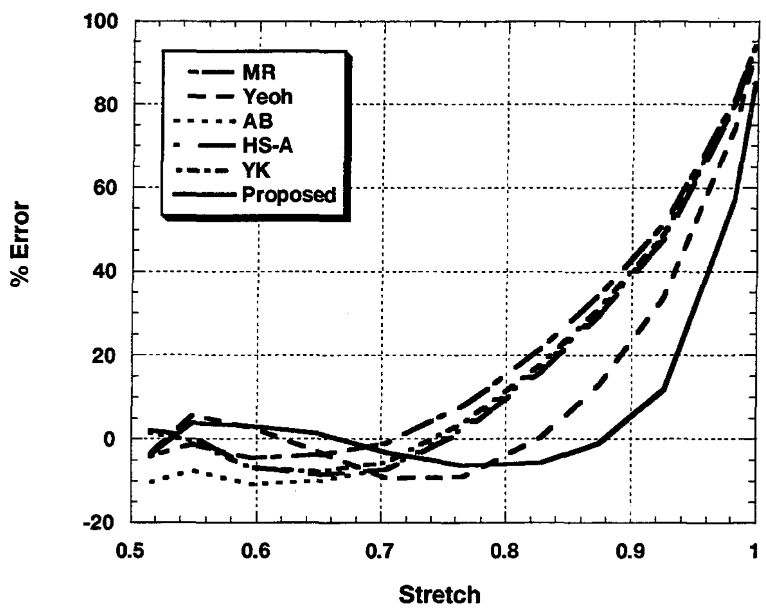

(b)

Figure 3.11 Comparative performances of conventional and proposed hyperelasticity models in representing HDR responses at different strain rates . (a) 0.001/s, (b) 0.88/s. MR: Mooney Rivlin model, Yeoh: Yeoh model, AB: Arruda-Boyce model, HS-A: Hart Smith-Alexander model, YK: Yamashita-Kawabata model, Proposed: Proposed model.

(This page is intentionally left blank)

Chapter 4

Finite Deformation Viscoelasticity Modeling

4.1 GENERAL

The experimental evidences (reported in Chapter 2) indicated the obvious presence of rate-dependent effect in the loading path of the response of NR and HDR. In addition, the significant presence of the hysteresis effect together with the absence of rate-dependent effect was noticed in the unloading path. Therefore, a complete constitutive model representing all these aspects should inevitably contain three model components namely, a hyperelasticity model to account for the nonlinear elastic behavior, a viscosity model to include the viscosity effect, and a damage/plasticity model to describe the hysteresis effect. Nevertheless, a rheological model structure based on the actual material behavior is also required to connect these model components. Moreover, the constitutive model is also required to be formulated on the basis of the finite deformation kinematics in order to account for the large strain effects.

To this end, an improved hyperelasticity model has been proposed (Chapter 3) to model the rate-independent elastic response. However, the model cannot represent the other effects and therefore needs further modeling beyond these efforts. Accordingly, the objective of the present chapter is extended to include the viscosity effect in the constitutive model. In this context, an up-to-date review of the available literatures on modeling the large strain viscoelastic behavior of rubbers was made to choose a suitable finite deformation rate-dependent model structure. The fundamental viscoelastic behavior of solids (Chapter 1) was considered as the main motivation in selecting such a model structure. The proposed hyperelasticity model (Chapter 3) was incorporated into the finite deformation model structure to describe the elastic boundaries, namely, the equilibrium and instantaneous responses (Fig. 1.5). Finally, the behavior of the derived constitutive model in terms of the equilibrium, the instantaneous and the viscoelastic responses was studied. The following sections depict these aspects.

4.2 LITERATURE REVIEW

4.2.1 Initial efforts

Decades ago, the presence of viscosity-induced effects in the response of rubbers was experimentally detected (Greensmith 1960; Dannis 1962; Gent 1962). Yet, the report of any successful attempt on modeling the effect was somewhat delayed. The classical theories of linear viscoelasticity (Flugge 1975) were then the major tools to describe the stress-strain-time relations either in differential or integral forms and to employing Boltzmann superposition principle (Tschoegl 1989). However, application of linear viscoelasticity theories to modeling rubbers could not fetch any successful model because of a strong nonlinearity of the viscoelastic response.

Some investigators tried to overcome such a difficulty by using a modified hyperelastic model and thereby employing time-dependent energy functions (Sullivan et al 1979; Johnson and Stacer 1993; Johnson et al 1993). In other efforts, internal variables were proposed within the strain energy description in continuum mechanics based models (Johnson et al 1994; Quigley and Mead 1994). This approach was also further generalized for finite element implementation (Johnson et al 1995). Subsequently, it was O'Dowd and Knauss (1995) who also attempted to generalize the rubber elastic behavior by using intrinsic relaxation function and strain energy density functional. A similar effort by Spathis (1997) was found, where an internal variable was used for generating theoretical large strain viscoelastic response in uniaxial condition.

However, in general, the choice of all these different kinds of internal variables and associated evolution equations, especially in the case of large deformations were found not to be so evident as well as not unique (Reese and Govindjee 1998a,b). Hence, these approaches failed to find any reasonable physical justification in describing the fundamental viscoelastic behavior (Section 1.3.3).

4.2.2 Micromechanics based approach

Drozdov (1997, 1998) considered the micromechanics of molecular chains in an explicit way to describe the viscoelastic behavior of rubber. The concepts of entanglements in polymer molecules, rates of breakage and reformation were utilized in the formulation of such a model.

In a contemporary work, Park and Schapery (1997) proposed an axisymmetric mechanical model to describe the time- and the temperature-dependent deformation behavior of filled rubber composites with changing microstructure. A rate-type equation was applied to describe the evolution of microstructure due to micro cracking. Subsequently, Ha and Schapery (1998) extended the axisymmetric model for three dimensional stress states.

Bergstrom and Boyce (1998) proposed another micromechanism inspired model to incorporate the time-dependent behavior. The foundation of the model was based on the mechanical behavior that can be decomposed into two parallel branches. The first branch was the equilibrium state that is usually approached during the long time relaxation tests. The second branch of response was incorporated to describe the nonlinear rate-dependent deviation from the equilibrium state. The motion of the molecules having the ability to change the conformation significantly and thereby relaxing the overall stress state was considered as the motivation in employing the second state.

However, in none of these micromechanics-based approaches, the description of instantaneous state response is available.

4.2.3 Phenomenological approach

Gurtin and Herrera (1965) discussed the physical notion for describing the viscoelastic material properties in terms of the instantaneous and the equilibrium responses (Section 1.3.3). Subsequently, Krempl (1987); Lubliner (1985); Tsakmakis (1996); and Lion (1996, 1997) conceived and used the idea to express the increase in response with increasing strain rate and subsequent approach of the material towards instantaneous state. The 'overstress concept' in the phenomenological model forms the basis of the advanced phenomenological theories at the present days.

To this end, the finite linear viscoelasticity theories were proposed by a number of researchers. For example, the initial works of Christensen (1980); Le Tallec et al (1993) can be referred. The equations of evolution belonging to this range of theories were the linear differential equations with non-constant coefficients like deformation dependent relaxation times. The theories of this range were capable of taking account of large perturbations away from the equilibrium state, and those theories therefore offered a more general constitutive model. Simo (1987) presented one of the first finite element implementation of such theories using the 'over-stress' as an internal variable. The finite viscoelasticity was also discussed in detail in Haupt (1993) whereas Lion (1997) further developed the theory into a practically usable finite viscoelastic material model and simulated the experimental results.

Reese and Govindjee (1998a,b) studied further on this theory to come up with a compressible version of a finite viscoelastic law. They also proposed nonlinear evolution laws for material viscosity and included thermal effects on the viscosity property through such evolution laws. Holzapfel and Simo (1996) as well as Holzapdel (1996) presented other information in terms of internal variables to account for the thermal changes into the material viscosity in three dimension and subsequent finite element implementation. Miehe and Keck (2000) also exploited the overstress feature in their model and used the nonlinear evolution laws for material viscosity.

Finally, a simpler version of finite deformation viscoelasticity law came to light through the work of Huber and Tsakmakis (2000) for incompressible materials subjected to isothermal deformation. Based on the objectives and the subsequent experimental observations of the present research, the finite deformation rate-dependent model proposed by Huber and Tsakmakis (2000) was employed to derive the rate-dependent constitutive model for NR and HDR. The salient features of the model are presented in the following sections.

4.3 FINITE DEFORMATION KINEMATICS: PRILIMINERY DEFINITIONS

This section deals with the kinematics of finite deformation to study the motion of a body. In the kinematics, the relationship of the elemental vectors in undeformed and deformed configurations is described by the deformation gradient tensor $\mathbf{F}$.

As a general measure of deformation, the right and the left Cauchy Green deformation tensors $\mathbf{C}$ and $\mathbf{B}$ are defined respectively as:

$$\mathbf{C} = \mathbf{F}^T\mathbf{F} \tag{4.1}$$

$$\mathbf{B} = \mathbf{F}\mathbf{F}^T \tag{4.2}$$

Here the superscript 'T' denoted the transpose of the second order tensor. The Lagrangian or Green tensor, **E** is expressed as:

$$\mathbf{E} = \frac{1}{2}(\mathbf{C}-\mathbf{1}) \tag{4.3}$$

where $\mathbf{1}$ is an identity second-order tensor. The Cauchy stress and weighted Cauchy stress are denoted by $\mathbf{T}$ and $\mathbf{S}$, respectively, where:

$$\mathbf{S} = (\det\mathbf{F})\mathbf{T} \tag{4.4}$$

However, for incompressible materials, the condition $\det\mathbf{F} = \mathbf{1}$ implies, $\mathbf{S} = \mathbf{T}$.

Furthermore, the velocity gradient tensor, $\mathbf{L}$ is defined as:

$$\mathbf{L} = \dot{\mathbf{F}}\mathbf{F}^{-1} = \mathbf{D} + \mathbf{W}, \quad \mathbf{D} = \frac{1}{2}\left(\mathbf{L}+\mathbf{L}^T\right) \quad \mathbf{W} = \frac{1}{2}\left(\mathbf{L}-\mathbf{L}^T\right) \tag{4.5}$$

Here, the 'dot' over $\mathbf{F}$ stands for its material time derivative. For incompressible materials and uniaxial loading, the tensors $\mathbf{F}$, $\mathbf{B}$, $\mathbf{B}^{-1}$, $\mathbf{L}$ and $\mathbf{S}$ are given by:

$$F_{ij} = \begin{pmatrix} \frac{l}{l_0} & & \\ 0 & \sqrt{\frac{l_0}{l}} & \\ 0 & & \sqrt{\frac{l_0}{l}} \end{pmatrix} = \begin{pmatrix} e^{\zeta} & 0 & 0 \\ 0 & e^{-(\zeta/2)} & 0 \\ 0 & 0 & e^{-(\zeta/2)} \end{pmatrix} \tag{4.6}$$

$$B_{ij} = \begin{pmatrix} e^{2\zeta} & 0 & 0 \\ 0 & e^{-\zeta} & 0 \\ 0 & 0 & e^{-\zeta} \end{pmatrix}, \quad B^{-1}{}_{ij} = \begin{pmatrix} e^{-2\zeta} & 0 & 0 \\ 0 & e^{\zeta} & 0 \\ 0 & 0 & e^{\zeta} \end{pmatrix} \tag{4.7}$$

$$L_{ij} = \begin{pmatrix} \dot{\zeta} & 0 & 0 \\ 0 & -\frac{\dot{\zeta}}{2} & 0 \\ 0 & 0 & -\frac{\dot{\zeta}}{2} \end{pmatrix} \tag{4.8}$$

$$S_{ij} = \begin{pmatrix} \sigma & 0 & 0 \\ 0 & 0 & 0 \\ 0 & 0 & 0 \end{pmatrix} \tag{4.9}$$

where, $l=l(t)$, $l_o=l$ $(t=0)$, $\zeta=\zeta(t)=\ln(l/l_o)$,and $\sigma=\sigma(t)$. Here, l stands for the length of the specimen at time, t.

4.4 A RATE-DEPENDNET MODEL STRUCTURE

4.4.1 Model configuration

A three-parameter parallel model illustrated in Fig. 4.1 was considered. Although the linear spring elements are used in the standard three-parameter model for linear viscoelasticity, hyperelasticity formulation presented in Chapter 3 was employed in the present three-parameter model to represent the nonlinear elastic behavior of each spring element. For the dash–pot element, the conventional linear viscosity was assumed in the present investigation for simplicity. In this model, the hyperelastic element A represented the equilibrium response. The other branch consisting of hyperelastic element B and viscous dash-pot C represented the over-stress feature resulting from the rate-dependent effect. The total strain ε was decomposed into elastic strain e_e and inelastic strain e_i components.

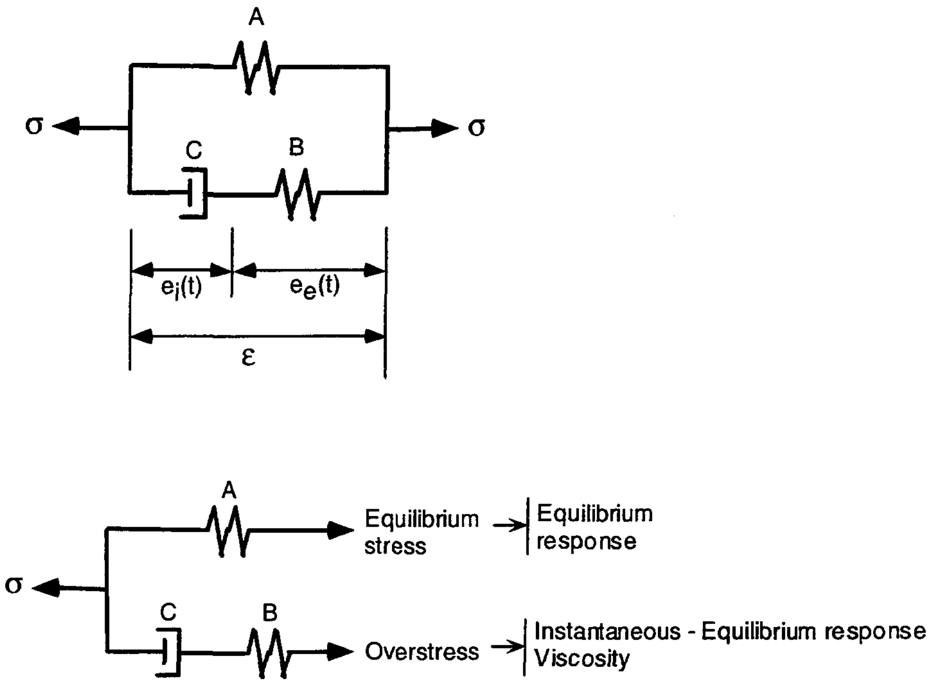

Figure 4.1. Three-parameter parallel model.

4.4.2 Description of elasticity

In the hyperelasticity under the assumption of isotropy, the stress-strain relationship was derived from a strain energy density function W which was expressed either in terms of the strain invariants or principal stretches (Chapter 3). To this end, an improved strain-invariant based hyperelasticity model was proposed (Eqs. 3.22 and 3.23). In this course, each spring element (Fig. 4.1) was modeled in terms of hyperelasticity relation. The equilibrium Cauchy stress, $T_E^{(E)}$ and overstress, $T_E^{(OE)}$ were expressed as follows:

$$
\begin{aligned}
T_E^{(E)} &= \frac{\partial W^{(E)}}{\partial \varepsilon}, \quad \text{for spring A} \\
T_E^{(OE)} &= \frac{\partial W^{(OE)}}{\partial e_e}, \quad \text{for spring B}
\end{aligned}
\qquad (4.10)
$$

4.4.3 Introduction of viscosity

The stress and strain components of the three-parameter parallel model (presented in Fig. 4.1) were converted into a finite deformation model following the formulation of Huber and Tsakmakis (2000). The finite deformation model was formulated under the framework of multiplicative decomposition of the deformation gradient tensor, $\mathbf{F}$. The deformation gradient tensor was decomposed into:

$$\mathbf{F} = \mathbf{F_e F_i} \tag{4.11}$$

where, $\mathbf{F}_e$ and $\mathbf{F}_i$ are the deformation gradients associated with e_e and e_i, respectively. There $\mathbf{F}_i$ component introduced an intermediate equilibrium configuration. Such a configuration is resulted, when the stress is unloaded at an infinitely fast rate to an equilibrium state at constant value of $\mathbf{F}_i$ during the unloading process. Such an unloading process is local, hence, neither $\mathbf{F}_e$ nor $\mathbf{F}_i$ components needs to satisfy global compatibility conditions.

Subsequently, the stress was decomposed into distortional part and volumetric part according to the proposal of Flory (1961). This led to the expression of the Cauchy stress tensor $\mathbf{T}$ and rate of left Cauchy-Green deformation tensor $\mathbf{B}$ as follows:

$$\begin{aligned}
\mathbf{T} &= -p\mathbf{1} + \mathbf{T_E} \\
\mathbf{T_E} &= \mathbf{T_E^{(E)}} + \mathbf{T_E^{(OE)}} \\
\mathbf{T_E^{(E)}} &= 2\frac{\partial W^{(E)}}{\partial \mathbf{I_{1B}}}\mathbf{B} - 2\frac{\partial W^{(E)}}{\partial \mathbf{I_{2B}}}\mathbf{B}^{-1} \\
\mathbf{T_E^{(OE)}} &= 2\frac{\partial W^{(OE)}}{\partial \mathbf{I_{1Be}}}\mathbf{B_e} - 2\frac{\partial W^{(OE)}}{\partial \mathbf{I_{2Be}}}\mathbf{B_e}^{-1} \\
\dot{\mathbf{B}}_e &= \mathbf{B_e L^T} + \mathbf{LB_e} - \frac{2}{\eta}\mathbf{B_e}\left(\mathbf{T_E} - \mathbf{T_E^{(E)}}\right)^D
\end{aligned} \tag{4.12}$$

where, p is the hydrostatic pressure of $\mathbf{T}$ and sub-script 'E' denotes the extra part of corresponding stress tensor. $\mathbf{1}$ is the identity tensor. The subscript 'e' denotes the quantities related to $\mathbf{F}_e$. $\mathbf{L}$ is the velocity gradient tensor. Superscript 'D' denotes the deviatoric part of stress. The subscripts B and Be denote the parts of the strain-invariants associated with e_e and e_i, respectively. η is the material viscosity represented by the dash-pot.

4.5 INCORPORATION OF THE PROPOSED HYPERELASTICITY LAW INTO THE MODEL STRUCTURE

In deriving the explicit expressions for $\mathbf{T}$ and rate of $\mathbf{B}_e$, the hyperelasticity function presented in Eq. 4.12 was used together with Eq. 3.22. Eq. 4.13 presents the final form of the $\mathbf{T}$ and the rate of $\mathbf{B}_e$.

$$\begin{aligned}
\mathbf{T} &= -p\mathbf{1} + 2C_5^{(E)}\mathbf{B} + 2C_3^{(E)}(\mathbf{I}_{1\mathbf{B}}-3)^{N^{(E)}}\mathbf{B} + 2C_4^{(E)}(\mathbf{I}_{1\mathbf{B}}-3)^{M^{(E)}}\mathbf{B} + \\
&\quad 2C_5^{(OE)}\mathbf{B}_e + 2C_3^{(OE)}(\mathrm{I}_{1\mathrm{B}}-3)^{N^{(OE)}}\mathbf{B}_e + 2C_4^{(OE)}(\mathrm{I}_{1\mathrm{B}}-3)^{M^{(OE)}}\mathbf{B}_e \\
\dot{\mathbf{B}}_e &= \mathbf{B}_e\mathbf{L}^T + \mathbf{L}\mathbf{B}_e - \\
&\quad \frac{4}{\eta}\mathbf{B}_e\left(C_5^{(OE)}\mathbf{B}_e + C_3^{(OE)}(\mathbf{I}_{1\mathbf{B}}-3)^{N^{(OE)}}\mathbf{B}_e - C_4^{(OE)}(\mathbf{I}_{1\mathbf{B}}-3)^{M^{(OE)}}\mathbf{B}_e\right)^D
\end{aligned} \tag{4.13}$$

The material parameters of the proposed model expressed in Eq. 4.13 are summarized (Table 4.1).

Table 4.1 Material parameters

Response components	Material Parameters				
Equilibrium stress	$C_5^{(E)}$	$C_3^{(E)}$	$C_4^{(E)}$	$M^{(E)}$	$N^{(E)}$
Overstress	$C_5^{(OE)}$	$C_3^{(OE)}$	$C_4^{(OE)}$	$M^{(OE)}$	$N^{(OE)}$
Viscosity	η				

4.6 MODEL BEHAVIOR IN UNIAXIAL COMPRESSION

The incorporation of the proposed hyperelasticity relation has completed the modification of the Huber and Tsakmakis (2000) model for the present purpose. At this moment, the behavior of the derived model with the change of viscosity parameter and applied strain rate was studied in a qualitative way. The motivation for presenting this study is to examine the behavior of the resulting model when subjected to some standard strain histories. Table 4.2 presents the qualitative values of elastic parameters used in the study. The model was implemented using MATHEMATICA© (Wolfram 1999).

Table 4.2. Elastic material parameters for qualitative study of model behavior

Responses	C_5	C_3	C_4	M	N
	MPa	MPa	MPa		
Equilibrium	80.0	20.0	-60.0	0.25	1.00
Overstress	180.0	70.0	-180.0	0.25	1.00

4.6.1 Effect of viscosity parameter

In order to investigate the effect of viscosity parameter on the model response, the value of η was varied in numerical experiments with step strain followed by relaxation hold times. Figure 4.2 presents the applied stretch history and obtained deformation history related to $\mathbf{B}_e$ from the model for η = 300 MPa-s and 900 MPa-s respectively. The delayed response in $\mathbf{B}_e$ with the increase of η is clearly noted from the model results. In addition, with the increase of η, the magnitude of response of instantaneous response of $\mathbf{B}_e$ component also increased significantly. This is also directly associated with the delayed response feature to highlight the effect of viscosity represented by the dashpot. Figure 4.3 presents the obtained stress histories for different η values. In the following section, the strain-rate dependency feature introduced in the model due to the viscosity modeling will be further investigated.

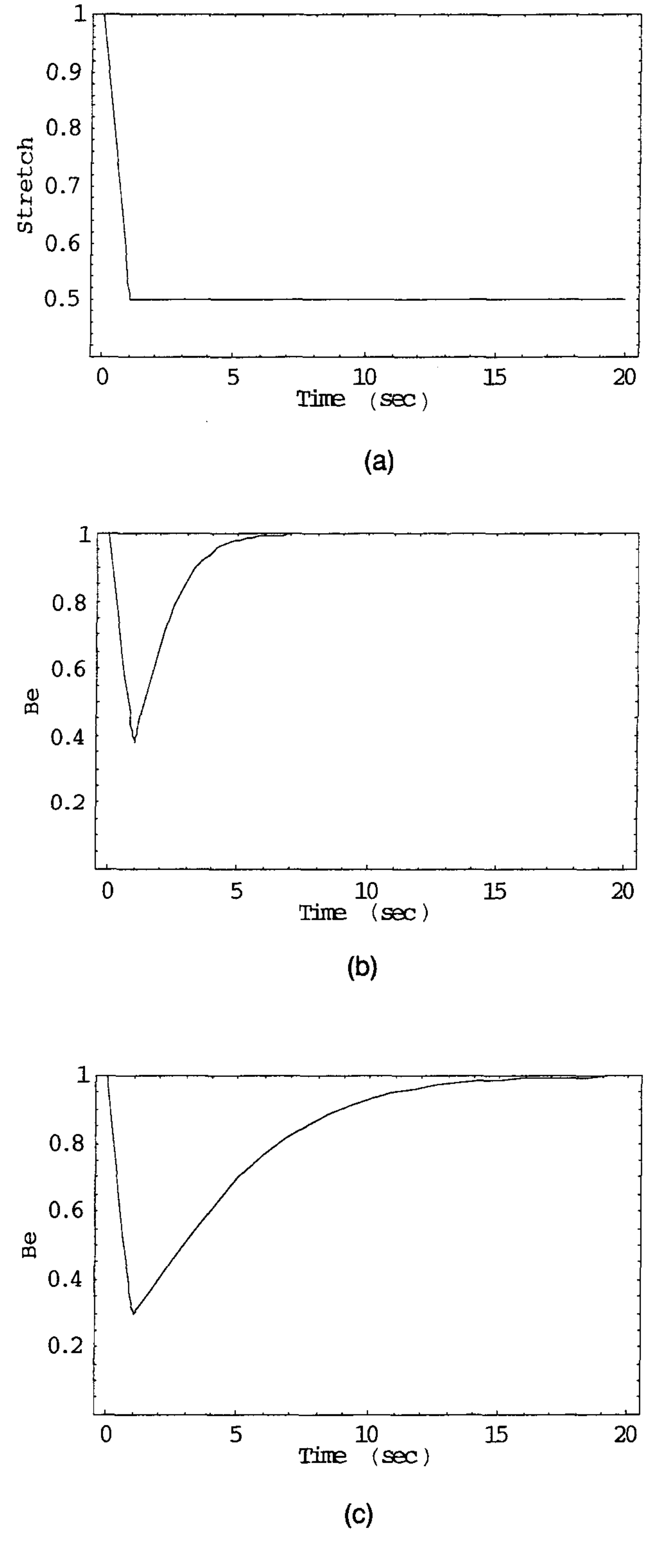

Figure 4.2 Effect of viscosity parameter on the model behavior. (a) Applied stretch history; (b) Obtained $\mathbf{B}_e$ history for η = 300 MPa-s; (c) Obtained $\mathbf{B}_e$ history for η = 900 MPa-s.

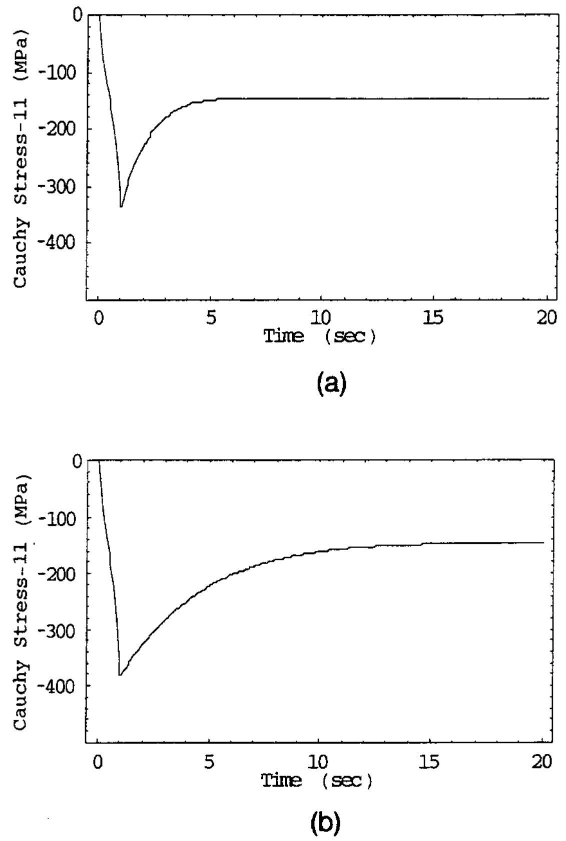

Figure 4.3 Effect of viscosity parameter on the model behavior. (a) Obtained stress history for η = 300 MPa-s; (b) Obtained stress history for η = 900 MPa-s.

4.6.2 Effect of strain rate

Figure 4.4 to 4.8 present the applied stretch history, the corresponding stress history and the stress-stretch responses. The comparison of these figures clearly shows the increase in stress response in the loading path with the increase of applied strain rate. This must be due to the viscosity effect represented by the model.

However, when the unloading paths at different strain rates are considered, the model showed some other features. At slower strain rate of 0.001/s (Fig. 4.4), the unloading response of the model was found to approach the loading path, while at intermediate strain rates like 0.025/s (Figs. 4.5) and 0.075/s (Fig. 4.6), the unloading responses were found to shift significantly from the loading response due to viscosity effect. However, at the faster strain rates like 0.25/s (Fig. 4.7) and 1.0/s (Fig. 4.8), due to the approach of the instantaneous state, the unloading response again tends to merge with the loading response.

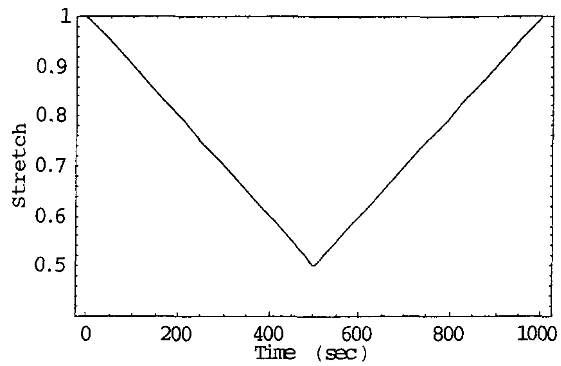

(a)

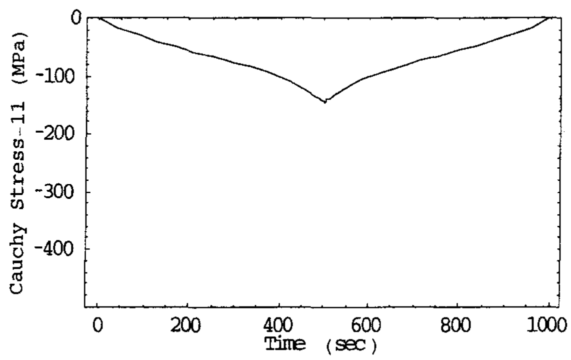

(b)

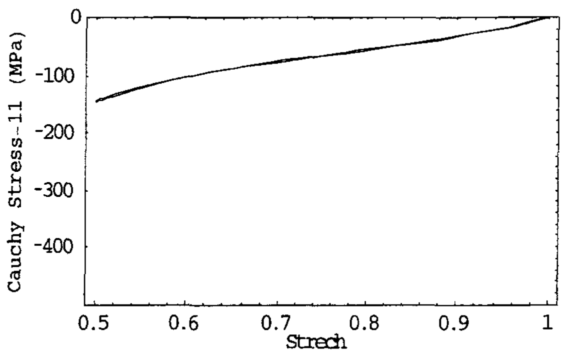

(c)

Figure 4.4 Cyclic response obtained from the model at 0.001/s strain rate. (a) Applied stretch history; (b) Obtained stress history; (c) Obtained Stretch-stress response

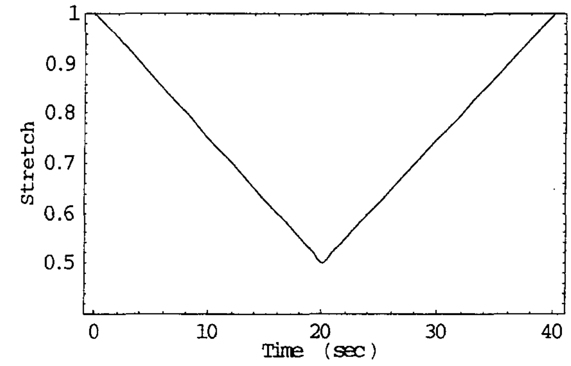

(a)

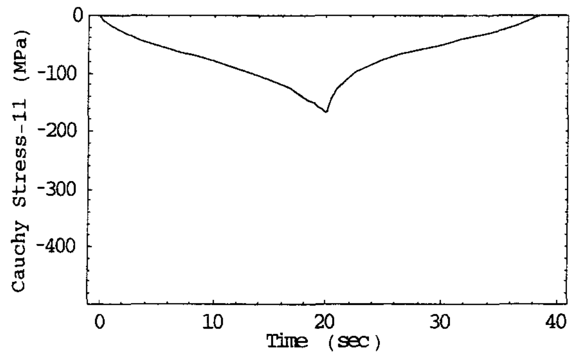

(b)

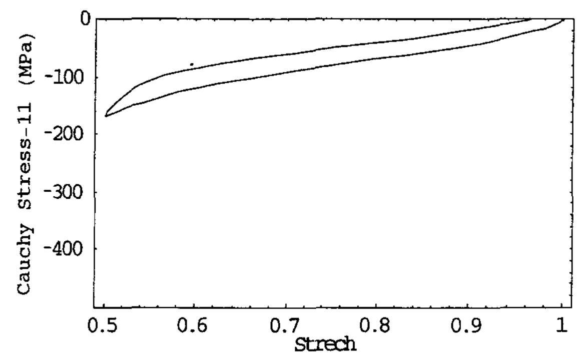

(c)

Figure 4.5 Cyclic response obtained from the model at 0.025/s strain rate. (a) Applied stretch history; (b) Obtained stress history; (c) Obtained Stretch-stress response

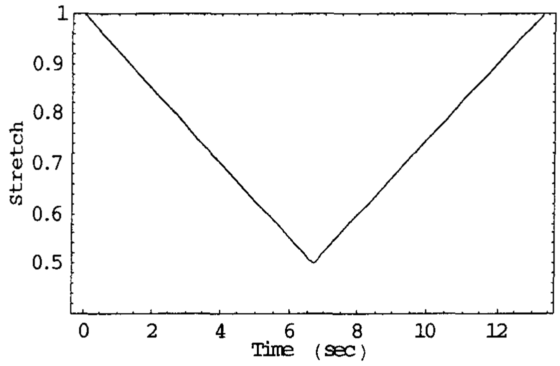

(a)

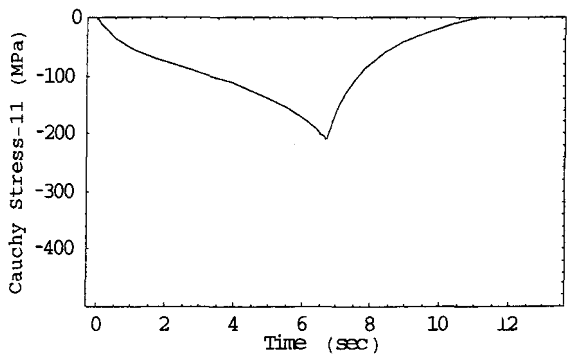

(b)

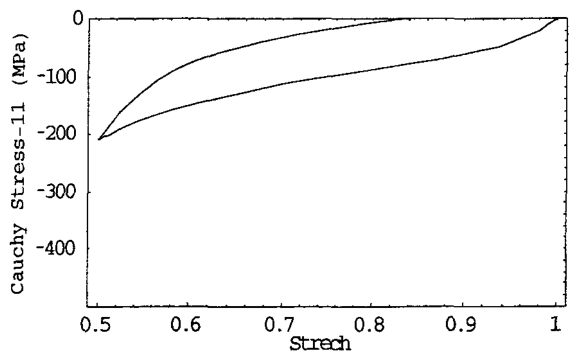

(c)

Figure 4.6 Cyclic response obtained from the model at 0.075/s strain rate. (a) Applied stretch history; (b) Obtained stress history; (c) Obtained Stretch-stress response

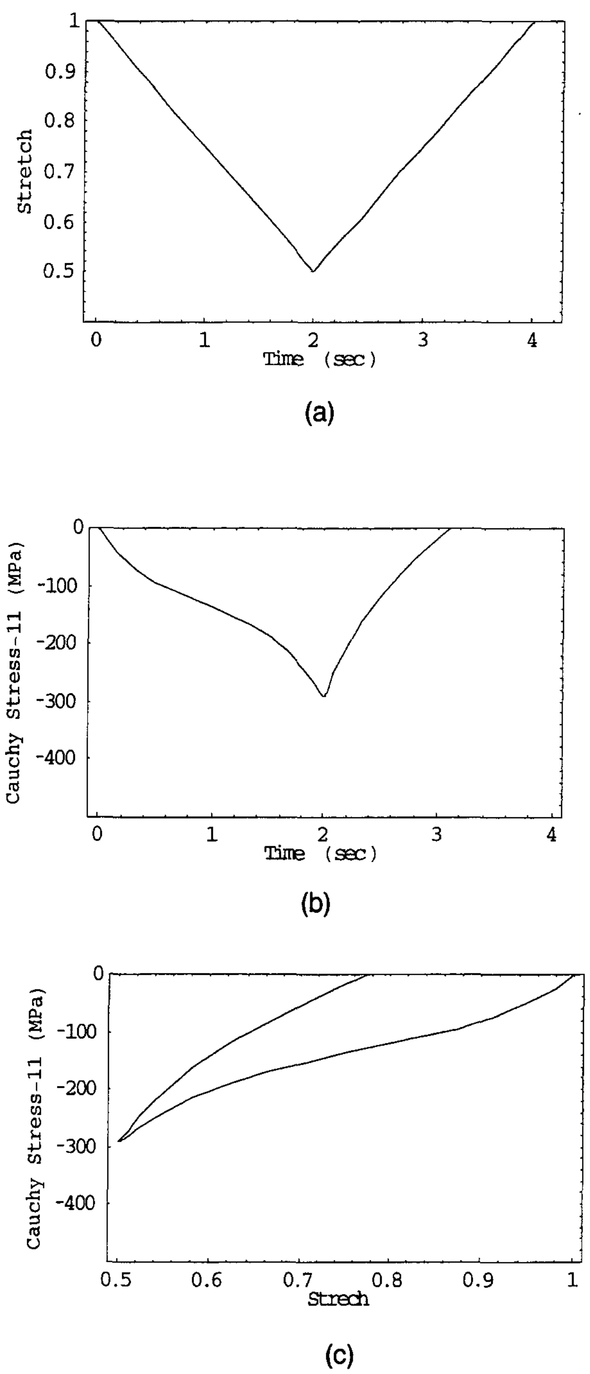

Figure 4.7 Cyclic response obtained from the model at 0.25/s strain rate. (a) Applied stretch history; (b) Obtained stress history; (c) Obtained Stretch-stress response

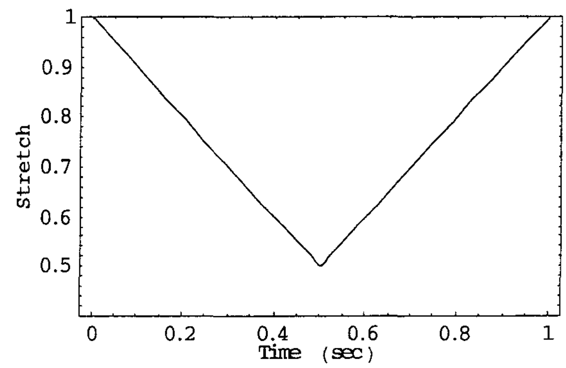

(a)

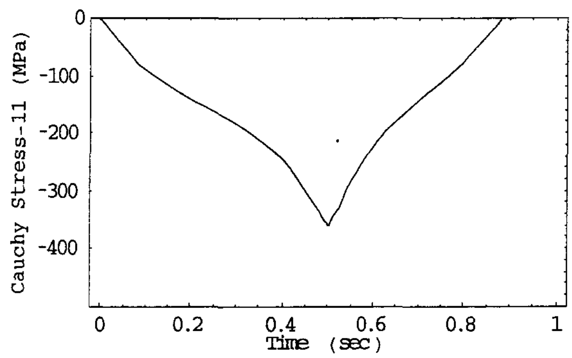

(b)

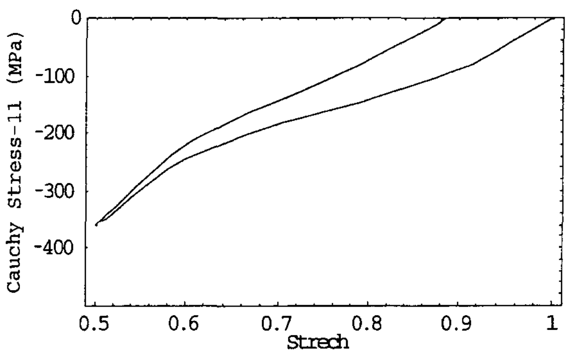

(c)

Figure 4.8 Cyclic response obtained from the model at 1.0/s strain rate. (a) Applied stretch history; (b) Obtained stress history; (c) Obtained Stretch-stress response

(This page is intentionally left blank)

Chapter 5

Parameter Identification

5.1 GENERAL

The identification of material parameters is one of the major requirements for the successful application of any constitutive model to practical problems. The model parameters represent the material properties in a quantitative way and therefore need to be identified from an explicit experimental scheme (Haupt 1993). Hence the objective of any experimental technique is targeted to achieve a picture of specimen's behavior that is complete in the context of the specified constitutive model.

To this end, the experimental observations presented in Chapter 2 have portrayed the fundamental rate-dependent property of NR and HDR, while Chapters 3 and 4 have presented the construction of a constitutive model derived from the physical viewpoint of materials' viscoelastic behavior. At this stage, the interest of the work focuses on identifying the model parameters in a specific way based on the experimental data. The following section presents a review of the existing parameter identification procedures of viscoelastic solids and highlights their physical limitations. Following the review, a step-by-step method of identifying the elasticity and the viscosity parameters for the proposed constitutive model has been presented.

5.2 LITERATURE REVIEW

The up-to-date literatures on the viscoelasticity modeling were reviewed in Section 4.2, where the initial modeling efforts using the modified hyperelasticity relations with time dependent internal variables (Section 4.2.1) and the micromechanics-based modeling approaches (Section 4.2.2) were recorded. However, the review indicated that the models developed on the basis of these approaches could not comprehensively take into account the elastic responses and the viscosity effect (Section 1.3.3). These models thus suffered a lacking in originality from the physical viewpoint.

On the other hand, the phenomenological approaches based on the overstress concept presented in Section 4.2.3 provided some means to express the physical aspects of the viscoelastic material. Hence, the models derived in that approach contained three groups of material parameters describing the instantaneous response, the equilibrium response, and the viscosity effect. In this context, the suggestive approaches to identify the parameters are summarized in the following paragraphs.

Lion (1996, 1997) conducted some monotonic experiments in tension and compression at different strain rates (0.0002/s to 0.2/s) to observe the viscoelastic effect. In some other monotonic tests carried out at 0.2/s, a series of hold times were inserted at different strain levels to allow the specimens to relax for removing the viscosity effect. In the monotonic tests, Lion found the stress to increase nonlinearly with increasing applied strain rate. Whereas in the test with hold times, he found the stresses to relax to some time-independent equilibrium states at the respective strain levels. The connecting curve of these equilibrium states was defined as the equilibrium stress strain curve. The difference between the 'total' stress and the equilibrium stress was regarded as the overstress. However, the appearance of the instantaneous state was neither noticed nor clarified in those experiments and discussion. Subsequently Lions (1997) frankly stated that he relied on a lot of experiences in combination with a large number of numerical simulations and comparisons with experimental data to determine all the model parameters. The contemporary information of Holzapfel (1996); Reese and Govindjee (1998a, b); Miehe and Keck (2000) also entirely depended on the numerical trials to find some material parameter values that could represent the respective experimental observations. However, the estimation of material parameter values from numerical trials and comparing the data obtained from the experiments performed in the middle of the viscous domain (Fig. 1.5) carries only a very little physical meaning.

On the other hand, although the continuum-mechanics-based formulations of Lubliner (1985); Holzapfel and Simo (1996); Huber, and Tsakmakis (2000) included the consideration of the equilibrium state, the instantaneous state and the viscosity effect, such a theoretical work could not throw any light in regard to the parameter identification procedure. Subsequently, the application of these models in practical problems was stalled. Hence, attention was given in the following sections to proposing a parameter identification scheme for identifying the elasticity and the viscosity parameters from explicit experimental observations.

5.3 IDENTIFICATION OF ELASTICITY PARAMETERS

The equilibrium response and the instantaneous response bound the viscosity domain. These two are elastic responses and they need to be identified by experiments. Once, these two boundary states are reached, the identification of viscosity parameter lies just at a step away. The experimental identification of equilibrium response and the instantaneous response therefore lie at the core of the identification of elasticity parameters. In order to identify the elastic parameters, the responses obtained from the loading paths of the cyclic compression and the monotonic tension tests at different strain rates along with the cyclic relaxation tests are considered here once again to identify the elastic boundary states.

5.3.1 Identification of elastic boundary states

Figure 5.1 presents the loading paths obtained at different strain rates in the cyclic compression tests described in Section 2.6.3. A comparison of the curves at different strain rate cases in each specimen shows that with increasing strain rate, the stresses increase due to viscosity effect. At higher strain rates, however, a diminishing trend in the increase of stress response was observed indicating the approach of an instantaneous state in each specimen. Consequently, the stress response of NR-I obtained at and over 0.47/s strain rate can be considered as the neighborhood of instantaneous state boundary of viscous domain (Fig. 1.5). In NR-II and HDR the corresponding strain rates are 0.072/s and 0.47/s.

To get a clearer picture of the viscous domain, the equilibrium loci of the loading path (presented in Section 2.6.5) are compared here with stress-stretch response in different strain rate cases. Invariably, these loci represent the equilibrium state boundary of the viscous domain for each material. A comparison of the Figs. 5.1a, 5.1b, and 5.1c shows that the equilibrium loci estimated for all the specimens are comparable. However, stress-response of NR-II at faster strain rates is much lower

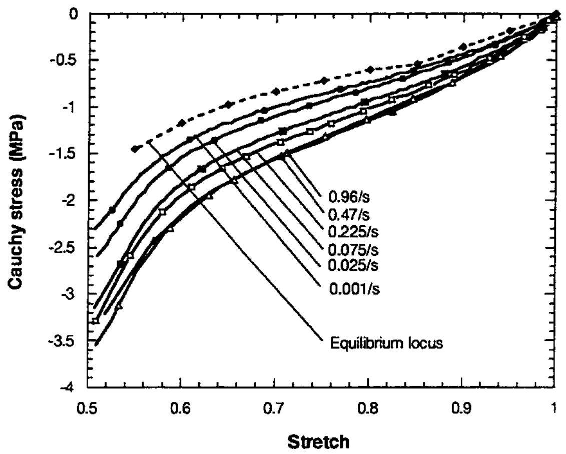

(a)

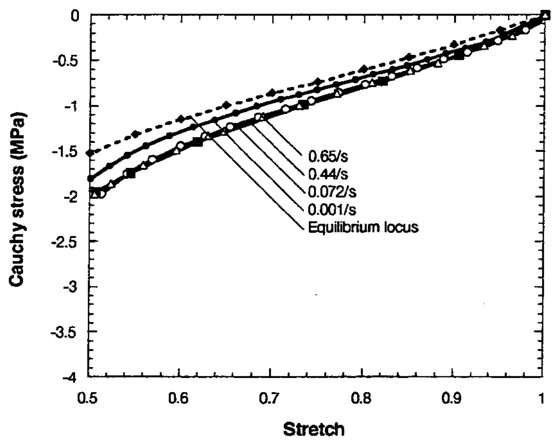

(b)

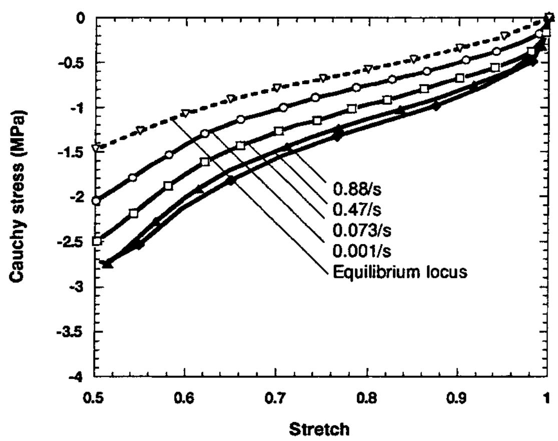

(c)

Figure 5.1. Comparison of monotonic compression test stretch-stress responses at different strain rates along with the equilibrium locus. (a) NR-I (b) NR-II (c) HDR

than those of NR-I and HDR. This results in a smaller viscous domain for NR-II characterizing a low viscosity. In this connection, the higher viscosity in NR-I than that of NR-II can be interpreted by the presence of microstructural voids in NR-I (Section 2.5). However, the present experimental observations can not yield any such conclusion about the presence of higher viscosity in HDR.

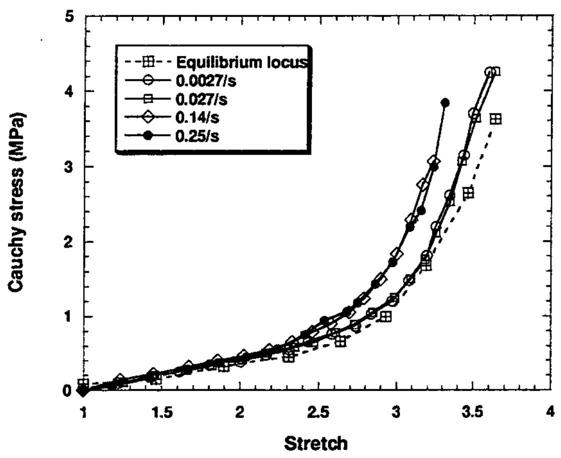

(a)

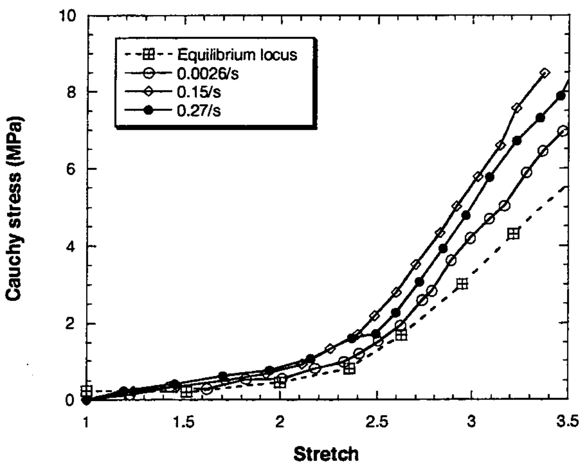

(b)

Figure 5.2. Comparison of monotonic tension test stretch-stress responses at different strain rates along with the equilibrium locus. (a) NR-II (b) HDR.

Figure 5.2 presents the corresponding viscous domains obtained for NR-II and HDR observed in the tension regime. To construct these domains, the monotonic tension responses at different strain rates (Section 2.7.3) were combined with the loading paths of the equilibrium loci obtained from the cyclic relaxation tests. The appearance of the instantaneous state at strain rates larger than 0.14/s is evident in NR-II. However, in HDR, such a feature could not be confirmed due to the limitation of the experimental results at faster strain rates.

5.3.2 Determination of equilibrium response parameters

The equilibrium locus obtained from the cyclic relaxation tests (Figs. 5.1 and 5.2) has confirmed the identification of the path of the equilibrium response. This identification has thus eliminated the problems and the subsequent uncertainties associated with a slow loading rate on a rubbery material of unknown viscosity and therefore approximated the equilibrium locus. At this point, the coefficients of the hyperelasticity relation (Equations 3.19, 3.20 and Table 4.1) for the locus can be readily determined by a least-square method. The values of the parameters are listed for compression regime (Tables 5.1 to 5.3) and tension regime (Tables 5.4 and 5.5).

Table 5.1 Elastic material parameters in compression regime (NR-I)

Responses	C_5	C_3	C_4	M	N
	MPa	MPa	MPa		
Equilibrium	0.99	0.40	-0.89	0.25	1.00
Instantaneous	1.89	0.86	-1.80	0.25	1.00

Table 5.2. Elastic material parameters in compression regime (NR-II)

Responses	C_5	C_3	C_4	M	N
	MPa	MPa	MPa		
Equilibrium	0.67	0.07	-0.31	0.25	1.00
Instantaneous	1.04	0.22	-0.68	0.25	1.00

Table 5.3. Elastic material parameters in compression regime (HDR)

Responses	C_5	C_3	C_4	M	N
	MPa	MPa	MPa		
Equilibrium	0.79	0.18	-0.55	0.25	1.00
Instantaneous	2.35	0.74	-2.28	0.25	1.00

Table 5.4. Elastic material parameters in tension regime (NR-II)

Responses	C_5	C_3	C_4	M	N
	MPa	MPa	MPa		
Equilibrium	0.03	3.49×10^{-5}	0.01	0.25	3.30
Instantaneous	0.10	1.02×10^{-4}	-0.03	0.25	3.30

Table 5.5. Elastic material parameters in tension regime (HDR)

Responses	C_5	C_3	C_4	M	N
	MPa	MPa	MPa		
Equilibrium	-0.09	-0.002	0.110	0.50	1.00
Instantaneous	0.06	0.031	0.001	0.50	1.00

5.3.3 Determination of instantaneous response parameters

The monotonic responses presented in Figs. 5.1 and 5.2 displayed a diminishing trend in the increase of the stress response at higher strain rates indicating the approach of the instantaneous state. Interestingly, the overall stress-stretch response at each strain rate has a characteristic curve, which can be described by the hyperelasticity model. On the basis of this feature, the constants, i.e. C_5, C_4 and C_3 were determined for each monotonic compression test with different strain rates ranging from 0.001/s to 0.96/s. In the Cauchy stress-stretch relation of the hyperelasticity model (Equations 3.19 and 3.20), each of the contributions from the 2nd and 3rd terms is related to two parameters, i.e. C_3, N and C_4, M respectively. However, the values of M and N have a weaker sensitivity on the whole relation. On this basis, constant values of M and N as determined from the equilibrium locus of each material were used for determining C_3 and C_4 parameters. The C_5, C_3 and C_4 parameters determined by this way are plotted respectively in Figs. 5.3 and 5.4 against the corresponding strain rate values.

It is interesting to note that the values of C_5, C_3 and C_4 parameters (Fig. 5.3) follow an asymptotic trend with the increase of applied strain rate. This must be due to the approach of the instantaneous state. In case of NR-I such a feature is noticed over a strain rate of 0.25/s, while in NR-II the corresponding strain rate is 0.1/s. For HDR it is around 0.7/s. The parameters for the instantaneous response are estimated from this

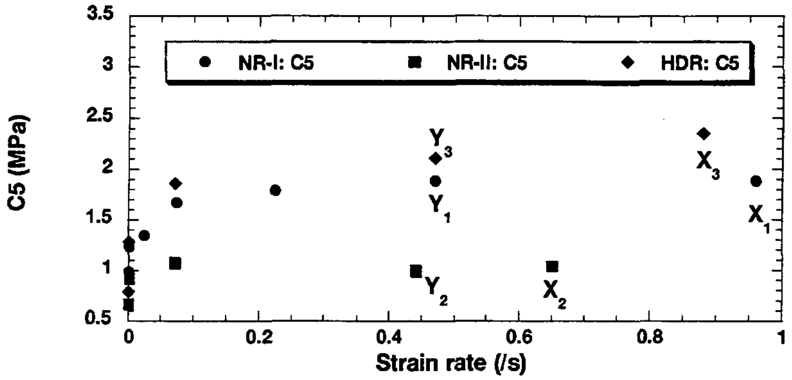

(a)

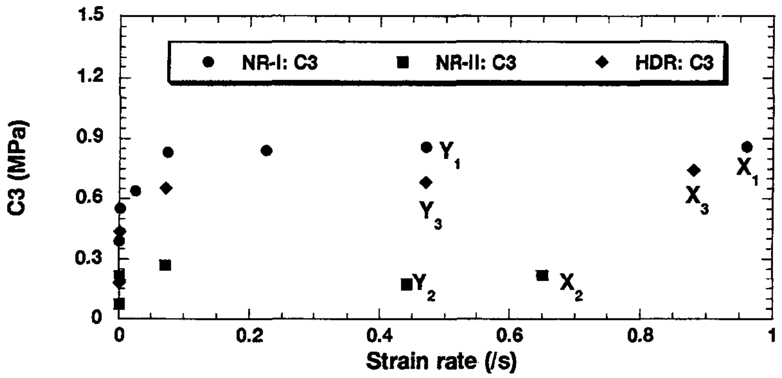

(b)

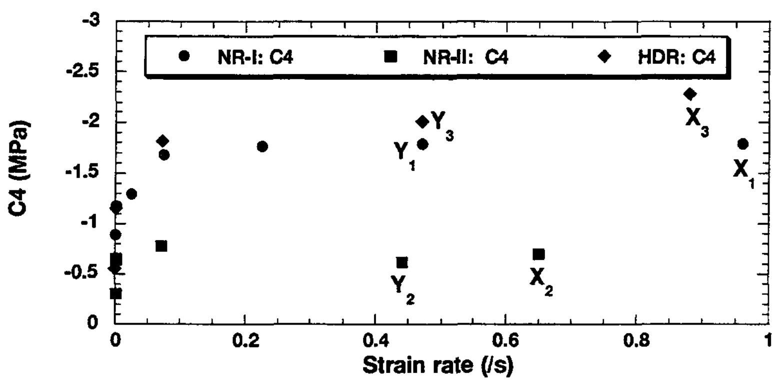

(c)

Figure 5.3. Best-fit hypereleasticity coefficients for monotonic compression tests at different strain rates (a) C_5 (b) C_3 (c) C_4 values.

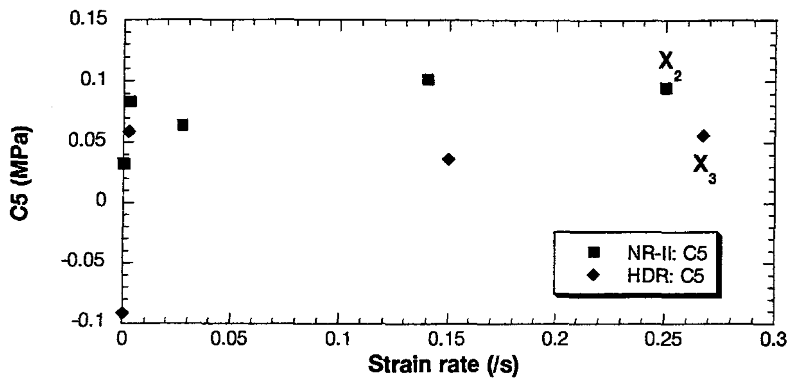

(a)

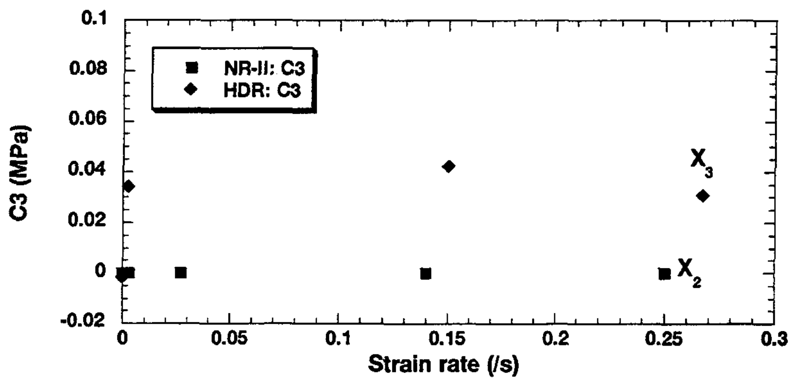

(b)

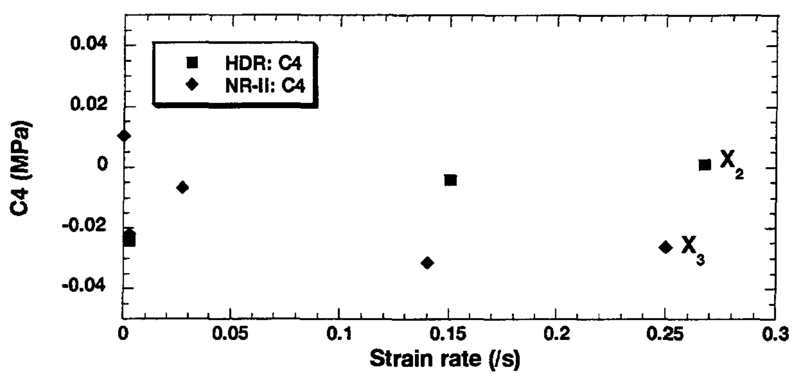

(c)

Figure 5.4. Best-fit hypereleasticity coefficients for monotonic tension tests at different strain rates (a) C_5 (b) C_3 (c) C_4 values.

asymptotic trend within finite strain rate region. The values obtained from the highest strain rate case in each specimen and denoted by X_1, X_2 and X_3 (Fig. 5.3) were taken for representing the instantaneous response. The values are presented in Tables 5.1 to 5.3. The subtraction of the values of C_5, C_3 and C_4 from the instantaneous to the equilibrium state gives the parameter values for the overstress response as mentioned in Table 4.1.

In a similar way, the instantaneous response parameters were also estimated in tension regime for NR-II and HDR. However, unlike the compression regime findings, the appearance of the instantaneous state in an asymptotic trend was little less prominent in tension regime. Further experiments are required in this regard to arrive at a definite conclusion.

Apart from these aspects, for both NR-II and HDR, the material parameters presented in Tables 5.2 to 5.5 differed widely from compression regime to tension regime. The effect of specimen size and the temperature might be the major reasons behind such a deviation.

5.4 IDENTIFICATION OF VISCOSITY PARAMETER

The determination of elastic parameters completes the representation of the viscosity domain boundary and leaves the material viscosity represented by η (Fig. 4.1, Equation 4.14) as the only unknown quantity. In this situation, simple relaxation test results presented in Sections 2.6.4 and 2.7.4 were utilized to estimate the viscosity parameter.

In the compression regime tests, the loading strain rate for each specimen was maintained at 0.5/s, while in the tension regime tests the corresponding strain rate was 0.15/s. All these strain rates lie in the neighborhood of respective instantaneous states for all the materials (Section 5.3.3). In this situation, all the tests (presented in Sections 2.6.4 and 2.7.4) illustrate the fundamental stress relaxation phenomena of the materials from the instantaneous to the equilibrium state and thus include the entire viscosity domain.

In this context, to find an adequate value of η, simulation trials of the rate-dependent hyperelasticity model (Chapter 4) were carried out and the experimental data were compared with those of the simulation results. The values obtained for different specimens at different regimes are summarized in Table 5.6.

Table 5.6 Viscosity parameter values in compression and tension regime

Regimes	Specimens		
	NR-I	NR-II	HDR
	MPa-s		
Compression	2.00	3.50	3.00
Tension	–	3.50	15.50

Figure 5.5 presents the representation of stress relaxation feature by the linear viscosity parameter, η at different compressive stretch levels in NR-I. The comparison indicates an adequate representation at each stretch level.

The corresponding results obtained for NR-II are presented in Fig. 5.6 with a similar conclusion. Figure 5.6 presents the stress-relaxation representation of NR-II in tension regime, where the model could not reach the instantaneous and the equilibrium states. However, the stress relaxation behavior represented by the model was in conformity with the experimental results.

Figure 5.8 presents the representation of the stress relaxation feature of HDR by the proposed model at two compressive stretch levels, where a good correlation between the theory and the experiments is observed. The corresponding result in tension regime (Fig. 5.9) also illustrates an encouraging capability of the model.

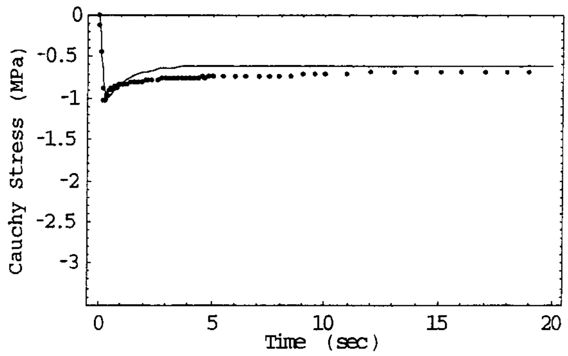

(a)

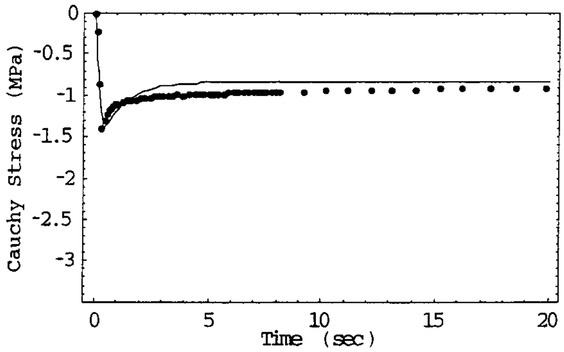

(b)

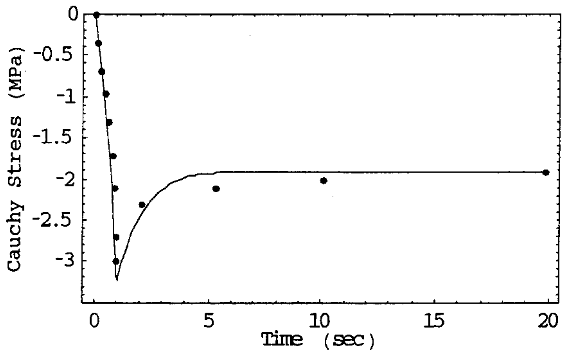

(c)

Figure 5.5. Estimation of viscosity parameter by simulating the simple relaxation test result at different stretch levels in NR-I; (-) Numerical simulation, (•) Experiment.
(a) 0.8 stretch, (b) 0.7 stretch, (c) 0.5 stretch levels.

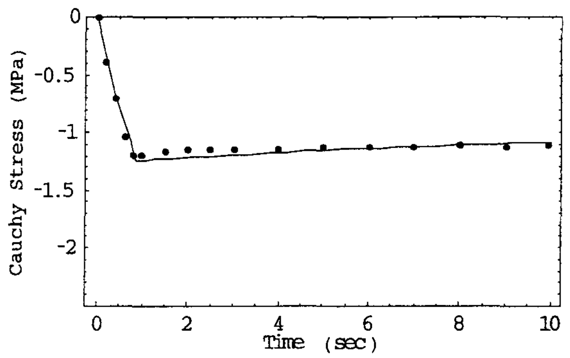

(a)

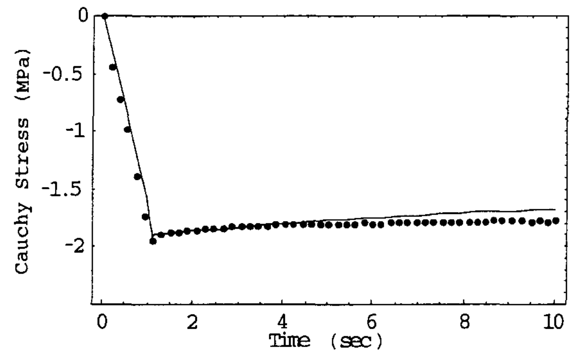

(b)

Figure 5.6. Estimation of viscosity parameter by simulating the simple relaxation test result at different stretch levels in NR-II; (-) Numerical simulation, (•) Experiment.
(a) 0.65 stretch, (b) 0.50 stretch levels.

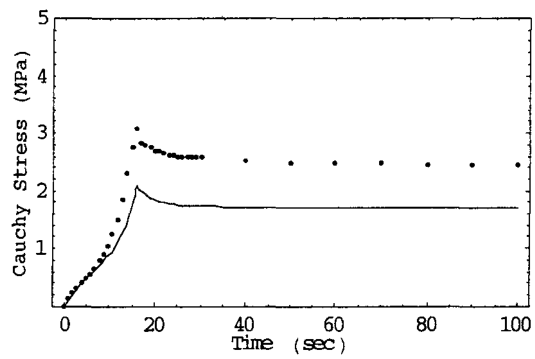

Figure 5.7. Estimation of viscosity parameter by simulating the simple relaxation test result at 3.24 stretch levels in NR-II; (-) Numerical simulation, (•) Experiment.

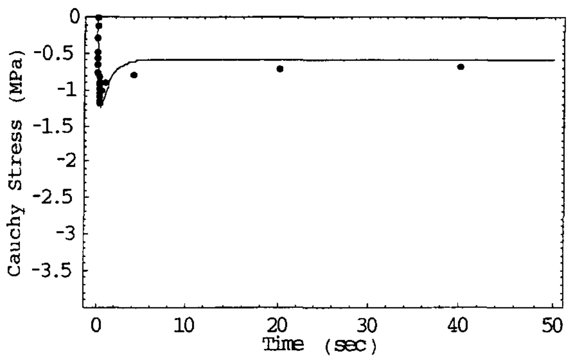

(a)

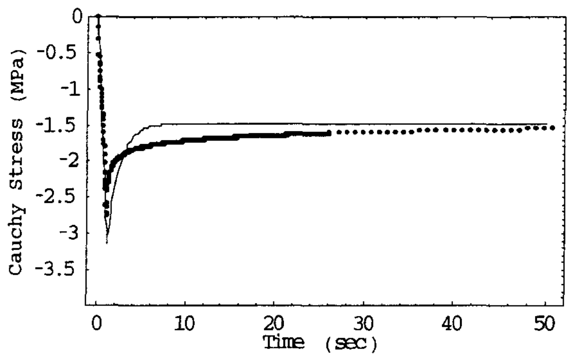

(b)

Figure 5.8. Estimation of viscosity parameter by simulating the simple relaxation test result at different stretch levels in HDR; (-) Numerical simulation, (•) Experiment.
(a) 0.80 stretch, (b) 0.50 stretch levels.

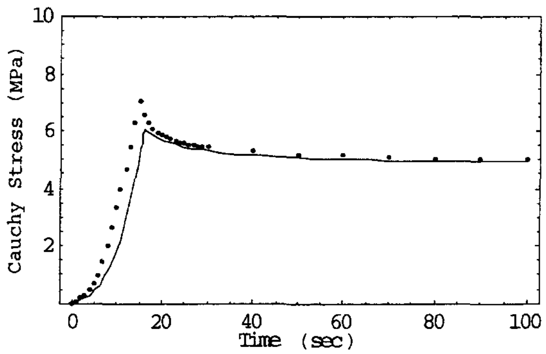

Figure 5.9. Estimation of viscosity parameter by simulating the simple relaxation test result at 3.37 stretch level in HDR; (-) Numerical simulation, (•) Experiment.

Chapter 6

Numerical Simulation

6.1 GENERAL

The experimental findings presented in Chapter 2 indicated the presence of strain-rate effect induced by the material viscosity in all the specimens on NR and HDR. Such an effect was evident in the loading path and was quite indistinguishable in the unloading path. However, hysteresis and residual strain effects dominated the unloading behavior. In this context, a constitutive model was constructed in Chapters 3 and 4 on the standpoint of phenomenology and under the framework of large strain kinematics to model the strain-rate dependent behavior. Furthermore, an explicit scheme was proposed in Chapter 6 to identify the elastic and the viscous parameters of the materials in a physically meaningful way. To this end, the identified material parameters were employed in the constitutive model to carry out the numerical simulation of monotonic compression and tension tests. Further efforts were also made to simulate the multi-step relaxation tests. The following section is devoted in discussing the performance of the model by comparing the simulation results with experimental data. The final section of this chapter is offered to studying the sensitivity of the instantaneous state parameters on the stress prediction and thereby to discuss the asymptotic convergence of the instantaneous response with increasing strain rate observed in Section 5.1.1.

6.2 SIMULATION RESULTS

6.2.1 Monotonic compression tests

Figures 6.1 to 6.3 show the simulation results in comparison with experimental data for NR-I, NR-II and HDR specimens, where a good conformity can be observed in all the cases. The capability of the model in simulating the high initial stiffness feature at different strain rates is well portrayed in Figs. 6.1 and 6.3. In contrast, the performance of the model in predicting the response of NR-II containing no initial stiffness feature is also noticeable in Fig. 6.2. Furthermore, the model was also found to show its capability in reproducing the intermediate large compression and large-strain hardening feature of all the specimens at slower and faster strain rates. The yielding of such ability is due to the inclusion of the newly proposed hyperelasticity relation in the finite deformation rate-dependent model and the adequacy of the proposed parameter identification procedure.

However, in all the specimens, the simulation result at 0.001/s strain rate is slightly poorer than those of other faster strain rate cases (Figs. 6.1 to 6.3). Such a performance might be related to the limitation of the present viscosity modeling, where only one relaxation rate can be modeled in contrast to the experimental observation presented in Section 2.6.4, where the co-existence of two relaxation rates is possible. In this case, the viscosity parameter was estimated in Section 5.2 to represent the faster relaxation rate that completes the major part of total stress relaxation within the first 10~50 sec of the stress history (Figs. 5.5 to 5.9). In contrast to this, the time history duration of monotonic compression test at 0.001/s up to 0.5 stretch level is 500 sec. This is much longer than the duration of relaxation stress history (10~50 sec) modeled by that single viscosity parameter.

Figure 6.4 presents an evaluation of the performance of the model in representing the stress response at a slower and a faster strain rates at different stretch levels. To evaluate the performance, the performance index is represented as:

$$\text{Error}(\%) \ \text{in stress} = \frac{T_{\text{Expt}} - T_{\text{Predicted}}}{T_{\text{Expt}}} \text{x}100 \tag{6.1}$$

The evaluation shows that the model performs better at higher strain rates than at higher stretch levels. When compared between the two specimens, the performance was found better in NR than HDR.

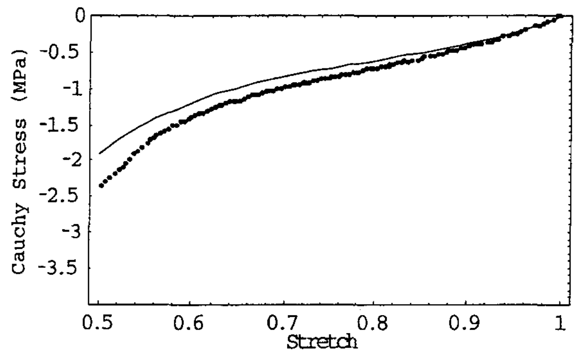

(a)

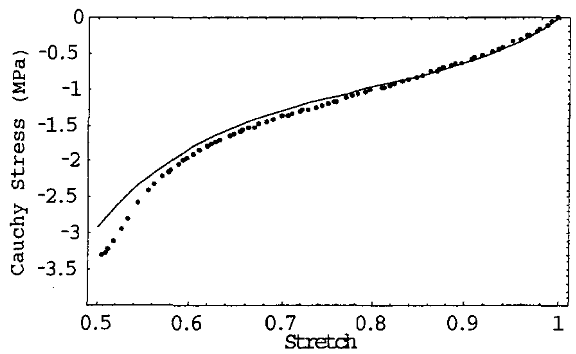

(b)

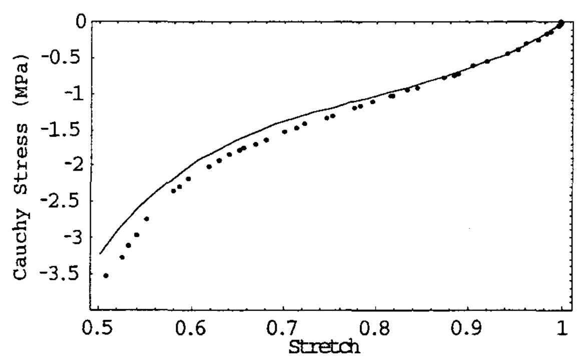

(c)

Figure 6.1. Numerical simulation of monotonic compression test at different strain rates for NR-I; (-) Numerical simulation, (•) Experiment. (a) 0.001/s (b) 0.075/s strain rates (c) 0.47/s.

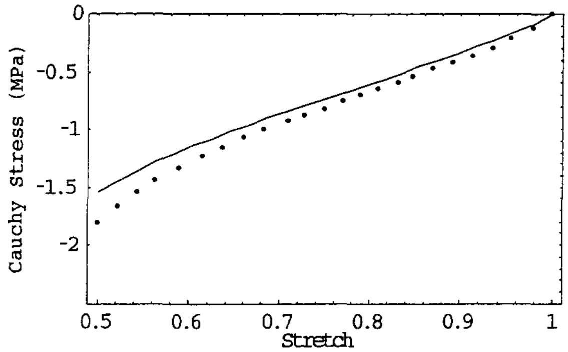

(a)

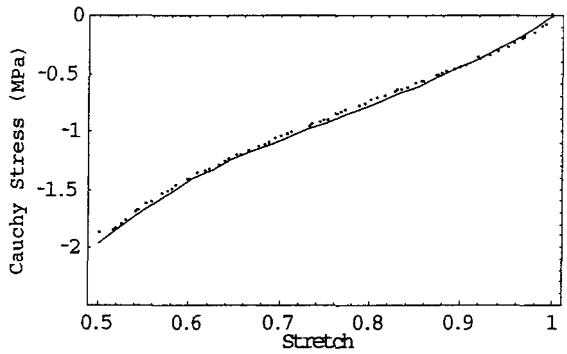

(b)

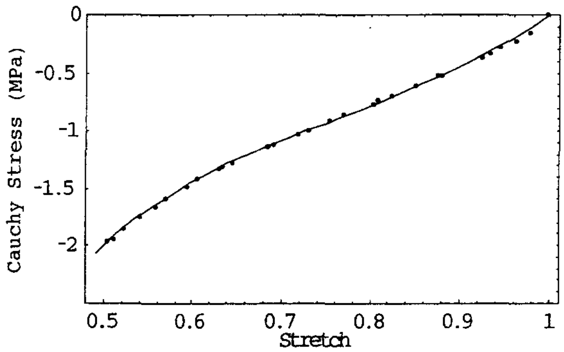

(c)

Figure 6.2. Numerical simulation of monotonic compression test at different strain rates for NR-II; (-) Numerical simulation, (•) Experiment. (a) 0.001/s (b) 0.25/s strain rates (c) 0.65/s.

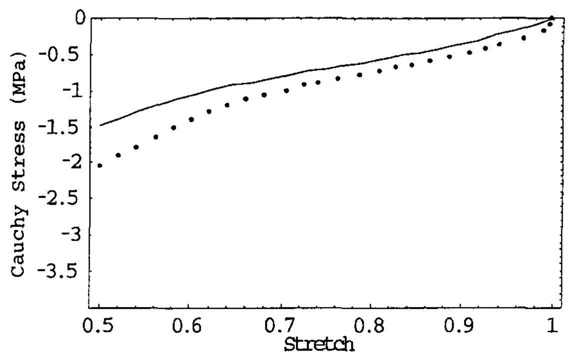

(a)

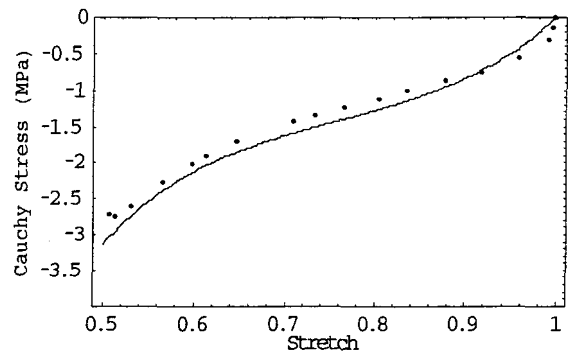

(b)

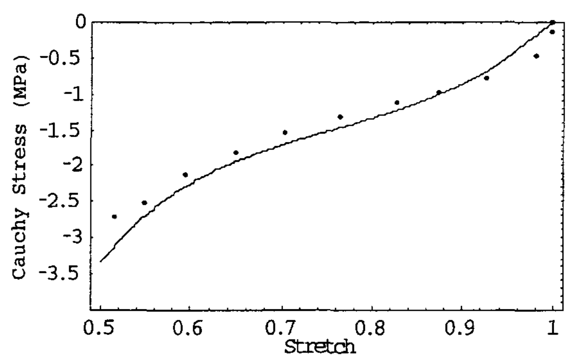

(c)

Figure 6.3. Numerical simulation of monotonic compression test at different strain rates for NR-II; (-) Numerical simulation, (•) Experiment. (a) 0.001/s (b) 0.47/s strain rates (c) 0.88/s.

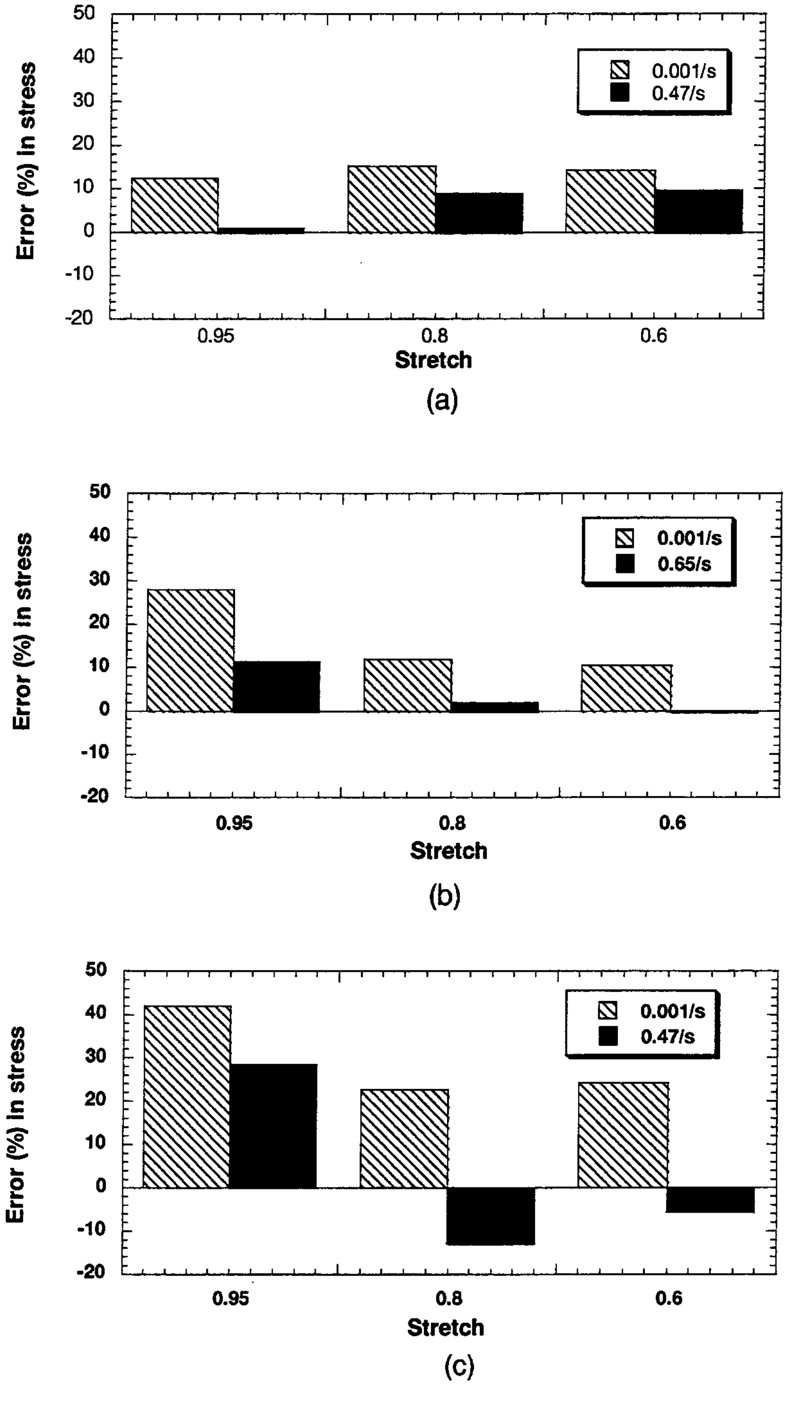

Figure 6.4. Comparative performance of the model in simulating strain-rate dependency effect. (a) NR-I (b) NR-II (c) HDR.

6.2.2 Monotonic tension tests

Figures 6.5 and 6.6 present the monotonic tension simulation results for NR-II and HDR at different strain rates. In both specimens, the simulation tended to give a better performance in faster strain rates. Such a model characteristics is in line with those found in the compression regime. However, at a higher stretch level, the performance of the model in representing the hardening feature was not as good as those in the compression regime.

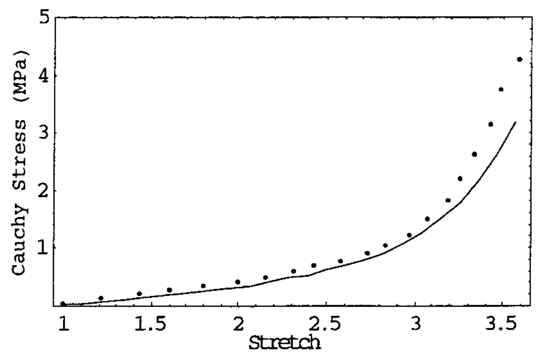

(a)

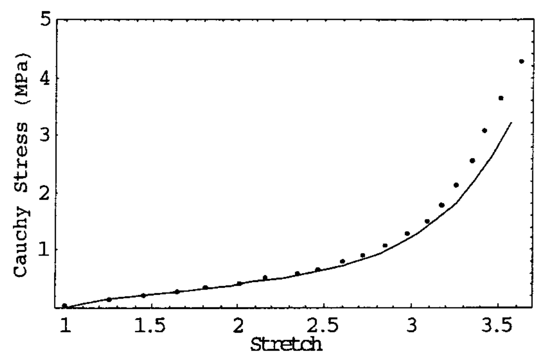

(b)

Figure 6.5. Numerical simulation of monotonic tension test at different strain rates for NR-II; (-) Numerical simulation, (•) Experiment. (a) 0.0027/s (b) 0.027/s strain rates.

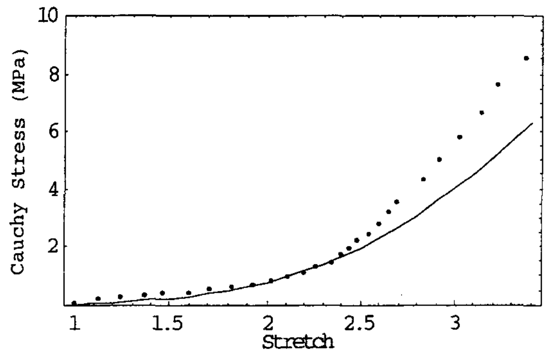

(a)

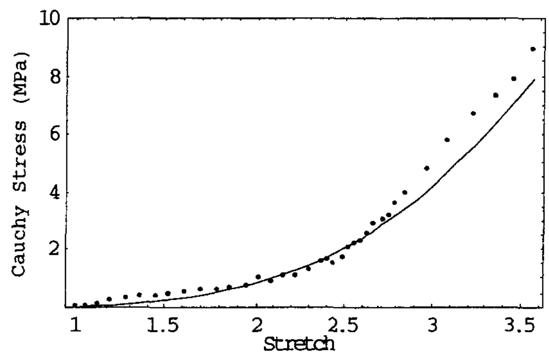

(b)

Figure 6.6. Numerical simulation of monotonic tension test at different strain rates for HDR; (-) Numerical simulation, (•) Experiment. (a) 0.0026/s (b) 0.267/s strain rates.

6.2.3 Multi-step relaxation tests in compression

Figures 6.7 and 6.8 illustrate the model capability in representing the multi-step relaxation tests in the compression regime. In the example of simulation of test on NR-I (Fig. 6.7), the performance was observed to be better than that of HDR (Fig. 6.8). In both cases, the approach of the equilibrium state due to stress relaxation feature was quite well modeled. However, the loading paths of the steps other than the first one could not be modeled in a proper way. This indicates the need for inclusion of some state variables to model such a behavior.

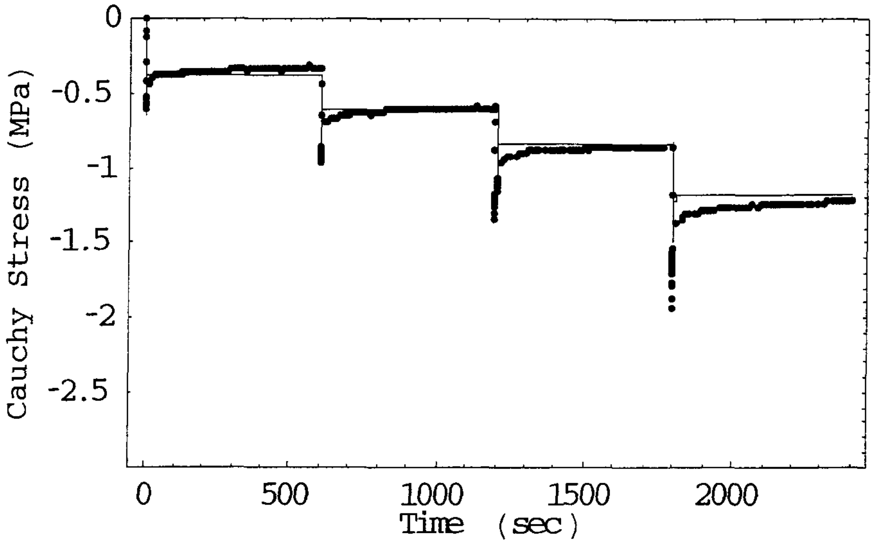

(a)

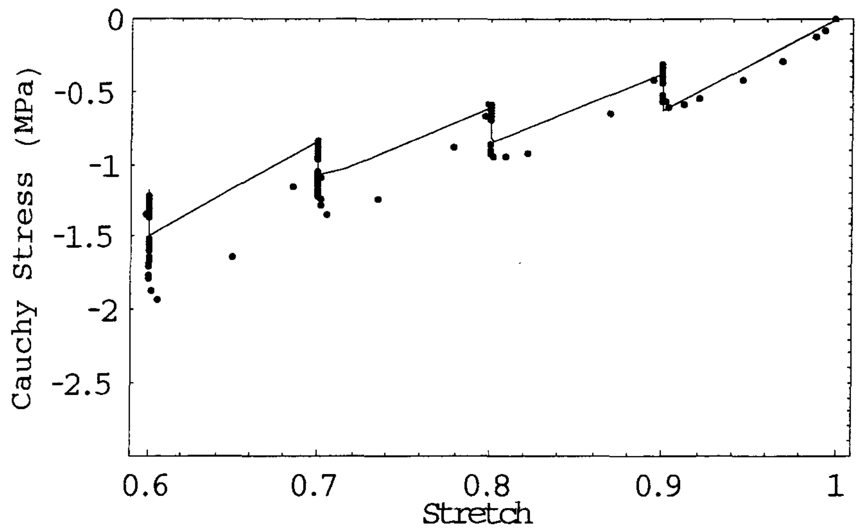

(b)

Figure 6.7. Numerical simulation of multi-step relaxation test in compression for NR-I; (-) Numerical simulation, (•) Experiment. (a) Stress history (b) Stress-stretch response.

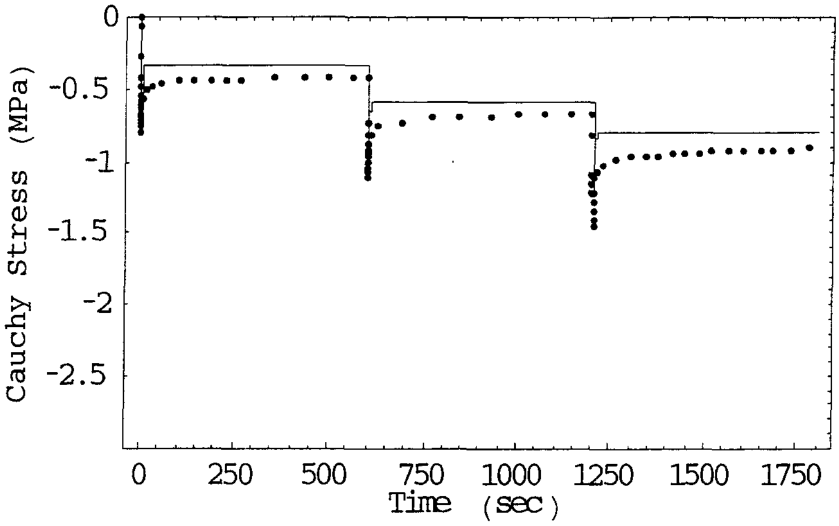

(a)

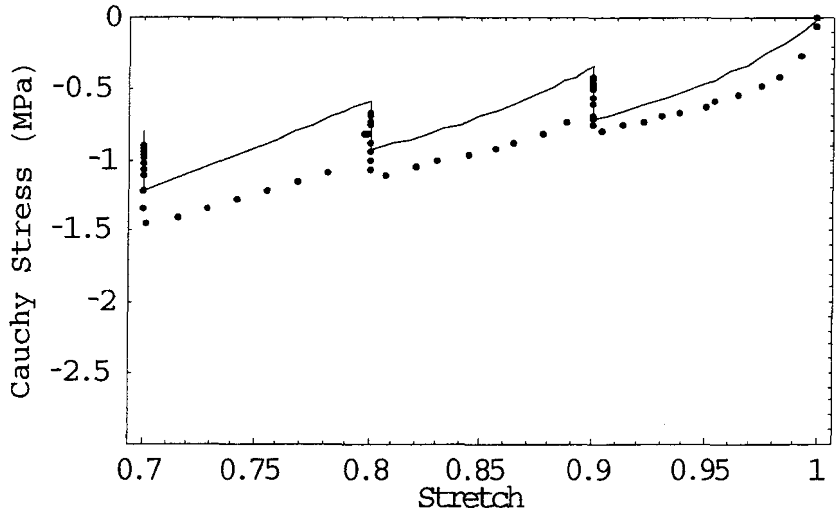

(b)

Figure 6.8. Numerical simulation of multi-step relaxation test in compression for HDR; (-) Numerical simulation, (•) Experiment. *(a) Stress history (b) Stress-stretch response.*

6.3 SENSITIVITY STUDY

In determining the elastic parameters, the proposed scheme requires only one test for the equilibrium response in contrast to the case of the instantaneous response, where the required number of experiments is somewhat large. In addition, a large number of monotonic compression experiments from the slower to the faster rates were carried out in this study to clarify the convergence of the hyperelasticity parameters to the asymptotic value with the increasing strain rate. However, the values of C_5, C_3 and C_4 determined at different strain rates (Fig. 5.3) indicate the possibility of reducing the strain rate in approximating the instantaneous response for a practical application. Hence, at this stage, the effect of using the instantaneous state parameter values estimated from different but slower strain rate cases on the simulation results was studied through a sensitivity study. The study was carried out with a view to checking the robustness of the proposed scheme and thereby to investigate the possibility of using a reduced strain rate for estimating the instantaneous response parameters.

To do this, in the case of NR-I, we take the value of one of the parameters C_5, C_3 and C_4 for the instantaneous response from the strain rate case of Y_1 (Fig. 5.3) while taking the other parameter from X_1 case. The resulting errors in stress prediction that occur due to this parametric variation are presented as a function of stretch in Fig. 6.9 where,

$$\text{Error}(\%) \;\; \text{in} \;\; \text{stress} \; = \; \frac{T_X \; - \; T_Y}{T_X} \text{x100} \qquad (6.2)$$

Simulation of monotonic compression tests at three different strain rates were considered. In case of NR-II and HDR, a similar study was carried out for X_2 - Y_2 and X_3 – Y_3 cases respectively (Figs. 6.10 and 6.11).

In NR-I, the considered reduction of strain rate from X_1 to Y_1 is 52%, while in NR-II and HDR, the corresponding shifts are 32% and 47% respectively. In contrast to such a large reduction of strain rate in selecting the instantaneous parameters, the errors in stress prediction remain within 15% in NR specimens as revealed from Figs. 6.9 and 6.10. However, for HDR, the errors in stress prediction swelled up to 30% indicating a very high material viscosity.

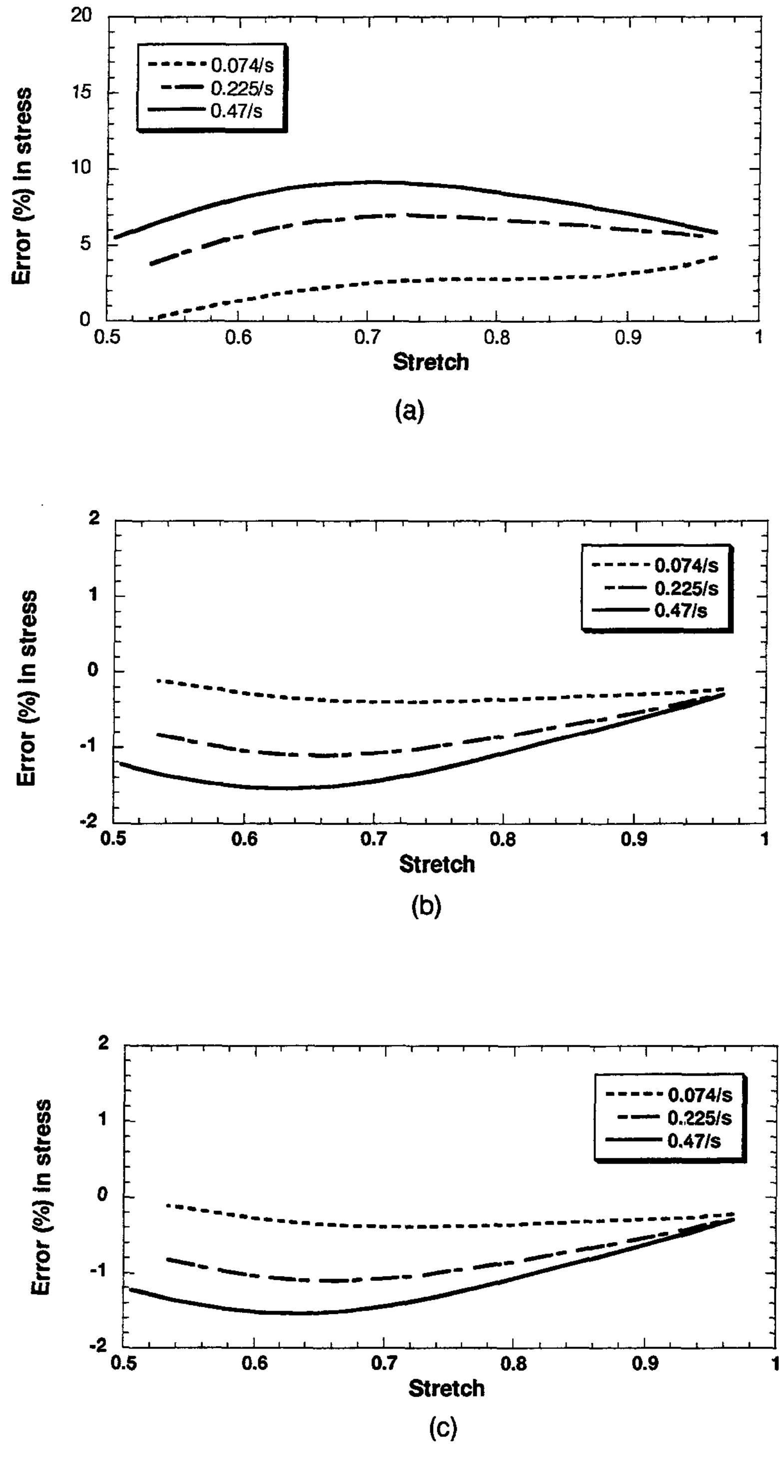

Figure 6.9. Effect of instantaneous response parameter variation on monotonic compression test simulation result in NR-I ; (a) C_5 variation, (b) C_3 variation, (c) C_4 variation

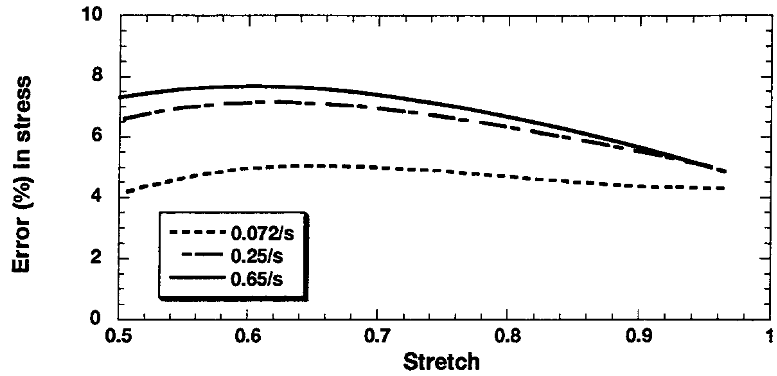

(a)

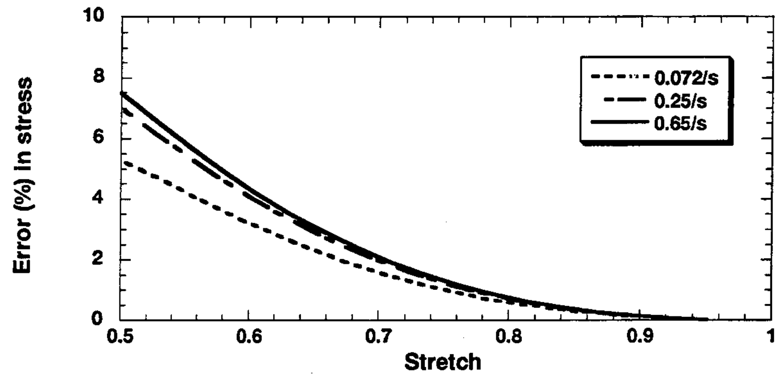

(b)

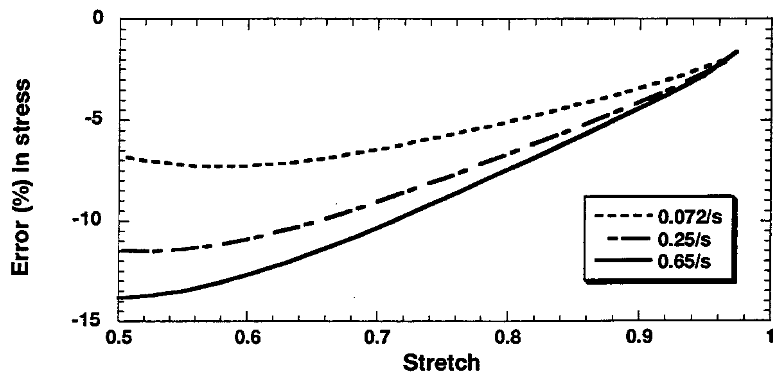

(c)

Figure 6.10. Effect of instantaneous response parameter variation on monotonic compression test simulation result in NR-II ; (a) C_5 variation, (b) C_3 variation, (c) C_4 variation

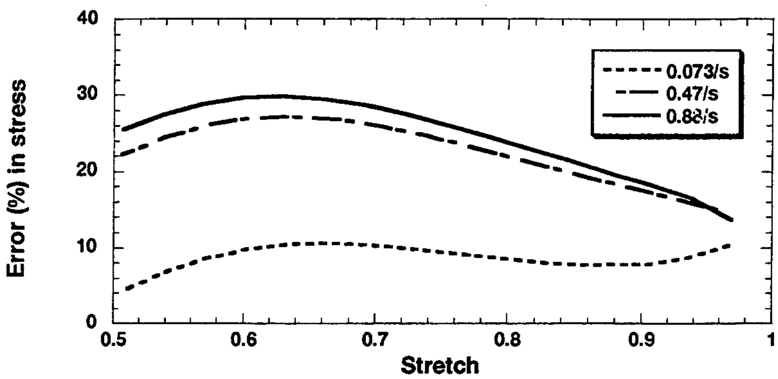

(a)

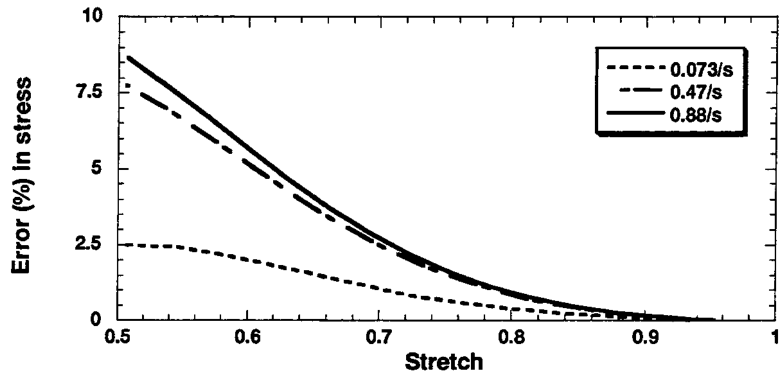

(b)

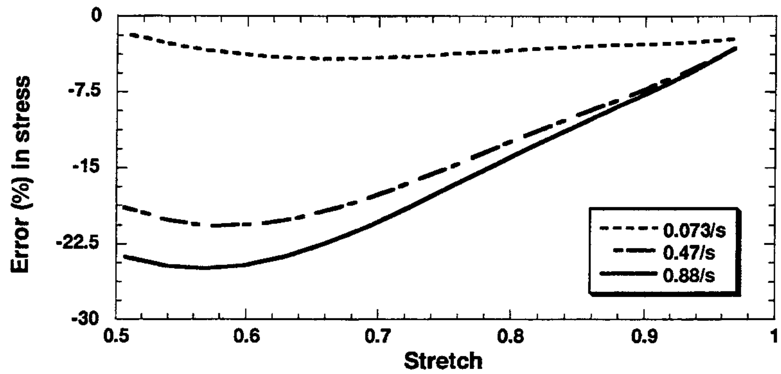

(c)

Figure 6.11. Effect of instantaneous response parameter variation on monotonic compression test simulation result in HDR; (a) C_5 variation, (b) C_3 variation, (c) C_4 variation

In general, the study indicated a higher amount of error in stress prediction in simulation of high strain-rate response than slower ones. This confirms the necessity of the confirmation of the instantaneous response boundary through adequate experiments in faster strain rates for a viscous material to estimate the instantaneous response parameters in the viscous materials. However, in materials of low viscosity, a high strain rate experiments might not be required to estimate some instantaneous response parameters, which is sufficient enough for use in numerical simulation.

A detail look over the Figs. 6.9 to 6.11 shows that the effect of C_5 and C_4 parameter variation was more dominant over the entire stretch range in stress prediction contrast to that of the C_3 parameter.

(This page is intentionally left blank)

Chapter 7

Summary and conclusions

7.1 MICROSTRUCTURE AND MECHANICAL MEHAVIOR

SEM observations revealed a void dominated microstructure in NR-I in contrast to NR-II and HDR, where the occurrence of void is rare. However, in spite of the presence of the microstructural voids in NR-I, the validity of incompressibility assumption in uniaxial case was verified from the measurement of the deformed cross-section. The results of the SEM image analysis further substantiated the validity of this assumption.

The mechanical tests in the compression regime demonstrated the existence of Mullins' softening effect in all the specimens. However, with the passage of time a slow healing of the softening effect was observed. A preloading sequence had been applied before all the tests were carried out to remove the Mullins' effect from other inelastic phenomena. In order to keep the healing effect constant in each specimen, a constant 20 min time interval was maintained between the pre-loading and the actual test.

Cyclic compression tests carried out at different strain rates gave a picture of the significant strain-rate dependency property in the loading-path. The simple relaxation tests were carried out at different maximum stretch levels to clarify the effect of the viscosity property in the material. However, in the cyclic loading tests, the absence of the strain-rate dependency phenomena was noticed in the unloading path together with significant hysteresis and a residual strain effect.

In order to remove the strain-rate dependency and thereby to identify the equilibrium locus as well as equilibrium hysteresis, the cyclic relaxation tests were carried out with different maximum stretch levels. The test results identified the strong dependence of the equilibrium state hysteresis on the experienced maximum strain and the current strain.

The studies on the history dependence of the residual strain identified a direct effect of the applied strain rate. Furthermore, a logarithmically linear relation in the recovery of residual strain with time was uncovered in all the specimens.

Finally, the mechanical tests in tension also confirmed the existence of strain-rate dependency and the hysteresis effect in the tension regime as well.

When the extent of the Mullins' effect, strain-rate dependency, hysteresis, residual strain and recovery properties were compared with the NR specimens, these effects were found to be more significant in NR-I than those of NR-II. The presence of microstructural voids in NR-I might be a reason behind such effects.

However, the existence of all these mechanical effects was also found to be very significant in HDR. In addition, HDR exhibited a stronger nonlinearity in the stress-stretch response under compression than that of NRs. Although the related literatures suggest the presence of higher amount of filler concentration behind such effects in HDR, the available data on the microstructural observation made in the present study could not explain such effects. In such a situation, the phenomenological approach was considered in the present research for constructing a constitutive model that would represent the behaviors of not only the HDR but also the NR.

7.2 CONSTITUTIVE MODELING FOR STRAIN-RATE DEPENDENCY

The mechanical tests indicated the presence of high initial stiffness at a low stretch level in the compressive response of the HDR. In the NR specimens, such an effect was less prominent. In this context, a hyperelasticity model was proposed to represent the rate-independent response including the initial stiffness feature of the HDR and the NR in the compression. The performances of the conventional and the proposed hyperelasticity models in representing the rate-independent response of the NR and the HDR were evaluated. The evaluation displayed the superiority of the proposed model over the conventional ones in representing the low stretch level response. However, at higher stretch levels, all the models were found to perform well.

In order to model the strain-rate dependency observed in the experiments, a finite deformation model structure formulated based on overstress concept was employed. The proposed hyperelasticity model was successfully incorporated to represent the equilibrium and the instantaneous states. A qualitative study of the model behavior showed the capability of representing the viscosity induced strain-rate effect.

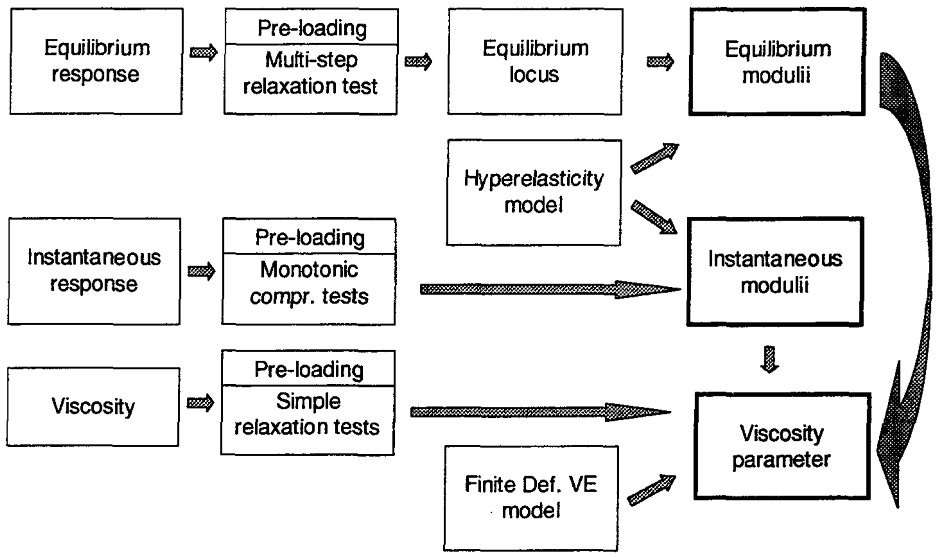

Figure 7.1 The proposed scheme for identifying the viscoelasticity parameters

7.3 PARAMETER IDENTIFICATION

On the basis of the physical interpretation of the strain-rate effect observed in a viscoelastic solid, a sequential method comprising of experimentation and computation were proposed to identify the constitutive parameters.

A multi-step relaxation test was proposed to identify the equilibrium response. In order to estimate the instantaneous response, a series of constant-rate monotonic tests at different strain rates was proposed. After identifying the responses, the hyperelasticity model can be used to find out the parameters for the equilibrium as well as the instantaneous response from these tests. When the elastic parameters of the material are known, the rate-dependent finite deformation hyperelasticity model can be used to find out the viscosity parameter by comparing the simple relaxation test data. Figure 7.1 illustrates the proposed parameter identification scheme. The viability of applying the scheme in the compression as well as in the tension regime was verified.

7.4 NUMERICAL SIMULATION

In order to verify the adequacy of the proposed model and the parameter identification scheme, a series on numerical simulations in the compression and the tension regimes were carried out. To do this, the constitutive model with the identified parameters was used in the simulation. The experimental results were used for the verification. The simulations of the monotonic tests and the multi-step relaxation tests portrayed the adequacy of the proposed model and the scheme in modeling the strain-rate dependency of the NR and the HDR. However, if modeling of any rubber with more than one prominent relaxation rates is needed, the numerical model may need some improvements.

Finally, the sensitivity of the instantaneous state parameters on the stress response prediction was studied. The investigation hinted the possibility of the strain rate reduction for estimating the instantaneous response for materials of low viscosity.

7.5 SCOPES FOR FUTURE STUDIES

In the present research studies, the mechanical behavior of the NR and the HDR was studied to reveal the Mullins' effect, the strain-rate dependency, the hysteresis and the residual strain effect. On the basis of the experimental observation, a rate-dependent constitutive model and a parameter identification scheme were proposed.

In doing this, experiments were carried out in compression and tension regimes. Due to limitations, the identical experimental conditions could not be maintained in both the regimes. This led to obtain a different set of parameters for the tension and the compression responses. It would be interesting to put further efforts to identify the material parameters with experiments to be carried out in similar conditions. Direct shear experiment may be one of the viable options in this regard for future studies.

Furthermore, the capability of the present model lies in simulating the strain-rate dependency phenomena observed in the monotonic response. In contrast, the experimental observations of the present research indicated the absence of such an effect in the unloading paths of the cyclic tests together with the presence of hysteresis effect. To model this kind of behavior, further formulations are needed to incorporate a damage/plasticity model into the current model structure to increase its capability in simulating the cyclic response as well.

(This page is intentionally left blank)

References

Aklonis, J. J., Macnight, W. J. and Shen, M., 1972. *Introduction to Polymer Viscoelasticity,* John Wiley & Sons, Canada.

Alam, M. Shah, Takanezawa, S., Amin, A. F. M. S. and Okui, Y., 2000. Mechanical Behavior of Elastomers Under Compression and Its Microstructure, Proceedings of 55th Annual Conference of Japan Society of Civil Engineers, Sendai, Japan, September 2000, I-A9.

Alexander, H., 1968. A constitutive relation for rubber-like materials, *Int. J. Engrg. Sci.,* **6**, 549-563.

Ali, H. M. and Abdel-Ghaffar, A.M., 1995. Modeling of rubber and lead passive-control bearings for seismic analysis, *J. Struct. Engrg,* **121**, 1134-1144.

Amin, A. F. M. S., Alam, M. Shah and Okui, Y., 2001a. Development of Rate Dependent Constitutive Model for Elastomers, Creative Systems in Structural and Construction Engineering, Singh (ed.), Balkema, Rotterdam.

Amin, A. F. M. S., Alam, M. Shah and Okui, Y., 2001b. An Improved Hyperelasticity Relation For Modeling Strain Rate Dependency Of High Damping Rubber, Proceedings of 55th Annual Conference of Japan Society of Civil Engineers, Kumamoto, Kyushu, Japan, (accepted).

Amin, A. F. M. S., Alam, M. Shah and Okui, Y., 2001c. Nonlinear viscoelastic response of elastomers: Experiments, parameter identification and numerical simulation, *J. Struct. Engrg, JSCE,* **47A**, 181-192.

Amin, A. F. M. S., Alam, M. Shah and Okui, Y., 2000. Hyperelasticity Modeling of High Damping Rubber and Finite Element Simulation, Proceedings of 55th Annual Conference of Japan Society of Civil Engineers, Sendai, Japan, September 2000, I-A8.

Anand, L., 1996. A constitutive model for compressible elastomeric solids, *Computational Mechanics,* **18**, 339-355.

Arruda, E. M., and Boyce, M. C., 1993. A three-dimensional constitutive model for the large stretch behavior of rubber elastic materials, *J. Mech. Phys. Solids,* **41**, 389-412.

ASTM Standard D 395-98, *Standard Test Methods for Rubber Property-Compression Set,* American Society for Testing and Materials, Philadelphia, USA.

ASTM Standard D 412-98a, *Standard Test Methods for Vulcanized Rubber and Thermoplastic Elastomers-Tension,* American Society for Testing and Materials, Philadelphia, USA.

Bathe, K., 1996. *Finite Element Procedures,* Prentice Hall International Editions, USA.

Berger, M., 1960. Response of elastomers to any forcing function, *J. Appl. Polym. Sci,* **4**, 269-276.

Bergstrom, J. S. and Boyce, M. C., 2000a. Large strain time-dependent behavior of filled elastomers, *Mech. Mater.,* **32**, 627-644.

Bergstrom, J. S. and Boyce, M. C., 2000b. Mechanical behavior of particle filled elastomers, *Rubber Chem. Technol.,* **72**, 633-656.

Bergstrom, J. S. and Boyce, M. C., 1998. Constitutive Modeling of the Large Strain Time-Dependent Behavior of Elastomers, *J. Mech. Phys. Solids,* **46**, 931-954.

Bogert, P.A.J. van den and Borst, R. de, 1994. On the behavior of rubber-like materials in compression and shear, *Arch. Appl. Mech.,* **64**, 136-146.

Bogert, P.A.J. van den, 1991. *Computational Modeling of Rubberlike Materials,* PhD Thesis, Delft University of Technology, The Netherlands.

Bonet, J. and Wood, R. D., 1997. *Nonlinear Continuum Mechanics for Finite Element Analysis,* Cambridge University Press, Cambridge.

Boyce, M.C. and Arruda, E.M., 2000. Constitutive models of rubber elasticity: A review, *Rubber Chem. Technol.,* **73**, 504-523.

Bueche, F., 1961. Mullins effect and rubber-filler interaction, *J. Appl. Polym. Sci.,* **5**, 271-281.

Bueche, F., 1960a. Mechanical degradation of high polymers, *J. Appl. Polym. Sci.,* **4**, 101-106.

Bueche, F., 1960b. Molecular basis for the Mullins effect, *J. Appl. Polym. Sci.,* **4**, 107-114.

Castellani, A., Kajon, G., Panjeri, P. and Pezzoli, P., 1998. Elastomeric Materials Used for Vibration Isolation of Railaway Lines, *J. Engrg. Mech.,* **124**, 614-621.

Charlton, D. J., Yang, J. and Teh, K. K., 1993. A review of methods to characterize rubber elastic behavior for use in finite element analysis, *Rubber Chem. Technol.,* **67**, 481-503.

Christensen, R. M., 1980. A nonlinear theory of viscoelasticity for application to elastomers, *J. Appl. Mechanics,* **47**, 762-768.

Cornwell, L.R. and Schapery, R. A., 1975. SEM study of microcracking in strained solid propellant, *Metallography,* **8**, 445-452.

D'Ambrosio, P., Tommasi, D.D. and Marzano, S., 1995. Nonlinear elastic deformations and stability of laminated rubber bearings, *J. Engrg. Mech. ASCE,* **121**, 1041-1048.

Dannis, M. L., 1962. Stress-strain testing of rubbers at high rates of elongation, *J. Appl. Polym. Sci.,* **6**, 283-296.

Davis, C.K.L., De, D.K. and Thomas, A.G., 1994. Characterization of the behavior of rubber for engineering design purposes. 1. Stress-strain relations, *Rubber Chem. Technol.,* **67**, 716-728.

Dorfmann, A. and Burtscher, S. L., 2000. Aspects of cavitation damage in seismic bearings, *J. Struct. Engr., ASCE,* **126**, 573-579.

Drozdov, A., 1998. A model for the nonlinear viscoelastic response in polymers at finite strains, *Int. J. Solids Structs,* **35**, 2315-2347.

Drozdov, A., 1997. A constitutive model for nonlinear viscoelastic media, *Int. J. Solids Structs,* **34**, 2685-2707.

Finney, R.H, Kumar, A., 1987. Development of material constants for nonlinear finite-element analysis, *Rubber Chem. Technol.,* **61**, 879-891.

Fishman, K.L. and Machmer, D., 1994. Testing techniques for measurement of bulk modulus, *J. Testing and Evaluation, ASME,* **22**, 161-167.

Flory, P.J., 1961. Thermodynamic relations for high elastic materials, *Trans. Faradey Soc.,* **57**, 829-838.

Flugge, W., 1975. *Viscoelasticity,* Second Edition, Springer-Verlag, New York.

Fried, I. and Johnson, A.R., 1988. A note on elastic energy density functions for largely deformed compressible rubber solids, *Comp. Methods. Appl. Mech. Engrg.,* **69**, 53-64.

Fujita, T., Fujita, S., Tazaki, S., Yoshizawa, T. and Suzuki, S., 1990. Research, development and implementation of rubber bearings for seismic isolations, *JSME Internation Journal,* **33**, 394-403.

Fukahori, Y. and Seki, W., 1992. Molecular behavior of elastomeric materials under large deformation: 1. Re-evaluation of the Mooney-Rivlin plot, *Polymer,* **33**, 502-508.

Gent, A. N., 1962a. Relaxation Processes in Vulcanized Rubber. I. Relation among Stress Relaxation, Creep, Recovery, and Hysteresis, *J. Appl. Polym. Sci.,* **6**, 33-441.

Gent, A. N., 1962b. Relaxation Processes in Vulcanized Rubber. II. Secondary relaxation due to network breakdown, *J. Appl. Polym. Sci.,* **6**, 442-448.

Govindjee, S., 1996. An evaluation of strain amplification concepts via Monte Carlo simulations of an ideal composite, *Rubber Chem Technol.,* **70**, 25-37.

Govindjee, S. and Simo, J.C., 1992a. Mullins' effect and strain amplitude dependence of the storage modulus, *Int. J. Solids Structs,* **29**, 1737-1751.

Govindjee, S. and Simo, J.C., 1992b. Transition from micro-mechanics to computationally efficient phenomenology: Carbon black filled rubbers incorporating Mullins' effect, *J. Mech. Phys. Solids,* **40**, 213-233.

Govindjee, S. and Simo, J.C., 1991. A micromechanically based continuum damage model for carbon black filled rubbers incorporating Mullins' effect, *J. Mech. Phys. Solids,* **39**, 87-112.

Govindjee, S., 1991. *Physical and Numerical Modeling in Filled Elastomeric Systems,* PhD Thesis, Stanford University, USA.

Gurtin, M. E. and Herrerra, I., 1965. On the dissipation inequalities and linear viscoelasticity, *Q. Appl. Math.,* **23**, 235-245.

Ha, K., Schapery, R.A., 1998. A three dimensional viscoelastic constitutive model for particulate composites with growing damage and its experimental validation, *Int. J. Solids Structs.,* **35**, 3497-3517.

Haggblad, B. and Sundberg, J.A., 1983. Large strain solutions for rubber components, *Computers and Structures,* **17**, 835-843.

Hamed, G.R. and Hatfield, S., 1988. On the role of bound rubber in carbon black reinforcement, *Rubber Chem. Technol.,* **62**, 143-156.

Hart-Smith, L.J. and Crisp, J.D.C., 1967. Large elastic deformations of thin rubber membranes, Int. J. Engrg. Sci., **5**, 1-24.

Hart-Smith, L. J., 1966. Elasticity parameters for finite deformations of rubber-like materials, *Z. Angew. Math. Phys.* **17**, 608-626.

Harwood, J.A.C. and Payne, A.R., 1966. Stress softening in natural rubber vulcanizates. Part III. Carbon black filled vulcanizates, *J. Appl. Polym.Sci.,* **10**, 315-324.

Harwood, J.A.C., Mullins, L. and Payne, A.R., 1965. Stress softening in natural rubber vulcanizates. Part II. Stress softening effects in pure gum and filled loaded rubbers, *J. Appl. Polym. Sci.,* **9**, 3011-3021.

Haupt, P., 1993. On the mathematical modeling of material behavior in continuum mechanics, *Acta Mechanica,* **100**, 129-154.

Hernandez, J. Y., 1998. *Modeling of Highly-deformable Polymeric Damping Materials for Use in Seismic Protective Devices,* Master of Science Thesis, Department of Civil and Environmental Engineering, Saitama University, Japan.

Herrmann, L.R., Ramaswamy, A. and Hamidi, R., 1989. Analytical parameter study for class of elastomeric bearings, *J. Struct. Engrg, ASCE,* **115**, 2415-2434.

Herrmann, L.R., Hamidi, R., Shafigh-Nobari, F. and Lim, C.K., 1988. Nonlinear behavior of elastomeric bearings. I: Theory, *J. Engrg. Mech., ASCE,* **114**, 1811-1830.

Holzapfel, G.A., 1996. On large strain viscoelasticity: Continuum formulation and finite element applications to elastomeric structures, *Int. J. Num. Methods Engrg,* **39**, 3903-3926.

Holzapfel, G.A. and Simo, J. C., 1996. A new viscoelastic constitutive model for continuous media at finite thermomechancial changes, *Int. J. Solids Structures,* **33**, 3019-3034.

Huber, N. and Tsakmakis, C., 2000. Finite deformation viscoelasticity laws, *Mech. Mater.,* **32**,1-18.

Hwang, J.S., Ku, S.W., 1997. Analytical modeling of high damping rubber bearings, *J. Struct. Engrg,* **123**, 1029-1036.

Irons, B. and Ahmad, S., 1980. *Techniques of Finite Elements,* Ellis Horwood Limited.

James, A.G., Green, A. and Simpson, 1975a. Strain energy functions of rubber. I. Characterization of gum vulcanizates, *J. Appl. Polym. Sci.,* **19**, 2033-2058.

James, A.G., Green, A. and Simpson, 1975b. Strain energy functions of rubber. II. The characterization of filled vulcanizates, *J. Appl. Polym. Sci.,* **19**, 2319-2330.

Jankovich, E., Leblanc, F., and Durand, M., 1981. A finite element method for the analysis of rubber parts, experimental and analytical assessment, *Computers and Structures,* **14**, 385-391.

Johnson, A.R., Quigley, C.J. and Freese, C.E., 1995. A viscohyperelastic finute element model for rubber, *Comput. Methods Appl. Mech. Engrg.,* **127**, 163-180.

Johnson, A.R., Quigley, C.J. and Mead, J.L., 1994. Large strain viscoelastic constitutive models for rubber, Part I: Formulations, *Rubber Chem. Technol.,* **67**, 904-917.

Johnson, A.R., Quigley, C.J., Young, D.G. and Danik, J.A., 1993. Viscohyperelastic modeling of rubber vulcanizates, *Tire Science and Technology,* **21**, 179-199.

Johnson, A.R., Stacer, R.G., 1993. Rubber viscoelasticity using the physically constrained system's stretches as internal variables, *Rubber Chem. Technol.,* **66**, 567-577.

Johnson, M.A. and Beatty, M.F., 1993a. A constitutive equation for the Mullins effect in stress controlled uniaxial extension experiments, *Continuum Mech. and Thermodyn.,* **5**, 301-318.

Johnson, M.A. and Beatty, M.F., 1993b. Mullins effect in uniaxial extension and its influence on transverse vibration of a rubber string, *Continuum Mech. and Thermodyn.,* **5**, 83-115.

Kar, K.K, Bhowmick, A.K., 2000. High strain hysteresis loss of rubber vulcanizates under pure shear and constrained extension and influence of filler, *Rubber Chem. Technol.,* **73**, 56-73.

Kawabata, S. and Kawai, H., 1977. Strain energy density functions of rubber vulcanizates from biaxial extension, *Adv. Polym. Sci.,* **24**, 90-124.

Kawabata, S., Matsuda, M., Tei, K. and Kawai, H., 1981. Experimental survey of the strain energy density function of isoprene rubber vulcanizate, *Macromolecules,* **14**, 154-162.

Kelly, J. M., 1997. *Earthquake Resistant Design with Rubber,* Springer-Verlag, London.

Kelly, J.M., 1991. *Dynamic and Failure Characteristics of Bridgestone Isolation Bearings,* Report no. UCB/EERC-91/04.

Kilian, H.G., Strauss, M., Hamm, W., 1994. Universal properties of filler loaded rubbers, *Rubber Chem. Tech.* **67**, 1-16.

Krempl, E., 1987. Models of viscoplasticity, Some comments on equililibrium (back) stress and drag stress, Acta Mechanica, **69**, 25-42.

Krinshnaswamy, S. and Beatty, M.F., 2000. The Mullins effect in compressible solids, *Int. J. Engrg, Sci.,* **38**, 1397-1414.

Kugler, H. P., Stacer, R. G. and Steimle, C., 1989. Direct measurement of Poisson's ratio in elastomers, *Rubber Chem. Technol.,* **63**, 473-487.

Lambert-Diani, J. and Rey, C., 1999. New phenomenological behavior laws for rubbers and thermo plastic elastomers, *Eur. J. Mech. A/Solids,* **18**, 1027-1043.

Le Tallac, P., Rahier, C. and Kaiss, A., 1993. Three dimensional incompressible viscoelasticity in large strain formulation and numerical approximation, *Comput. Meth. Appl. Mech. Engrg.,* **109**, 233-258.

Lim, C.K. and Herrmann, L.R., 1987. Equivalent homogeneous FE model for elastomeric bearings, *J. Struct. Engrg., ASCE,* **113**, 106-125.

Lion, A., 1997. A physically based method to represent the thermo-mechanical behavior of elastomers, *Acta Mechanica,* 123, 1-25.

Lion, A., 1996. A constitutive model for carbon black filled rubber: Experimental investigations and mathematical representation, *Continuum Mech. Thermodyn.,* **8**, 153-169.

Liu, Z.H., Zhang, X.D., Zhu, X.G., Li, R.K.Y, Qi, Z.N. and Wang, F.S., 1998. Effect of morphology on the brittle ductile transition of polymer blends:2. Analysis on poly(vinyl chloride)/nitrile rubber blends, *Polymer,* **39**, 5019-5025.

Lubliner, J., 1985. A model for rubber viscoelasticity, *Mech. Res. Comm.*, **12**, 93-99.

Mason, P., 1960. The strain dependence of rubber viscoelasticity, Part II. The influence of carbon black, *J. Appl. Polym. Sci.,* **4**, 212-218.

Meinecke, E.A. and Taftaf, M.I., 1987. Effect of carbon black on the mechanical properties of elastomers, *Rubber Chem. Technol.,* **61**, 534-547.

Miehe, C. and Keck, J., 2000. Superimposed finite elastic-viscoelastic-plastoelastic stress response with damage in filled rubbery polymers. Experiments, modeling and algorithmic implementation, *J. Mech. Phys. Solids,* **48**, 323-365.

Migwi, C.M., Darby, M.I., Wostenholm, G.H. and Yates, B., 1993. A method of determining the shear modulus and Poisson's ratio of polymer materials, *J. Mater. Sci.,* 3430-3432.

Mooney, M., A theory of large elastic deformation, 1940. *J. Appl. Phys.,* **11**, 582-592.

Mullins, L., 1987. Engineering with rubber, *Chemtech,* 720-727.

Mullins, L., 1969. Softening of rubber by deformations, *Rubber Chem. Technol.,* **42,** 339-362.

Mullins, L. and Tobin, N.R., 1965. Stress softening in rubber vulcanizates. Part I. Use of a strain amplification factor to describe the elastic behavior of filler-reinforced vulcanized rubber, *J. Appl. Polym. Sci.,* **9**, 2993-3009.

Mullins, L., Tobin, N.R., 1956. Theoretical model for the elastic behavior of filler reinforced vulcanized rubbers, Proc. Of the 3rd Rubber Technology Conference, 397-412.

Mullins, L., 1950. Thixotropic behavior of carbon black in rubber, *Phys. Colloid. Chem.,* **54**, 239-251.

Mullins, L., 1947. Effect of stretching on the properties of rubber, *J. Rubber Res.,* **16**, 275-289.

Nicholson, D.W., Nelson, N.W., Lin, B., and Farinella, A., 1998. Finite element analysis of hyperelastic components, *Appl. Mech. Rev.,* **51**, 303-320.

O'Dowd, N.P. and Knauss, W.G., 1995. Time dependent large principan deformation of polymers, *J. Mech. Phys. Solids,* **43**, 771-792.

Ogden, R.W., 1986. Recent advances in the phenomenological theory of rubber elasticity, *Rubber Chem. Technol.,* **59**, 361-383

Ogden, R. W., 1984. *Non-linear Elastic Deformations,* Ellis Horwood Ltd., Chichester.

Ogden, R.W., 1972. Large deformation isotropic elasticity: on the correlation of theory and experiment for compressible rubberlike solids, *Proc. R. Soc. Lond. A.,* **328**, 567-583.

Park, S.W. and Scapery, R.A., 1997. A viscoelastic constitutive model for particulate composites with growing damage, *Int. J. Solids Structs,* **34**, 931-947.

Peeters, F. J. H. and Kussner, M., 1999. Material law selection in the finite element simulation of rubber-like materials and its practical application in the industrial design process, Constitutive Models for Rubber, A. Dorfmann & A. Muhr ed., A. A. Balkema, Rotterdam, 29-36.

Peng, S.H. and Chang, S.H., 1997. A compressible approach in finite element alanysis of rubber elastic materials, *Comput. Struct.,* **62**, 573-593.

Peng, S.H., Shimbori, T. and Naderi, A., 1994. Measurement of elastomer's bulk modulus by means of a confined compression test, *Rubber Chem. Technol.,* **67**, 871-879.

Peng, T. J. and Landel, R. F., 1972. Stored energy function of rubberlike materials derived from simple tensile date, *J. Appl. Phys.* **43**, 3064-3067.

Plumtree, A., Cheng, G.X., 1998. Monotonic and cyclic compressive behavior of elastomers, *Plastics, Rubber and Composites Processing and Applications,* **27**, 349-355.

Quigley, C.J. and Mead, J., 1994. Large strain viscoelastic constitutive models for rubber, Part II: Determination of material constants, *Rubber Chem. Technol.,* **68**, 230-247.

Reese, S. and Govindjee, S., 1998a. A theory of finite viscoelasticity and numerical aspects, *Int. J. Solids Structures,* **35**, 3455-3482.

Reese, S. and Govindjee, S., 1998b. Theoretical and numerical aspects in the thermo viscoelastic material behavior of rubber-like polymers, *Mech. Time Dependent Mater.,* **1**, 357-396.

Rivlin, R. S. and Saunders, D. W., 1951. Large elastic deformations of isotropic materials VII. Experiments on the deformation of rubber, *Phil. Trans. Roy. Soc.* **243**, 251-288.

Rivlin, R.S. and Thomas, A.G., 1951. Large elastic deformations of isotropic materials VIII. Strain distribution around a hole in a sheet, *Phil. Trans. Roy. Soc.* **244**, 289-298.

Rivlin, R.S., 1949. Large elastic deformations of isotropic materials VI. Further results in the theory of torsion, shear and flexure, *Phil. Trans. Roy. Soc.* **242**, 173-195.

Rivlin, R. S., 1948a. Large elastic deformations of isotropic materials: Fundamnetal concepts, *Philos. Trans. R. Soc. London A,* **240**, 459-490.

Rivlin, R.S., 1948b. Large elastic deformations of isotropic materials IV. Further developments of the general theory, *Phil. Trans. Roy. Soc.*, **241**, 379-397.

Rivlin, R.S., 1948c. Large elastic deformations of isotropic materials V. The problem of flexure, *Phil. Trans. Roy. Soc.* **241**, 463-473.

Rivlin, R.S., 1947. Torsion of a rubber cylinder, *J. Appl. Phys.*, **18**, 444-449.

Roeder, C. W. and Stanton, J. F., 1983. Elastomeric Bearings: State-of-the-Art, *J. Struct. Engrg., ASCE,* **109**, 2853-2871.

Scion Image 2000. *User Manual,* Scion Corporation.

Seibert, D. J. and Schoche N., 2000. Direct comparison of some recent rubber elasticity models, *Rubber Chem. Technol.,* **73**, 366-384.

Shariff, M.H.B.M., 2000. Strain energy function for filled and unfilled rubberlike material, *Rubber Chem. Technol.,* **73**, 1-18.

Simo, J.C. and Taylor, R.L., 1991. Quasi-incompressible finite elasticity in principal stretches. Continuum basis and numerical algorithms, *Comp. Methods. Appl. Mech. Engrg.,* **85**, 273-310.

Simo, J.C., 1987. On a fully three dimensional finite strain viscoelastic damage model: Formulation and computational aspects, *Comput. Methods. Appl. Mech. Engrg.,* **60**, 153-173.

Simo, J.C., Taylor, R.L. and Pister, K.S., 1985. Variational and projection methods for the volume constraint in finite deformation elasto-palsticity, *Comput. Methods Appl. Mech. Engrg.,* **51**, 177-208.

Simo, J.C. and Taylor, R.L., 1982. Penalty function formulations for incompressible nonlinear elastics, *Comput. Methods Appl. Mech. Engrg.,* **35**, 107-118.

Spathis, G., 1997. Non-linear constitutive equations for viscoelastic behavior of elastomers at large deformations, *Polymer Gels and Networks,* **5**, 55-68.

Sullivan, J.L., Morman, K.N. and Pett, R.A., 1979. A nonlinear viscoelastic characterization of a natural rubber gum vulcanizate, *Rubber Chem. Technol.,* **53**, 805-822.

Sussman, T. and Bathe K., 1987. A finite element formulation for nonlinear incompressible elastic and inelastic analysis, *Computers and Structures,* **26**, 357-409.

Taylor, R.L., 2000. *FEAP – A Finite Element Analysis Program, User Manual,* Version 7.3.

Treloar, L. R. G., 1975. *The Physics of Rubber Elasticity,* Clarendon Press, Oxford.

Trealor, L.R.G., 1973. The elasticity and related properties of rubbers, *Rep. Prog. Phys.,* 755-826.

Treloar, L. R. G., 1944. Stress-strain data for vulcanized rubber under various types of deformations, *Trans. Faradey Soc.,* 59-70.

Truesdell, C., Noll, W., 1992. The non-linear field theories of mechanics. Second edition, Springer-Verlag, Berlin.

Tsakmakis, C., 1996. Formulation of viscoplasticity laws using overstress, *Acta Mechanica,* **115**, 179-202.

Tschoegl, N. W., 1989. *The Phenomenological Theory of Linear Viscoelastic Behavior: An Introduction,* Springer-Verlag Berlin.

Tschoegl, N. W., 1972. Constitutive equations for elastomers, *Rubber Chem. and Technol.,* **45**, 60-70.

Valanis, K. C. and Landel, R. F., 1967. The strain-energy density function of a hyperelastic material in terms of the extension ratios, *J. Appl. Phys.,* **38**, 2997-3002.

Wang, L. Y., Kuo, C.S. and Chiang, L.Y., 1997. Microscopic surface characterization of polyaniline-based conducting elastomers, *Synthetic Metals,* **84**, 587-588.

Ward, I. M., 1985. *Mechanical Properties of Solid Polymers,* John Wiley & Sons. New York, USA.

Wischt, C.E., 1998. *The Effect of Carbon Black on Elastic and Viscoelastic Properties of Elastomers,* PhD Thesis, University of Akron, USA.

Wolfram Research Inc., 1999. USA, *Mathematica,* Version 4.0.

Yamashita, Y. and Kawabata, S., 1992. Approximated form of the strain energy density function of carbon-black filled rubbers for industrial applications, *J. Soc. Rubber Ind. (Jpn),* **65**, 517-528. *(in Japanese).*

Yeoh, O.H., 1993. Some forms of strain energy function for rubber, *Rubber Chem Technol.,* **66**, 754-771.

Yeoh, O. H., 1990. Characterization of elastic properties of carbon-black filled rubber vulcanizates, *Rubber Chem. Technol.,* **63**, 792-805.

Yoshida, J., 1999. *Construction of the Constitutive Law for High Damping Rubber Material,* Masters Thesis, Department of Civil Engineering, Tokyo University Japan.

Zienkiewicz, O.C. and Taylor, R.L., 1996. *The Finite Element Method,* 4th Edition, Mc Graw Hill, New York.